Institute of Thermoelectricity, Academy of Sciences and Ministry of Education and Science of Ukraine

Journal of THERMOELECTRICITY

International Research

Founded in December, 1993

published 4 times a year

No. 4 *2023*

Editorial Board

International Editorial Board

Founders – National Academy of Sciences, Ukraine
Institute of Thermoelectricity of National Academy of Sciences and Ministry of Education and Science of Ukraine

Certificate of state registration № КВ 15496-4068 ПР

Address of editorial office:
Ukraine, 58002, Chernivtsi, General Post Office, P.O. Box 86.
Phone: +(380-372) 90 31 65.
Fax: +(380-3722) 4 19 17.
E-mail: jt@inst.cv.ua
http://www.jt.inst.cv.ua

Signed for publication 25.12.2023. Format 70×108/16. Offset paper №1. Offset printing.
Printer's sheet 11.5. Publisher's signature 9.2. Circulation 400 copies. Order 5.

Printed from the layout original made by "Journal of Thermoelectricity" editorial board in the printing house of "Bukrek" publishers,
10, Radischev Str., Chernivtsi, 58000, Ukraine

CONTENTS

O.M. Manyk, *Cand.Sc (Phys-Math)*[1]
T.O. Manyk, *Cand.Sc. (Phys-Math)*[2]
V.R. Bilynskyi-Slotylo, *Cand.Sc. (Phys-Math)*[1]

[1] Yuriy Fedkovych Chernivtsi National University, 2 Kotsiubynskyi str.,
Chernivtsi, 58012, Ukraine;
e-mail: o.manyk@chnu.edu.ua, slotulo@gmail.com
[2] Military University of Technology Jaroslaw Dombrowski, str. gene Sylwester Kaliskiego, 2,
Warsaw 46, 00-908, Poland
e-mail: tetjana.manyk@wat.edu.pl

THEORETICAL MODELS OF ORDERED ALLOYS OF THERMOELECTRIC MATERIALS BASED ON *Bi-Sb-Te*

Theoretical models of ordered alloys of promising thermoelectric materials of Bi-Sb-Te ternary systems have been developed. Diagrams of distribution of phase regions in such systems have been constructed using binary state diagrams of the initial components (Bi-Sb, Bi-Te, Sb-Te). Calculations of electron density redistribution, dissociation energy, and effective radii of chemical bonds forming the crystal structure of Bi-Sb-Te depending on interatomic distances are given.
Key words: theoretical models, chemical bond, effective radii, dissociation energy, state diagrams, non-equivalent hybrid orbitals (NHO).

Introduction

Antimony compounds and tellurium compounds are considered to be promising thermoelectric materials among binary compounds [1]. Depending on the mode of heat treatment and the method of cooling, antimony and tellurium alloys can crystallize in accordance with stable and metastable state diagrams [2]. The nature of the chemical bond in such alloys can vary from metallic to ionic, covalent and intermediate.

Considering also that the search for new thermoelectric materials is increasingly reduced to the need of studying multicomponent systems, the research of ternary systems based on *Bi-Sb-Te* is becoming especially relevant both from the standpoint of chemical bond and from the standpoint of phase diagrams. The need to conduct such studies is due to the fact that ternary systems are complex, nonlinear, and known theoretical approaches to problems of phase transformations of simple systems no longer detect the conditions for the appearance of the desired properties with the prospect of changing them in the desired direction. There is no consistent theory of phase transformations from the standpoint of chemical bond yet. This, in turn, raises the question of the relationship between physics and chemistry in technological research.

Physics plays a major role in modern natural science. Not only quantum mechanics, but much earlier thermodynamics and the science of electricity gave rise to new directions of chemical and physico-chemical research. The emergence of quantum chemistry has changed traditional ideas about the relationship between these two scientific disciplines.

There is a point of view that scientific knowledge develops intensively and extensively. Intensive development means a significant deepening of knowledge, which leads to a new view of nature. Along this path, quantum mechanics arose. Then these ideas and concepts, which arose on the way of intensive development, are added to new facts and used to solve new problems. Along this path, quantum chemistry arose.

In each area of knowledge, one fundamental theory can be distinguished. But the theory does not consist of just the foundation. Non-fundamental theoretical constructions (they are called theories of medium generality) model reality in their own way and solve scientific problems in their own way. They can be considered as "models of reality", then fundamental theories can be called "models of models".

Principles of quantum mechanics are the foundation of the modern theory of the structure of matter. In the course of reduction, which means reducing a complex process to a simpler one by complicating the original model, quantum mechanics is overgrown with approximate methods, hypothetical and model representations and “goes over“ into quantum chemistry [3].

At the same time, the original model of quantum mechanics changed somewhat (the model of the hydrogen atom to the model of the hydrogen molecule) and the basis of the theory is no longer a one-center, but a two-center problem. In this regard, quantum chemistry is often called chemical bond theory. Now quantum chemistry explains and implies various properties of crystals based on the electronic structure of molecules.

In reality, the structure of scientific knowledge is even more complicated. Each theoretical construction of an average degree of generality contains within itself another concept of an average degree of generality, and that is even narrower, and so on until the "degeneration" of theoretical knowledge into some concepts of "common sense" occurs.

It is this approach that has made it possible to unite the multilayer structure of theoretical knowledge in different fields. In this case, the structural element of the system under consideration is no longer the hydrogen atom, as the original model for solving the Schrödinger equation in quantum mechanics, but a two-center formation – a model of the hydrogen molecule. This unification became possible due to interdisciplinary synthesis. The basis of such synthesis, according to [4], is the unification of the electronic, oscillatory and configurational components of the energy of the "molecule" as a single whole, as a general measure of different types of interaction. In this case, energy is considered both from the position of its organizational structure and from the position of the state function. This made it possible to calculate the ordering processes in alloys by statistical methods; regularities of the formation of the short-range order of the chemical bond in melts – by quantum-chemical methods; redistribution of electron density and dissociation energy of non-equivalent chemical bonds in ternary systems – by methods of microscopic theory using solutions of inverse problems and molecular models [5].

This work is a continuation of complex studies [4] and is devoted to the construction of theoretical models of ordered alloys of ternary systems of promising thermoelectric materials based on *Bi-Sb-Te*. The use of the triangulation method was new in the study of tellurides and antimonides [6]. In chemistry, this method allows for the distribution of ternary systems into simpler binary ones, taking into account the patterns of formation of compounds; the formation of solid solutions and mechanical mixtures. In this paper, the inverse problem of triangulation is solved: using the known phase diagrams of binary systems [7], taking into account the chemical interaction between the elements *Bi*; *Te*; *Sb*, a diagram of the distribution of phase regions for various isothermal sections of *Bi-Te*, *Bi-Sb*, *Sb-Te* in the *Bi-Sb-Te* system is constructed, and the parameters of phase transformations are calculated theoretically using quantum chemistry methods.

Theoretical models of *Bi-Sb-Te* state diagrams

When constructing theoretical models of *Bi-Sb-Te*, it was necessary to summarize the results of experimental studies of binary state diagrams of *Bi-Sb*, *Bi-Te* and *Sb-Te* [7]; physicochemical properties and the results of studying quantum regularities of the initial components [2]. This will make it possible to establish the boundaries of phase equilibrium in the liquid-crystal regions (melting diagrams) and predict cases of incongruent melting of metastable phases.

In this regard, the choice of bismuth as a constituent component of *Bi-Sb-Te* was not accidental. First of all, bismuth is part of Bi_2Te_3 – the most widely used material in thermoelectricity [8]. In addition, bismuth in compounds can have different oxidation states, which can take values from – 3 to + 5. Pentavalent bismuth salts are strong oxidizers. In humid air, bismuth is covered with an oxide layer. At high temperature, bismuth burns to Bi_2O_3. It does not dissolve in hydrochloric and dilute sulfuric acids. It dissolves easily in nitric acid and aqua regia.

Bismuth is extracted from concentrates by pyro- or hydrometallurgical methods. Much bismuth is extracted from copper and lead production waste. Metallic bismuth is used to make low-melting alloys as a coolant in nuclear reactors in devices for various purposes. Bismuth compounds are used in medicine as binding antiseptic and adsorption agents for the treatment of stomach and intestinal ulcers, skin and mucous diseases.

Such a wide set of physicochemical properties of Bi and the ability to change them under certain conditions allows forming the short-range order of the chemical bond in *Bi-Sb-Te* compounds and, accordingly, the physicochemical properties of the obtained material in the desired direction.

The choice of antimony as a component of the ternary *Bi-Sb-Te* system was also not accidental. Research into antimony-based semiconductor materials is currently of great value [4]. Increased attention to antimony is also due to its inherent polymorphic transformations, since each modification has a corresponding stability field of the state diagram, which leads to technological difficulties.

Antimony is known in four modifications: ordinary – crystalline and three amorphous – yellow, black and explosive. Under normal conditions, only crystalline antimony with a rhombohedral structure, $a = 0.45064$ μm, $\alpha = 57.1°$, is stable. Crystals of pure antimony consist of cells of a rhombohedral structure, the distance between atoms within which is equal to 2.87 Å, and the angles between covalent bonds are 94°. Melting antimony changes the nature of bonds from covalent to metallic. At the same time, the coordination number increases to six, and the interatomic distances increase from 2.87 Å to 2.89 Å. The type of crystal lattice also changes - from rhombohedral to hexagonal. The hexagonal cells are arranged so that the shortest distance between atoms of adjacent layers is 3.38 Å, and the lattice periods are $a = 4.307$ Å; $c = 11.127$ Å. Antimony easily forms alloys with many metals – antimonides. The most common antimonides are indium, gallium, aluminum, cobalt, zinc, tellurium, cadmium, calcium, mercury, chromium, iron, cesium, potassium and sodium.

In addition, according to the state diagram (*Bi-Sb*), both components (*Bi* and *Sb*) are infinitely soluble in liquid and solid states and do not form chemical compounds. At the same time, the state diagrams of *Bi-Te* and *Sb-Te* are diagrams with eutectics, where both compounds and solid solutions can be formed. In this regard, the task was set: to calculate the parameters of chemical bonds depending on interatomic distances and to construct phase distribution schemes in the *Bi-Sb-Te* system.

When building theoretical models, the results of experimental studies of binary systems were summarized; physicochemical properties and quantum regularities of the initial components, which made it possible to determine the quantitative ratios of congruent and incongruent melting.

The obtained results are shown in Figs. 1 – 4, where the following designations are entered:

α – solid phase based on *Bi*;

β – solid phase based on *Te*;
γ – solid phase based on *Sb*;
δ – solid phases based on *Bi-Sb*;
ρ – solid phases based on *Sb-Te*;
ε – solid phases based oni *Bi-Te*;
σ – solid phases based on *Bi-Sb-Te* intermediate compound;
L – liquid.

Fig. 1 shows the diagram of distribution of *Bi-Sb-Te* phase regions in the solid state. This approach made it possible to trace the division of the *Bi-Sb-Te* ternary system into six ordered ternary subsystems. It should also be noted that in the presence of additional experimental data, the number of ordered subsystems may be larger. This makes it possible to study in more detail the eutectic, peritectic, phase transitions of stable and metastable phases, the formation of short-range chemical bond order in ternary systems depending on the interatomic distances in a narrower range of concentrations.

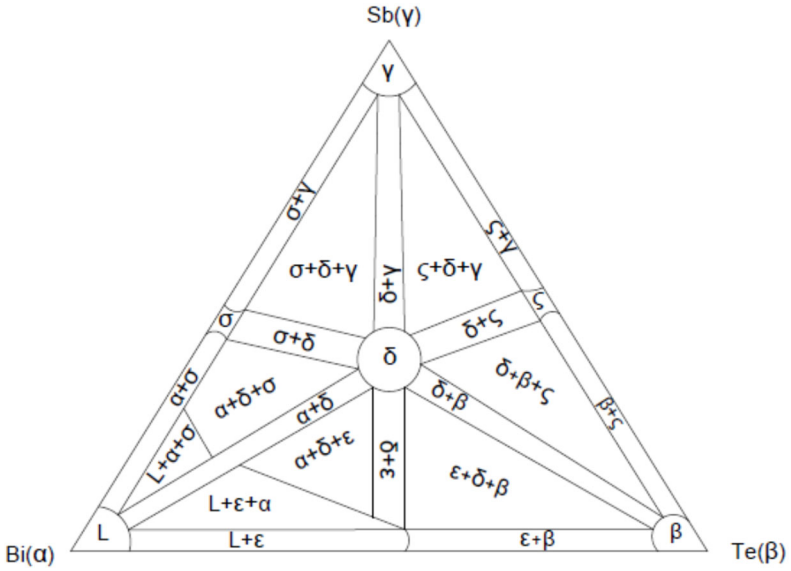

Fig. 1. Diagram of distribution of Bi-Sb-Te phase regions in the solid state.

Fig. 2 shows an isothermal section at a temperature of t = 300 °C. This temperature is higher than the melting point of bismuth (271.3 °C) and lower than the melting point of tellurium (450 °C) and antimony (630.5 °C). Part of the section (*Bi-Te*) and (*Bi-Sb*) is occupied by the liquid (*L*), and the two-phase equilibrium (*L*, α), (*L*, ε), (*L*, δ) is carried out by primary crystals α and crystals ε and β based on *Bi-Te* and *Bi-Sb*. In contrast to the previous case, the section contains conoid triangles with equilibrium phases (L + α + δ) and (L + α + ε), which are formed by primary crystals based on *Bi-Sb* and *Bi-Te* compounds. This division of ternary systems into separate sectors of dual state diagrams makes it possible to study the processes of formation of the short-range order of chemical bond and the fine structure of cooling and heating of individual elements depending on their environment in ternary systems.

Fig. 3 shows an isothermal section at a temperature of t = 425 °C, which is higher than the melting temperature of bismuth and higher than the temperatures of eutectics $Bi_{0.1}Te_{0.9}$ (t = 413 °C) and $Sb_{0.1}Te_{0.9}$ (t = 424 °C). In this case, liquid L occupies a larger part of the section (*Bi-Sb*) than in the previous case at t = 300 °C, and the equilibrium phases with conoid triangles (L + α + ε) and (L + α + δ) are replaced by phases (L + ε + δ).

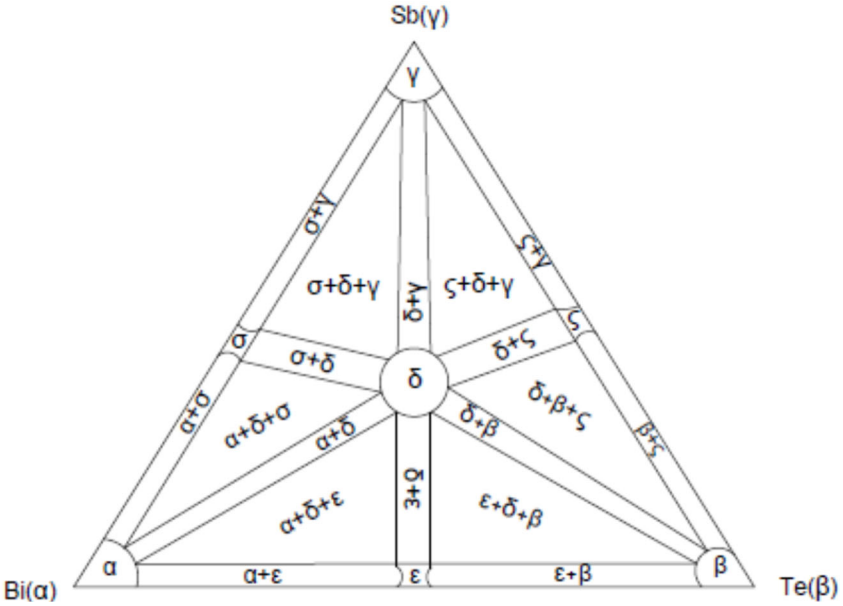

Fig. 2. Bi-Sb-Te isothermal section at t = 300 °C.

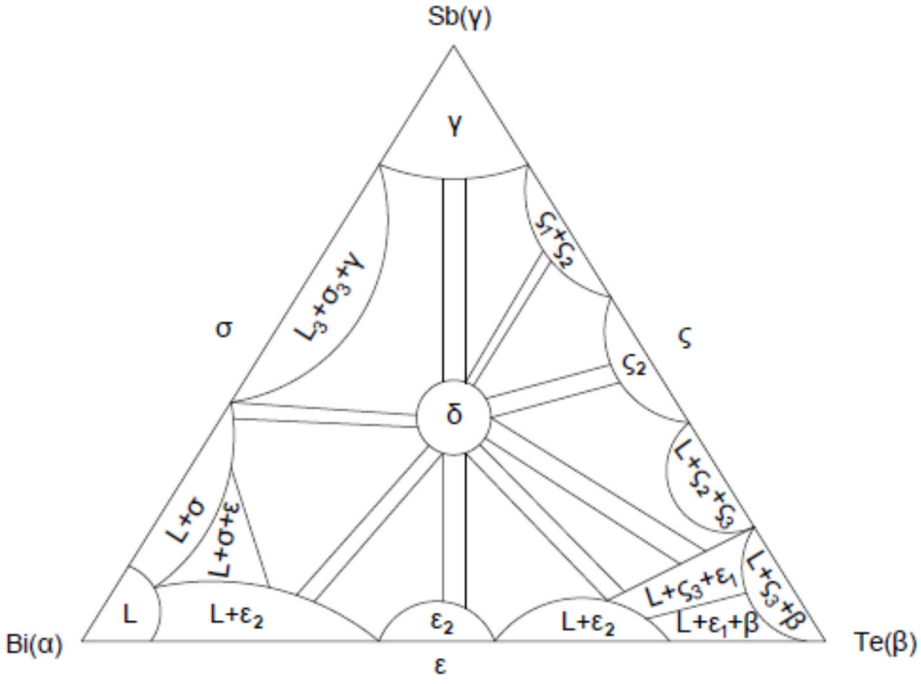

Fig. 3. Bi-Sb-Te isothermal section at t = 425 °C.

On the section (*Te-Sb*), the equilibrium phases ρ_1 ($Sb_{0.72}Te_{0.28}$); ρ_2 ($Sb_{0.4}Te_{0.6}$); ρ_3 ($Sb_{0.1}Te_{0.9}$) are clearly delineated. In this case, the compositions of phases ρ_1 and ρ_2 at this temperature remain stable and the concentration of components γ and ρ corresponds to the state diagram (*Te-Sb*), and does not change upon cooling. At the same time, in the area of tellurium concentrations from 60 % to 89 %, with a decrease in temperature from 622 °C to the eutectic of 425 °C, crystals of composition ρ_2 are released and the composition of the liquid changes towards increasing the component ρ_3. At the same time, the equilibrium phases ($L + \delta + \rho$) are replaced by intermediate phases ($L + \rho_3 + \sigma$) and ($L + \sigma + \rho_2$). This

makes it possible to study the fine structure of the formation of intermediate compounds in ternary systems depending on the concentration of the initial components.

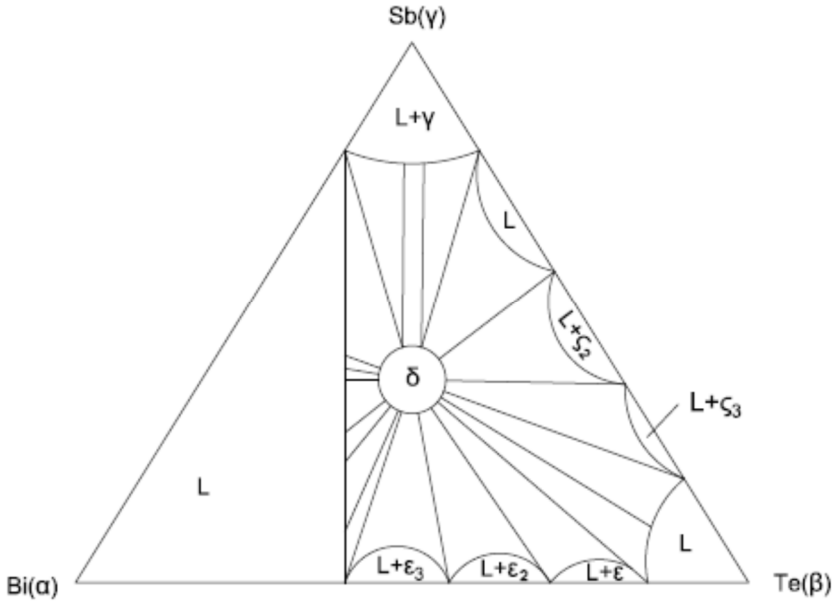

Fig. 4. Bi-Sb-Te isothermal section at t = 550 °C.

Fig. 4 shows an isothermal section at a temperature of t = 550 °C. In this case, a liquid phase is observed on the *Bi-Sb* diagram in the segment up to 75 % *Sb*. Both the solid phase of antimony and solid solutions based on *Sb-Bi* are observed in the segment 75 – 10 % *Sb*. A similar situation is observed in the *Sb-Te* diagram. Further, 25 – 35 % *Te* – a liquid phase is observed. In the 35 – 75 % segment, polymorphic transformations occur with the formation of Sb_2Te_3, and then – a liquid phase. As for the *Bi-Te* state diagram, in the segment from 30 to 50 %, polymorphic transformations occur with the formation of Bi_2Te_3, and in the other two – a liquid.

Thus, the above isothermal sections made it possible:

1. To establish the limits of phase equilibrium, their dynamics of change in the liquid-crystal regions and the region of existence in equilibrium of solid solutions.

2. To separate the boundaries of eutectic and peritectic state diagrams.

3. To predict cases of incongruent melting of chemical compounds of different composition.

However, it should be noted that isothermal sections alone do not provide the values of the phase transition parameters of multicomponent systems. Methods are needed that combine experimental approaches with calculations of the interaction energy in both phases when constructing phase diagrams of ternary systems. This will allow combining empirical information on the properties of atoms based on the experience and traditions of the crystal-chemical approach with analytical relationships reflecting the quantum laws of interatomic interaction; statistical laws – with the electron configurations of interacting atoms and the formation of a chemical bond between them.

Theoretical models of chemical bonding of ordered *Bi-Sb-Te* alloys

The theoretical analysis of empirical dependences of crystallization processes is connected with the revision of views on the problem of interatomic interaction. At the same time, there is still no single quantitative method for calculating the electronic structure of compounds and alloys based on both the quantum mechanical and empirical approaches.

On the other hand, taking into account statistical regularities made it possible to obtain the dependence of the number of electrons n on the outer shell of an atom on the Fermi radius r_F, and empirical information on the properties of atoms and ions can be combined on the basis of a crystal chemical approach, introducing the concept of unpolarized ionic radii R_{Un} [9]. Since the functions that include the Fermi radii $r_F = f(n)$ and the equations that include $R_{Un}^1 1$ determine the electronic configurations of the interacting atoms depending on the length and number of bonds they form, all this gives reason to consider r_F and R_{Un} identical and denote by one symbol R_U – effective ionic radii.

The relationship $tg\alpha = \frac{\Delta lgR_U}{\Delta n}$ where α is the slope of the lines in the coordinates $lgR_U = f(n)$, turned out to be useful when searching for the dependence of R_U on n. The latter should be given special attention. Despite the imperfection, from a theoretical point of view, of empirical criteria (crystal chemical radius, electronegativity, polarizability, and others), their positive role in the systematization of experimental data and the development of ideas about the nature of interatomic interaction does not raise doubts, since the determination of the numerical values of these criteria is based on the generalization of experimental data in combination with their interpretation from the standpoint of quantum chemistry, which contains important information about the nature of interatomic interactions.

A good agreement between the complex of research data on various physical and chemical properties of atoms and their ions and the values of R_U and tgα is given by the postulated [9] dependence: and tgα is given by the postulated [9] dependence:

$$lgR_{UA}^x = lgR_{UA}^0 - xtg\alpha, \tag{1}$$

where R_{UA}^0 is the radius of atoms A in an unexcited state, and x is the valence, which allows us to overcome the difficulties of chemical bond theory and obtain a physically substantiated result of interatomic interaction.

The use of ionic radii to describe the processes of formation of a chemical bond by rearrangement of valence shells made it possible to write equation (1) in the form:

$$lgR_{UA}^{+x} = lgR_{UA}^0 - xtg\alpha_{\mathrm{A}}, \tag{2}$$

$$lgR_{UB}^{-x} = lgR_{UB}^0 + xtg\alpha_{\mathrm{B}}, \tag{3}$$

$$d_1 = R_{UA}^{+x} + R_{UB}^{-x}, \tag{4}$$

where d_1 is the A – B internuclear distance.

From the point of view of the crystal-chemical approach, the presence of d_{min} and two possible values of effective charges r_{ef} for $d_1 > d_{min}$ is justified by the increase of the internuclear distance when the ionicity and covalency between the same partners change.

The main drawback of this approach is that in many cases the internuclear distances ($A – B$) in crystalline compounds and alloys are smaller than the d_{min} value, and it is impossible to calculate the charge of ions using the diagrams $Z_{ef} = f(d)$. Therefore, difficulties can be overcome only by abandoning the method of interpreting the solution of system (2) – (4) from the point of view of the crystal-chemical approach. Additional criteria are needed to translate system (2) – (4) into the language of quantum chemistry. It should be taken into consideration that in the zone of formation of a chemical bond, the spherical symmetry of the electron density of the initial components is broken and the formation of bonds ($A – B$) is accompanied by the transition of electrons to other directions of

interatomic interaction and this bond becomes a donor. This condition is fulfilled if the extraction $(+\Delta e)$ of electrons or their localization $(-\Delta e)$, in the given direction of communication equally change the value of the charges that this pair has at $d_1 = d_{min}$, i.e. $Z_{ef}A(B) = Z_{min}A(B) + \left(\frac{\Delta l}{2}\right)$. These conditions are described by a system of equations:

$$d_1 = R_{UA}^{ZA} + R_{UB}^{ZB}, \tag{5}$$

$$lgR_{UA}^{ZA} = lgR_{UA}^{0} - (Z_{minA} + \tfrac{\Delta e}{2})tg\alpha_A, \tag{6}$$

$$lgR_{UB}^{ZB} = lgR_{UB}^{0} - (Z_{minB} + \tfrac{\Delta e}{2})tg\alpha_B \tag{7}$$

Externally, equations (2) – (4) and (5) – (7) are similar, but in reality, replacing x with $(Z_{min} + \frac{\Delta e}{2})$ changes their physical meaning: if the function $d_1 = f(Z_{ef})$ according to (2) – (4) is calculated in the approximation $(Z_A = -Z_B)$ and is correct from a quantum point of view only when $d_1 = d_{min}$, this is enough for the system (5) – (7) to be solved when d_1 is known. Thus, taking into consideration the quantum interpretation of empirical material made it possible to obtain an expression for the energy of chemical bonds in the form:

$$D_{A-B}^{i} = \left(\frac{C_1(R_{UA}^0 + R_{UB}^0)}{(\mathrm{tg}\,\alpha_A + \mathrm{tg}\,\alpha_B)}\right)\left(\frac{C_2 d_i}{d_i^2 - R_{UA}R_{UB}} - \frac{1}{d_i}\right), \tag{8}$$

where $R_{UA(B)}^0$, $tg\alpha_{A(B)}$ are coefficients of equations (2) – (4) for atoms A and B; R_{UA} and, R_{UB} are effective radii of ions in bonds (A-B) with length d_i; i is the number of non-equivalent interatomic distances in the considered compounds; C_1 is a coefficient reflecting the interrelationship of dimensional characteristics of interatomic interaction (measured in electron volts); C_2 is a coefficient that depends on crystal structure and chemical bond and is chosen dimensionless.

The above equations were used in the calculations of effective charges, effective radii and dissociation energies of non-equivalent chemical bonds of compounds and alloys that are part of the ternary system *Bi-Sb-Te*.

The results of calculations of the coefficients of equations (2) – (4) R_U^0 and $tg\alpha$ of the initial components are given in Table 1.

Table 1

Coefficients of equations of the initial components.

Z	Element	R_U^0(Å)	$tg\alpha$
83	*Bi*	1.63	0.068
52	*Te*	1.57	0.076
51	*Sb*	1.45	0.074

Effective charges Δq_i, effective radii R_{Ui} and dissociation energies for the nearest neighbours at different interatomic distances $d_i (1 \le i \le 6)$ of the structural modifications of bismuth are given in Table 2.

Table 2

Effective charges (Δq_i), effective radii (R_{Ui}) and dissociation energies $D(\varphi_i)$ depending on interatomic distances d_i of Bi-Bi.

Bi-Bi NHO / Parameters	*Bi-Bi*					
	φ_1	φ_2	φ_3	φ_4	φ_5	φ_6
d_i (Å)	2.8	2.9	3.0	3.1	3.2	3.3
$R_{U_i}^{Bi}$ (Å)	1.40	1.45	1.50	1.55	1.60	1.65
Δq_i (φ_i)	+ 0.85	+ 0.70	+ 0.50	+ 0.30	+ 0.10	– 0.10
$D(\varphi_i)$ (eV)	2.8540	2.76	2.66	2.58	2.50	2.42

Results of calculations for antimony and tellurium are given in Tables 3 and 4.

Table 3

Effective charges (Δq_i), effective radii (R_{Ui}) and dissociation energies $D(\varphi_i)$ depending on interatomic distances d_i of Sb-Sb.

Sb-Sb NHO / Parameters	*Sb-Sb*					
	φ_1	φ_2	φ_3	φ_4	φ_5	φ_6
d_i (Å)	2.8	2.9	3.0	3.1	3.2	3.3
$R_{U_i}^{Sb}$ (Å)	1.40	1.45	1.50	1.55	1.60	1.65
Δq_i (φ_i)	0.2	0	– 0.2	– 0.39	– 0.6	– 0.75
$D(\varphi_i)$ (eV)	2.33	2.25	2.18	2.11	2.04	1.98

Table 4

Effective charges (Δq_i), effective radii (R_{Ui}) and dissociation energies $D(\varphi_i)$ depending on interatomic distances d_i of Te-Te.

Te-Te NHO / Parameters	*Te-Te*					
	φ_1	φ_2	φ_3	φ_4	φ_5	φ_6
d_i (Å)	2.8	2.9	3.0	3.1	3.2	3.3
$R_{U_i}^{Te}$ (Å)	1.40	1.45	1.50	1.55	1.60	1.65
Δq_i (φ_i)	0.65	0.45	0.26	– 0.01	– 0.11	– 0.28
$D(\varphi_i)$ (eV)	2.46	2.37	2.30	2.22	2.15	2.09

As regards the above parameters for *Sb-Te*, *Bi-Te* and *Bi-Sb* compounds, they are given in Tables 5, 6, 7.

Table 5

Effective charges (Δq_i), effective radii (R_{Ui}) and dissociation energies $D(\varphi_i)$ depending on interatomic distances d_i of Sb-Te.

Sb-Te NHO / Parameters	*Sb-Te*					
	φ_1	φ_2	φ_3	φ_4	φ_5	φ_6
d_i (Å)	2.8	2.9	3.0	3.1	3.2	3.3
$R_{U_i}^{Sb}$ (Å)	1.345	1.444	1.46	1.48	1.53	1.58
$R_{U_i}^{Te}$ (Å)	1.445	1.456	1.54	1.62	1.67	1.72
Δq_i (φ_i)	0.43	0.23	0.03	– 0.16	– 0.32	– 0.52
$D(\varphi_i)$ (eV)	2.39	2.31	2.24	2.16	2.09	2.03

Table 6

Effective charges (Δq_i), effective radii (R_{Ui}) and dissociation energies $D(\varphi_i)$ depending on interatomic distances d_i of Bi-Te.

Bi-Te NHO / Parameters	*Bi-Te*					
	φ_1	φ_2	φ_3	φ_4	φ_5	φ_6
d_i (Å)	2.8	2.9	3.0	3.1	3.2	3.3
$R_{U_i}^{Bi}$ (Å)	1.435	1.485	1.536	1.584	1.653	1.681
$R_{U_i}^{Te}$ (Å)	1.365	1.415	1.464	1.516	1.547	1.619
Δq_i (φ_i)	0.12	0.08	0.05	0.03	– 0.001	– 0.03
$D(\varphi_i)$ (eV)	2.64	2.57	2.47	2.40	2.31	2.24

Table 7

Effective charges (Δq_i), effective radii (R_{Ui}) and dissociation energies $D(\varphi_i)$ depending on interatomic distances d_i of Bi-Sb.

Bi-Sb NHO / Parameters	*Bi-Sb*					
	φ_1	φ_2	φ_3	φ_4	φ_5	φ_6
d_i (Å)	2.8	2.9	3.0	3.1	3.2	3.3
$R_{U_i}^{Bi}$ (Å)	1.852	1.542	1.583	1.642	1.688	1.742
$R_{U_i}^{Sb}$ (Å)	1.315	1.358	1.417	1.458	1.512	1.558
Δq_i (φ_i)	0.57	0.35	0.2	– 0.05	– 0.25	– 0.45
$D(\varphi_i)$ (eV)	2.57	2.48	2.40	2.32	2.25	2.18

In the tables, the values of coefficients C_1 and C_2 in the calculations in the first approximation are chosen to be equal to unity.

Discussion of the results

As follows from the obtained results presented in Figs.(1) – (4) and in Tables (1) – (7), the application of a complex approach to technological problems made it possible to build theoretical models combining generalized experimental information based on the analysis of isothermal sections of binary state diagrams of *Bi-Sb*, *Bi-Te* and *Sb-Te* at different temperatures, which allows describing phase transitions; processes of chemical bond formation in ternary systems *Bi-Sb-Te*.

This approach made it possible to describe the processes of formation of interatomic interaction at different technological levels by summarizing versatile theoretical studies from the standpoint of chemical bond. This is, first of all, the formation of a crystal structure based on the initial components (*Bi*, *Sb*, *Te*), where information on the physicochemical properties and chemical relationship of the initial elements (Tables 1 – 4), binary compounds based on a combination of the initial elements (*Bi-Sb*, *Bi-Te*, *Sb-Te*) – (Tables 5 – 7) was taken into account. What was new was that the work included calculations of the dependence of the parameters of the chemical bonds under consideration on interatomic distances (effective radii, redistribution of electron density on the corresponding chemical bonds and the dissociation energy of the bonds that form the crystal structure). This made it possible to establish the boundaries when the same chemical bond, depending on the crystal structure and interatomic distances, can be both donor and acceptor.

What was new in the study of ternary *Bi-Sb-Te* systems was that the method of inverse triangulation was used to construct the diagram of distribution of phase equilibrium regions using

information on binary compounds of the initial components and their state diagrams. This made it possible to determine the quantitative relationships between the phases and, in the liquid-crystal regions, to separate the boundaries of the eutectic and peritectic type diagrams to solve problems of stable and metastable phases, and to foresee cases of congruent and incongruent melting.

The obtained results can be used in the development of technological modes of obtaining new *Bi-Sb-Te* materials.

References

1. Anatychuk L.I. (2003). *Thermoelectric power converters*. Institute of Thermoelectricity, Kyiv: Naukova Dumka.
2. Belotskij D.P., Manik O.N. (1996). On the relationship between thermoelectric materials melts properties and structures and the state diagrams. 1. Regularities of eleavage manifestation in the state diagrams. *J. Thermoelectricity*, 1, 21 – 47.
3. Sleta L.O., Ivanov V.V. (2008). *Kvantova khimia [Quantum chemistry]*. Kharkiv: Gimnaziia [in Ukrainian].
4. Manyk O.M., Manyk T.O., Bilynskyi-Slotylo V.R. (2021). Theoretical models of ordered alloys of ternary systems of thermoelectric materials. 1. Chemical bond and state diagrams of *In-Cd-Sb*. *J. Thermoelectricity*, 2, 32 – 42.
5. Manik O.M. (1999). *Multi-factor approach in theoretical materials science*. Chernivtsi: Prut [in Ukrainian].
6. Barchii I.E., Peresh E.Yu., Rizak V.M., Khudolii V.O. (2003). *Heterogenni rivnovahy [Heterogeneous equilibria]*. Uzhhorod, Zakarpattia Publ. [in Ukrainian].
7. Hansen M., Anderko K. (1962). *Struktura dvoinykh splavov [Structure of double alloys].* Moscow: Metallurgizdat, v. 1,2.
8. Manyk O.M., Manyk T.O., Bilynskyi-Slotylo V.R. (2022). Theoretical models of ordered alloys of ternary systems of thermoelectric materials. 2. Chemical bond and state diagrams of *Bi-Pb-Te*. *J. Thermoelectricity*, 1, 5 – 15.
9. Prikhodko E.V. (1973). *Sistema nepolarizovannykh ionnykh radiusov i eio ispolzovaniie dlia analiza elektronnogo stroieniia i svoistv veschestv [The system of unpolarized ionic radii and its use for the analysis of the electronic structure and properties of substances].* Kyiv: Naukova Dumka.

Submitted: 26.10.2023.

Маник О.М., *канд. фіз.-мат. наук* [1]
Маник Т.О., *канд. фіз.-мат. наук* [2]
Білинський-Слотило В.Р., *канд. фіз.-мат. наук* [1]

[1] Чернівецький національний університет імені Юрія Федьковича,
вул. Коцюбинського 2, Чернівці, 58012, Україна;
e-mail: o.manyk@chnu.edu.ua, slotulo@gmail.com
[2] Військово-технічний університет ім. Ярослава Домбровського,
вул. ген. Сільвестра Каліського, 2, Варшава 46, 00-908, Польща
e-mail: tetjana.manyk@wat.edu.pl

ТЕОРЕТИЧНІ МОДЕЛІ ВПОРЯДКОВУВАНИХ СПЛАВІВ ТЕРМОЕЛЕКТРИЧНИХ МАТЕРІАЛІВ НА ОСНОВІ *Bi-Sb-Te*

Розроблено теоретичні моделі впорядковуваних сплавів перспективних термоелектричних матеріалів потрійних систем Bi-Sb-Te. Побудовано схеми розподілу фазових областей в таких системах з використанням бінарних діаграм стану вихідних компонентів (Bi-Sb, Bi-Te, Sb-Te). Приведено розрахунки перерозподілу електронної густини, енергії дисоціації та ефективних радіусів хімічних зв'язків, що формують кристалічну структуру Bi-Sb-Te в залежності від міжатомних віддалей.

Ключові слова: теоретичні моделі, хімічний зв'язок, ефективні радіуси, енергія дисоціації, діаграми стану, нееквівалентні гібридні орбіталі (НГО).

Література

1. Anatychuk L.I. (2003). *Thermoelectric power converters*. Institute of Thermoelectricity, Kyiv: Naukova Dumka.
2. Belotskij D.P., Manik O.N. (1996). On the relationship between thermoelectric materials melts properties and structures and the state diagrams. 1. Regularities of eleavage manifestation in the state diagrams. *J. Thermoelectricity*, 1, 21 – 47.
3. Слєта Л.О., Іванов В.В. Квантова хімія. –Харків: Гімназія, 2008. – 443 с.
4. Маник О.М., Маник Т.О., Білинський-Слотило В.Р. Теоретичні моделі упорядковуваних сплавів потрійних систем термоелектричних матеріалів. 1. Хімічний зв'язок та діаграми стану *In-Cd-Sb*. // Термоелектрика. – 2021. – №2. – С. 32 – 42.
5. Маник О.М. Багатофакторний підхід в теоретичному матеріалознавстві // Україна, Чернівці: Прут. – 1999. – 432 с.
6. Барчій І.Є., Переш Є.Ю., Різак В.М., Худолій В.О. Гетерогенні рівноваги // Україна, Ужгород: вид. Закарпаття. – 2003. – 211 с.
7. Хансен М., Андерко К. Структура двойних сплавов. – М: Металлургиздат, 1962, т. 1,2.
8. Маник О.М., Маник Т.О., Білинський-Слотило В.Р. Теоретичні моделі упорядковуваних сплавів потрійних систем термоелектричних матеріалів. 2. Хімічний зв'язок та діаграми стану *Bi-Pb-Te* // Термоелектрика. – 2022. – №1. – С. 5 – 15.
9. Prikhodko E.V. (1973). *Sistema nepolarizovannykh ionnykh radiusov i eio ispolzovaniie dlia analiza elektronnogo stroieniia i svoistv veschestv [The system of unpolarized ionic radii and its use for the analysis of the electronic structure and properties of substances].* Kyiv: Naukova Dumka.

Надійшла до редакції: 26.10.2023.

P.V. Gorskyi, *DSc. (Phys-Math)* [1,2]

[1] Institute of Thermoelectricity of the NAS
and MES of Ukraine, 1 Nauky str.,
Chernivtsi, 58029, Ukraine;
[2] Yuriy Fedkovych Chernivtsi National University,
2 Kotsiubynskyi str., Chernivtsi, 58012, Ukraine
e-mail: gena.grim@gmail.com

P.V. Gorskyi

DAMPING OF THERMOMECHANICAL STRESSES AS A MEANS OF INCREASING THE CYCLIC STABILITY OF THERMOELECTRIC ENERGY CONVERTERS

Based on a combination of the strength of materials methods with the Weibull approach, the requirements for the rigidity coefficients of damping elements are determined, which can be used to reduce thermomechanical stresses in thermoelectric legs in order to increase the cyclic stability of thermoelectric energy converters. The Coffin-Manson power model for the dependence of the acceleration factor on the temperature difference in the presence of cyclic temperature effects is substantiated. The calculation results are not only in qualitative but also in satisfactory quantitative agreement with the experimental data.

Key words: cyclic stability, thermoelectric energy converter, thermomechanical stresses, damping, strength of materials, Weibull approach, cracking strength, rigidity of elastic element.

Introduction

The need for damping of thermomechanical stresses arises from the fact that in the case of rigid fastening of thermoelectric legs to ceramic plates in the presence of cyclic temperature effects, thermomechanical stresses arise in thermoelectric legs, which significantly exceed their cracking resistance and significantly reduce the probability of failure-free operation of thermoelectric energy converters [1]. The purpose of the article is to determine the requirements for the rigidity of damping elements in order to obtain mechanical stresses in thermoelectric legs that are acceptable from the point of view of cyclic stability and the probability of failure-free operation of thermoelectric energy converters.

1. Physical model of thermomechanical stress damping and its consequences

Physical model of thermomechanical stress damping is shown in Fig. 1.

To determine the requirements for the rigidity coefficient of an elastic element, let us imagine that the thermoelectric leg expands partially freely. Its temperature deformation by the value x causes the reaction force kx from the elastic element. This reaction force corresponds to the mechanical stress kx/b^2, where b is the cross-sectional side of the leg. The following equation follows from the condition of mechanical equilibrium for determining x:

$$E\left(\alpha^T \Delta T - \frac{x}{l}\right) = \frac{kx}{b^2}. \quad (1)$$

where E is the Young's modulus of the thermoelectric material, α_T is the coefficient of its linear expansion, ΔT is the temperature difference across the thermoelectric leg, l is its length.

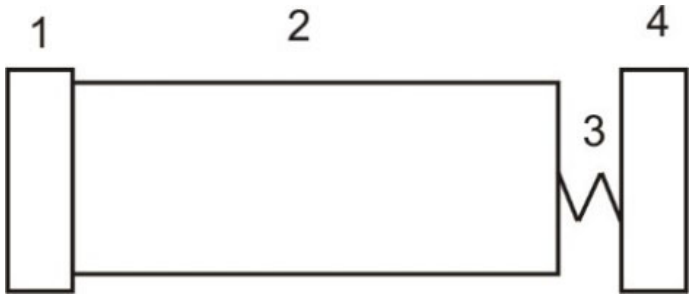

Fig. 1. Physical model of damping of a thermoelectric leg on the hot side,
1 – rigidly fastened ceramics on the cold side,
2 – thermoelectric leg with anti-diffusion layers and connections,
3 – elastic element; 4 – ceramics on the hot side.

Solving (1) and taking into account the generalized Hooke's law, we find the following expression for the residual mechanical stress that causes cracking of the thermoelectric leg in the presence of a damping element:

$$\sigma_f = \frac{kEl\alpha^T \Delta T}{\left(Eb^2 + kl\right)\left(1-\nu\right)} \quad (2)$$

where ν is the Poisson's ratio of the thermoelectric material.

It is clear that if the elastic element is perfectly compliant, then $k = 0$, the expansion is free and, therefore, there are no destructive stresses, and if we have a perfectly rigid fastening, then $k \to \infty$ and we get the traditional formula for the destructive stress of cracking under thermomechanical loads.

It is this stress that should be substituted into the Weibull distribution when calculating the probability of failure-free operation of a thermoelectric generator module in the presence of cyclic temperature effects. Taking into account the presence of a temperature gradient along the leg and approximately neglecting the temperature dependence of the thermal conductivity of the material, we obtain the following expression for the probability of failure-free operation of the module in the presence of cyclic temperature effects:

$$P\left(N_c\right) = \exp\left\{-\frac{2N_c N_L b^2 l}{m+1}\left(\frac{kEl\alpha^T \Delta T}{\left(Eb^2 + kl\right)\left(1-\nu\right)\sigma_0}\right)^m\right\}, \quad (3)$$

where N_c is the number of heating-cooling cycles, N_L is the number of legs in the module, m and σ_0 are the Weibull parameters of the thermoelectric material. And from formula (3) it is possible to determine such reliability indicators as the average cyclic stability and the percentage resource of cyclic stability γ. The results of these calculations are shown in Figs. 2, 3.

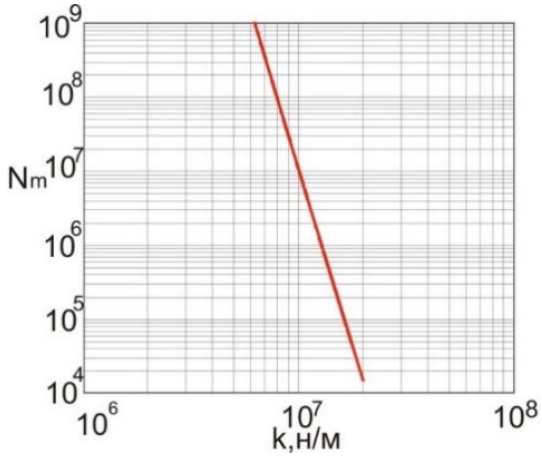

Fig. 2. Predicted dependence of the average cyclic stability of thermoelectric generator modules on the rigidity coefficient of the elastic element.

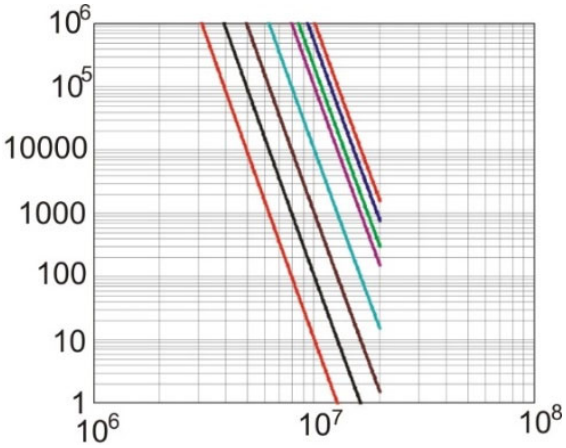

Fig. 3. Predicted dependence of gamma-percentage cyclic stability of thermoelectric generator modules on the rigidity coefficient of the elastic element in N/m. The lines from left to right correspond to values of γ equal to 0.999999, 0.99999, 0.9999, 0.9999, 0.99, 0.98, 0.95, 0.9.

In practice, stress relaxation is achieved either by proper selection of solders [2], or by installing special gaskets between the ceramic and copper connections [1].

It is evident from the figures that in going from absolutely rigid fastening of thermoelectric legs to fastening of albeit very high but finite rigidity, the predicted cyclic stability of thermoelectric energy converters grows very rapidly. This rapid growth is primarily due to the large value of the shape parameter *m.*

But this at first glance encouraging result is in fundamental contradiction with the approaches that have been formed and generally accepted within the disciplines of "Strength of Materials" and "Structural Mechanics". For these disciplines, the key characteristic of a material is its ultimate strength. And the Weibull probabilistic approach does not provide for such a characteristic. Therefore, within its framework, even at arbitrarily large thermomechanical stresses, there remains a probability, albeit very small, but significantly different from zero, of preserving the integrity of the thermoelectric leg. But from the basic principles of strength of materials and structural mechanics it follows that, regardless of the cyclic stability index, the “acceptable” rigidity coefficient of the damping element should be determined only by the requirement that the damped thermomechanical stresses do not exceed the

minimum cracking strength σ_f of the thermoelectric leg. And according to Griffiths' theory, it is defined as follows [3]:

$$\sigma_f = \frac{K_c}{\sqrt{\pi l}} \tag{4}$$

where K_c is the so-called load capacity of the thermoelectric leg material, l is the length of the thermoelectric leg along the temperature gradient. But in this case, it turns out that, for example, the rigidity coefficient of the damping element for a thermoelectric leg based on bismuth telluride in the form of a cube with an edge of 5 mm at a temperature difference of 150 °C should not exceed $1.17 \cdot 10^7$ n/m. And although this corresponds to the previous probabilistic estimates, it does not yet create a safety margin for crack resistance. There are no recommendations for safety margins in [3] for this case. For example, for a safety factor of 1.5, a rigidity coefficient value of no more than $7.636 \cdot 10^6$ N/m is required, and for a 10-fold safety factor – a rigidity coefficient value of no more than $1.106 \cdot 10^6$ N/m. To create a particularly large safety factor, such a damping element can be manufactured, for example, in the form of a miniature spring made of thin wire.

Its rigidity coefficient according to [3] is equal to

$$k = \frac{Ed^4}{16(1+\nu)D^3}, \tag{5}$$

where E and ν are Young's modulus and Poisson's ratio of the spring material, D and d are the diameters of the wire and the spring coil, respectively. From this formula it follows that acceptable damping of thermomechanical stresses is provided, for example, by a single-coil spring with a coil diameter greater than the wire diameter, made of aluminium wire with a diameter of no more than 5.6 mm, and damping with a 10-fold safety margin is provided by the same wire with a diameter of 3 mm with a coil diameter of 5 mm. The rigidity of the damping element is dramatically affected by the diameter of the wire; as a rule, such damping elements are made of wire of a significantly smaller diameter, so the condition of effective damping is well met. And the lower limit of the wire diameter is determined solely by the strength of the connection, and, therefore, the electrical connection of the thermocouples in the energy converter.

In this case, there is no need to worry about the "safe" value of thermal conductivity in terms of mechanical stability, and, consequently, the thermoelectric figure of merit and the efficiency of the thermoelectric material. In this case, the predicted cyclic stability in accordance with Fig. 2 will be no less than 10^7 cycles.

If we evaluate the rigidity coefficient of ceramics from the same point of view, taking into account its Young's modulus and thickness, it turns out to be equal to $2.7 \cdot 10^9$ N/m.

But elastic elements can also be made of rubber or polymers. Another way to reduce thermomechanical stress is to optimize the geometry of thermoelectric legs, but in itself it still does not provide a level that would guarantee acceptable cyclic stability of generator modules.

At first glance, the predicted cyclic stability and the allowable rigidity of the damping elements seem exaggerated. But it should be taken into account that in this case, the cyclic stability is considered relative to the destruction of thermoelectric legs. However, even without destruction, cyclic temperature effects can change the parameters of the thermoelectric energy converter due to such processes in the thermoelectric material that affect its thermoelectric characteristics. This issue was considered in detail in [4] for materials based on *Si-Ge*, but these processes are not the subject of this study.

The obtained results are at least qualitatively consistent with the results of [5], where it is shown that the highest predicted reliability is obtained when the hot end of the thermoelectric leg is not rigidly fastened, but is pressed, since pressing leads to additional compensation of thermomechanical stresses.

Let us now compare our calculations and estimates of the cyclic stability of thermoelectric energy converters with experimental data from other authors. In [6], accelerated cyclic tests of thermoelectric cooling modules were performed and their failures were analyzed during these tests. Studies have shown that the dependence of the relative number of failures on the number of heating-cooling cycles is described with satisfactory accuracy by Weibull curves. In this case, the shape parameters of the curves do not depend on temperature and are equal to 3.65877, and the scale parameters for temperature differences of 70 and 80 K are equal to 2324.91 and 1830.84, respectively. In this case, the presence of a temperature difference leads to deformation of the thermoelectric legs and bending of the ceramics. Therefore, failures are explained by cracking of the material due to the cyclic action of bending deformations. The probability of failures at the level of 10 % is observed after 1250 cycles at a temperature difference of 70 K and 1000 cycles at a temperature difference of 80 K. In the mentioned work there is no indication of the adoption by the manufacturers of modules of any special measures to reduce thermomechanical stresses.

But formula (3) can also be presented in the form of a Weibull distribution:

$$P\left(N_c\right)=\exp\left(-\frac{N_c}{N_0}\right). \tag{4}$$

The shape parameter of this distribution is 1, and the scale parameter is defined as:

$$N_0=\frac{m+1}{2N_L b^2 l}\left(\frac{\left(Eb^2+kl\right)\left(1-\nu\right)\sigma_0}{kEl\alpha^T\Delta T}\right)^m. \tag{5}$$

Let us introduce some effective temperature of activation of failures associated with the destruction of thermoelectric legs due to cracking, which will be equal to

$$T_{\text{efc}}=\frac{\left(Eb^2+kl\right)\left(1-\nu\right)\sigma_0}{kEl\alpha^T}\left(\frac{m+1}{2N_L b^2 l}\right)^{\frac{1}{m}}. \tag{6}$$

Then the scale parameter can be given as:

$$N_0=\left(\frac{T_{\text{efc}}}{\Delta T}\right)^m. \tag{7}$$

From this point of view, it seems appropriate to introduce a failure acceleration factor through a value inverse to the scale parameter:

$$Af=\left(\frac{\Delta T}{T_{\text{efc}}}\right)^m \tag{8}$$

This representation corresponds to the so-called Coffin-Manson model. According to the general definition of the acceleration factor in this model, it can be represented as follows:

$$AF = \left(\frac{\Delta T_{ALT}}{\Delta T_{nom}} \right)^m \tag{9}$$

where $\Delta T_{ALT}, \Delta T_{nom}$ are temperature differences during accelerated tests and in nominal mode, respectively.

Thus, it turns out that if the cyclic stability of thermoelectric modules is indeed determined by the processes of complete destruction of thermoelectric legs due to cracking under the influence of thermomechanical stresses, then its dependence on the temperature difference should directly characterize the Weibull distribution, which determines the "response" of the thermoelectric material to mechanical stress.

Now let us analyze to what extent such a preliminary conclusion is consistent with the available experimental data. In [6], the value of $m = 1.78914$ was obtained, while according to [7] it should be $m = 10$. Therefore, failures during accelerated cyclic endurance tests are mainly not caused by layer-by-layer cracking of thermoelectric legs as a whole under the influence of thermomechanical stresses. Moreover, the deviation from unity of the Weibull distribution shape parameter obtained during the tests indicates that failures in successive cycles are not independent. Thus, the observed failures depended significantly on the "prehistory" of the modules, which means that there is a gradual growth of fatigue cracks.

In this case, formula (5) can be written as follows:

$$P\left(N_c\right) = \exp\left\{ -\frac{2N_c^{\beta} N_L b^2 l}{m+1} \left[\frac{kEl\alpha^T \Delta T}{\left(Eb^2 + kl\right)\left(1-\nu\right)\sigma_0} \right]^m \right\}. \tag{10}$$

Therefore, taking into account the crack growth process, the scale parameter is now equal to:

$$N_0 = \left\{ \frac{m+1}{2N_L b^2 l} \left[\frac{\left(Eb^2 + kl\right)\left(1-\nu\right)\sigma_0}{kEl\alpha^T \Delta T} \right]^m \right\}^{\frac{1}{\beta}}, \tag{11}$$

and, hence, expression (9) for the acceleration factor takes the form:

$$AF = \left(\frac{\Delta T_{ALT}}{\Delta T_{nom}} \right)^{\frac{m}{\beta}}. \tag{12}$$

The modules studied in [6] contained 254 legs. This formula reflects the essence of the Coffin-Manson model, which is that the acceleration factor is the temperature difference of the legs connected in series. Considering that the studies were conducted without taking special measures to reduce thermomechanical stresses, assuming the dimensions of the legs to be $b = 3$ mm, $l = 2$ mm and considering σ_0 as a fitting parameter, we obtain that the studied modules at a temperature difference of 150 K could withstand about 106 cycles with a probability of 0.999, if they were given the opportunity to expand almost freely toward the hot side by placing the legs on this side on damping elastic elements with a rigidity coefficient of no more than 106 N/m. The corresponding calculated plot of cyclic stability is shown in Fig. 4.

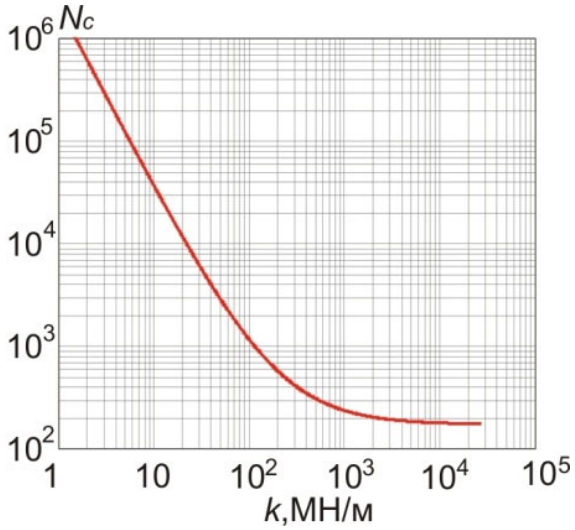

Fig. 4. The predicted cyclic stability of the module with a probability of failure-free operation equal to 0.999 depending on the rigidity coefficient of the elastic element in the presence of cyclic fatigue.

From the comparison of the plots in Figs. 3 and 4 it is seen that in the presence of cyclic fatigue the requirements for the compliance of the elastic element that damps thermomechanical stresses increase almost 10 times. On the other hand, based on the above estimate of ceramics rigidity, made on the basis of data on its Young's modulus and thickness, it can be stated that without additional stress damping this module with a probability of 0.99 will withstand only about 360 cycles at $\Delta T = 150$ °C. Taking into account the acceleration factor, we get that at $\Delta T = 80$ °C it should have withstood 1120 cycles with the same probability, but in reality it withstood 550 cycles. Such a coincidence of theory and experiment can be considered acceptable. Comparison of the prediction with the results of [6] allows us to conclude that in the manufacture of the tested modules special measures for damping thermomechanical stresses were not used. The above comparison of theory with experiment is only approximate and qualitative, since detailed data on the geometric parameters of the modules and the characteristics of the materials used are not provided in [6].

The discrepancy between the prediction results and the experimental data may also be due to the following factors:

1) The Weibull distribution was obtained empirically, its parameters are found exclusively experimentally and it only approximately describes the statistics of failure and cyclic fatigue, and no “first principles” that would allow obtaining more reasonable distributions exist today;

2) as a result, the Coffin-Manson power model for the acceleration factor in cyclic tests is only approximately valid;

3) when calculating the probability of failure-free operation of the module as a whole, we assume that during testing all legs are in the same conditions and fail with equal probability and independently;

4) as a result, we calculate the probability of failure of one leg and therefore assume that the ceramics is not subject to bending stresses and that it works purely on compression;

5) The presence of bending stresses in ceramics leads to the fact that the legs are in different conditions, and, therefore, the probabilities of their failure are different, as a result of which the presented theory ceases to be correct, which significantly complicates the calculations, since it requires determining the stresses in all the legs, and not just in one.

6) the traditional formula for the thermomechanical cracking stress of a layered material in the case of rigidly fastened thermoelectric leg is idealized.

The failure analysis showed first of all that despite the presence of significant shear thermomechanical stresses in the legs, no layer-by-layer cracking occurred. At the same time, bending stresses caused by the temperature gradient caused stress concentration in the most fragile parts of the soldered seams and solder failure. Long-term operation of the module in cyclic mode leads to the appearance of fatigue cracks, which gradually spread to the thermoelectric material. It was also found that moisture and material migration contribute to cracking to the greatest extent.

Thus, we see that the key means of increasing the cyclic stability of thermoelectric energy converters should be not only and not so much the search for hidden reserves in thermoelectric materials, but rather the leveling of thermomechanical stresses in thermoelectric legs due to design improvements of converters. Their developers quite often follow this path [7]. Incidentally, we note that in [1], the importance of damping thermomechanical stresses was emphasized in order to increase the cyclic stability of thermoelectric cooling modules, but specific requirements for damping elements of the design of thermoelectric energy converters were not determined.

Conclusions

1. By combining the strength of materials approach with the Weibull approach, a theory of damping of thermomechanical stresses in thermoelectric energy converters has been developed.

2. It has been established that the cyclic stability of thermoelectric energy converters increases significantly with increasing compliance of elastic damping elements. This increase is due to the large value of the Weibull shape parameter of the thermoelectric material.

3. It has been established that by properly selecting the rigidity coefficient, in particular the wire diameter and the diameter of the turns of the elastic damping elements in the form of cylindrical springs, it is possible to achieve complete compensation of the cracking stresses in thermoelectric legs caused by the temperature gradient, thereby dramatically increasing the cyclic stability of thermoelectric energy converters. As a result, there is no need to worry about the “safe” value of thermal conductivity from the point of view of thermomechanical cracking stresses, and, consequently, the thermoelectric figure of merit and efficiency of the thermoelectric material. An elastic element can be made, for example, in the form of a single-turn spring with an average diameter of 5 mm from aluminum wire with a diameter of no more than 3 mm. Since in practice a wire of a significantly smaller diameter is used, the lower limit of this diameter is determined not by the requirement for compensation of thermomechanical stresses, which is guaranteed to be performed with a significant reserve, but by its value, the minimum permissible from the point of view of the strength of connection.

4. The calculation results are in not only qualitative but also satisfactory quantitative agreement with the available experimental data.

5. The Coffin-Manson power model of the dependence of the acceleration factor in cyclic tests of thermoelectric energy converters on the temperature difference is substantiated. Its scope of applicability is the same as that of the Weibull approach, which relates the probability of maintaining the integrity of a thermoelectric leg to mechanical stresses therein. The Weibull parameters of a thermoelectric material are determined purely experimentally. The Coffin-Manson model is implemented in practice with acceptable accuracy.

References

1. Anatychuk L.I., Balaziuk V.M., Luste O.J., Malyshko V.V., Mikhalchenko V.P. (2003). On increasing the cyclic stability of thermoelectric cooling modules. *J. Thermoelectricity,* 4, 71 – 75.
2. Setty K., Sabbarayan G., Nguyen L. (2005). Power cycling reliability, failure analysis and acceleration factors of *Pb*-free solder joints. *Proceedings Electronic components and Technology Conference*, P. 907 – 915.
3. Pisarenko H.S., Kvitka O.L, Umanskyi E.S. (2004). *Strength of materials*: *manual*. Kyiv: Vyshcha shkola.
4. Sabo E.P. (2006). Mechanisms that determine the resource capabilities of thermoelectric converters. *J. Thermoelectricity,* 2, 59 – 70.
5. Karri N.K., Mo C. (2018). Reliable thermoelectric module design under opposing requirements from structural and thermoelectric considerations. *Journal of Electronic Materials,* 47, 3127 – 3135.
6. Park W., Barako M.T., Marconnet A.M., Asheghi M., Goodson K.E. (2012). Effect of thermal cycling on commercial thermoelectric modules. *13th IEEE ITHERM Conference*. (San Diego, CA, USA, 30 May 2012 – 01 June 2012).
7. Wereszczak A.A., Case E.D. (2015). *Mechanical response of thermoelectric materials.* Oak Ridge, TN: ORNL/TM-2015/227, U.S. Department of Energy.
8. *US Patent No 4011104* (1977). A. Basilius. Thermoelectric system.

Submitted: 10.10.2023.

Горський П.В., *док. фіз.-мат. наук* [1,2]

[1] Інститут термоелектрики НАН та МОН України,
вул. Науки, 1, Чернівці, 58029, Україна;
[2] Чернівецький національний університет імені Юрія Федьковича,
вул. Коцюбинського 2, Чернівці, 58012, Україна
e-mail: gena.grim@gmail.com

ДЕМПФУВАННЯ ТЕРМОМЕХАНІЧНИХ НАПРУЖЕНЬ ЯК ЗАСІБ ПІДВИЩЕННЯ ЦИКЛІЧНОЇ СТІЙКОСТІ ТЕРМОЕЛЕКТРИЧНИХ ПЕРЕТВОРЮВАЧІВ ЕНЕРГІЇ

На основі поєднання методів опору матеріалів з підходом Вейбулла, визначено вимоги до коефіцієнтів жорсткості демпфуючих елементів, які можна використати для зниження термомеханічних напружень у термоелектричних гілках з метою підвищення циклічної стійкості термоелектричних перетворювачів енергії. Обґрунтовано степеневу модель Коффіна-Менсона для залежності фактору прискорення за наявності циклічних температурних впливів від перепаду температури. Результати розрахунків знаходяться не лише у якісній, а й у задовільній кількісній згоді з експериментальними даними.

Ключові слова: циклічна стійкість, термоелектричний перетворювач енергії, термомеханічні напруження, демпфування, опір матеріалів, підхід Вейбулла, міцність на розтріскування, жорсткість пружного елемента.

Література

1. Анатичук Л.І., Балазюк В.М., Лусте О.Я., Малишко В.В., Михальченко В.П. Про підвищення циклічної стійкості термоелектричних модулів охолодження. // Термоелектрика. – 2003. – № 4. – С. 71 – 75.
2. Setty K., Sabbarayan G., Nguyen L. (2005). Power cycling reliability, failure analysis and acceleration factors of *Pb*-free solder joints. *Proceedings Electronic components and Technology Conference*, P. 907 – 915.
3. Писаренко Г.С., Квітка О.Л., Уманський Е.С. *Опір матеріалів*: підручник / за ред. Г.С. Писаренка. К.: Вища школа, 2004, 655 с.
4. Сабо Є.П. Механізми, що визначають ресурсні можливості термоелектричних перетворювачів. // Термоелектрика. – 2006. – № 2. – С. 59 – 70.
5. Karri N.K., Mo C. (2018). Reliable thermoelectric module design under opposing requirements from structural and thermoelectric considerations. *Journal of Electronic Materials,* 47, 3127 – 3135.
6. Park W., Barako M.T., Marconnet A.M., Asheghi M., Goodson K.E. (2012). Effect of thermal cycling on commercial thermoelectric modules. *13th IEEE ITHERM Conference*. (San Diego, CA, USA, 30 May 2012 – 01 June 2012).
7. Wereszczak A.A., Case E.D. (2015). *Mechanical response of thermoelectric materials.* Oak Ridge, TN: ORNL/TM-2015/227, U.S. Department of Energy.
8. *US Patent No 4011104* (1977). A. Basilius. Thermoelectric system.

Надійшла до редакції: 10.10.2023.

V.V. Lysko

V.V. Lysko, *Cand.Sc (Phys-Math)* [1,2]
O.V. Nitsovich, *Cand.Sc (Phys-Math)* [1,2]

[1]Institute of Thermoelectricity of the NAS
and MES of Ukraine,
1, Nauky str., Chernivtsi, 58029, Ukraine;
[2]Yuriy Fedkovych Chernivtsi National University,
2, Kotsiubynsky str., Chernivtsi, 58012, Ukraine
e-mail: anatych@gmail.com

O.V. Nitsovich

COMPUTER OPTIMIZATION OF THE VERTICAL ZONE MELTING METHOD FOR MANUFACTURING FLAT INGOTS OF THERMOELECTRIC MATERIALS BASED ON Bi_2Te_3

The results of computer simulation of the process of manufacturing flat ingots of thermoelectric materials based on Bi_2Te_3 by the method of vertical zone melting are presented. The dependences of the crystallization front shape on the geometric dimensions of the heater and coolers, their temperatures, speed of movement and other process parameters are given. Multifactor computer optimization of process modes and equipment design for growing flat ingots of thermoelectric materials based on Bi_2Te_3 is carried out. Bibl. 20, Figs. 14.

Key words: simulation, vertical zone melting, thermoelectric material, bismuth telluride.

Introduction

Thermoelectricity is finding more and more practical applications in various industries. According to estimates [1], the thermoelectric product market today is more than 800 million US dollars and is growing annually by approximately 9 %. More than 55 million thermoelectric modules are produced. At the same time, thermoelectric materials based on *Bi-Te* remain the main ones in production.

Self-contained thermoelectric power sources operating from the heat of combustion of any fuel are especially promising and can be used as autonomous low-power power sources for powering equipment for various purposes. They have a long service life, are highly reliable and resistant to climatic and impact loads, are universal, silent in operation and easy to use. Scientists and engineers of many countries are actively working on the creation of such sources. Thermoelectric generators with an electric power of 2 – 20 W designed for charging mobile phones, MP3 players, navigators during trips and tourist trips were developed by a number of foreign companies (TES, Power Pot, Biolite) [2 – 7]. Thermoelectric generators have also been developed, the operation of which is based on the use of heat from solid fuel furnaces [8 – 10]. They are serially produced by a number of enterprises [10 – 12]. At the same time, the main obstacle for their widespread practical use is a relatively high cost, primarily due to the high cost of the thermoelectric material from which they are made. Therefore, a lot of attention is paid to the improvement of methods of obtaining thermoelectric materials based on *Bi-Te* [13 – 18].

One of the possibilities for reducing the cost of the material and decreasing the technological defects when cutting ingots into thermoelements is the production of ingots in the form of flat rods. The creation of a technology for the production of such ingots requires multi-parameter optimization of the

controlled parameters of the growing process.

The work [19] shows the results of creating a computer model of the process of manufacturing flat ingots of thermoelectric materials by the method of vertical zone melting, which is one of the most common industrial methods of growing polycrystalline thermoelectric materials based on *Bi-Te*.

The purpose of this work is multifactorial computer optimization of technological modes and design of equipment for the production of flat ingots of thermoelectric materials based on Bi_2Te_3.

1. Physical, mathematical and computer models of vertical zone melting process

The quality of thermoelectric material obtained by vertical zone melting is affected by various factors, such as: impurity distribution coefficient; length of the molten zone; zone movement speed; degree of mixing of the molten zone; heater temperature, etc. The main technological characteristic of growth is the curvature of the crystallization front, determined by the values of the radial and axial temperature gradients in the ingot during growth.

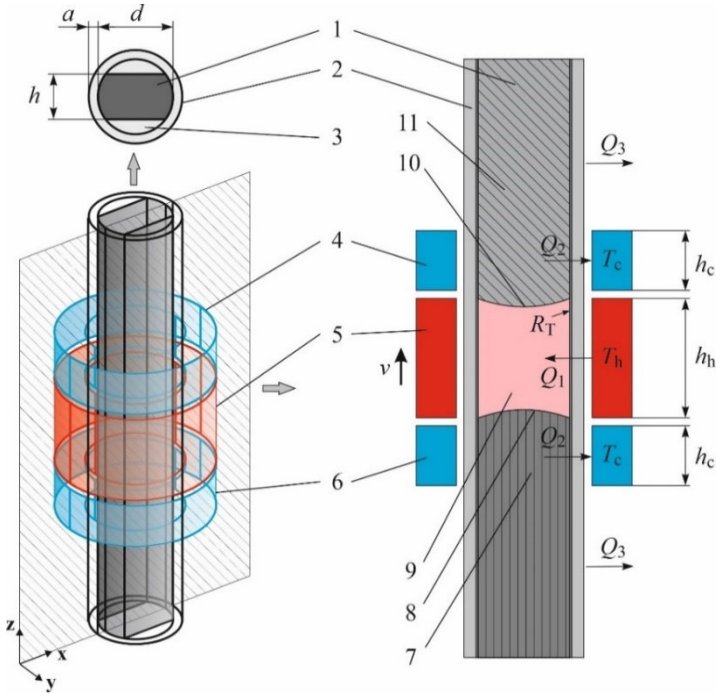

Fig. 1. Physical model of growing thermoelectric materials by vertical zone melting: 1 – thermoelectric material; 2 – container; 3 – quartz inserts; 4, 6 – coolers; 5 – heater; 7 –material in solid phase (structurally oriented crystal); 8 – crystallization front; 9 –melt zone; 10 – melt front; 11 – material in solid phase (polycrystal).

The shape of the crystallization front can be convex in the liquid phase, flat or concave in the solid phase. The most favorable for growing single crystals with a low density of defects is a flat crystallization front. To create a computer model of the process of growing flat ingots of thermoelectric materials based on Bi_2Te_3, which allows us to study the dependence of the crystallization front shape on various technological parameters, a physical model was constructed, shown in Fig. 1. The figure shows a fragment of an ingot, which includes polycrystalline material 11, a molten zone 9 and a single crystal 7. The ingot is placed in a container 2. With the help of a heater 5 and a system of coolers 4 and 6, a molten zone 9 is formed, which, moving together with the heater along the ingot, ensures the melting of

the polycrystal and the crystallization of the melt below the boundary 8, which is called the crystallization front.

The COMSOL Multiphysics package of application programs [20] was used for computer simulation of the process of growing Bi_2Te_3 thermoelectric material.

The temperature distribution in the sample under study consists of the solution of the differential equation of thermal conductivity, supplemented by the dependencies of the physical properties of the material under study, as a function of the phase state at a given point at a given temperature:

$$\rho\, C_p \frac{\partial T}{\partial t} + \rho\, C_p u\, \nabla T + \nabla q = Q, \tag{1}$$

$$q = -\kappa \nabla T, \tag{2}$$

$$\rho = \theta \rho_{phase1} + (1-\theta)\rho_{phase2}, \tag{3}$$

$$C_p = \frac{1}{2}\left(\theta \rho_{phase1}\, C_{p_{phase1}} + (1-\theta)\rho_{phase2}\, C_{p_{phase2}}\right) + L\frac{d\alpha_m}{dT}, \tag{4}$$

$$\alpha_m = \frac{1}{2} \cdot \frac{(1-\theta)\rho_{phase2} - \theta\rho_{phase1}}{\theta\rho_{phase1} + (1-\theta)\rho_{phase2}}, \tag{5}$$

$$\kappa = \theta \kappa_{phase1} + (1-\theta)\kappa_{phase2}, \tag{6}$$

where ρ is the density, C_p is the heat capacity of the material, κ is the thermal conductivity, u is the velocity of the medium which is zero in the problem under study, T is the temperature, θ is the phase ratio at a given temperature, α_m is the mass ratio between the phases, L is the latent heat of the phase transition, Q is the external heat flow. The $phase1$ and $phase2$ indices indicate which phase the properties belong to, the solid phase or the liquid phase, respectively.

When modeling zone melting, a stationary mode was considered, i.e. the movement of the thermal unit, including the heater and coolers, was not taken into account. It is known that bismuth telluride-based crystals are grown at a rate of 1.5 – 2.5 cm/hour. Having estimated the time required for the system to achieve thermal equilibrium, it was determined that during this time the heater would shift less than 0.2 mm. Heat loss in this area will be two orders of magnitude less than the heat transmitted from the thermal unit to the ampoule. Thus, these losses can be neglected in computer simulations, as they will have little effect on the overall temperature distribution.

For calculations in the created computer model, the geometric dimensions of the system elements, the temperatures of the heater and coolers, the liquidus and solidus temperatures of the thermoelectric material based on Bi_2Te_3, as well as the temperature dependences of the properties of the grown material are specified.

2. Results of computer optimization

Fig. 2 shows an example of the crystallization front shape obtained by simulation using the method described above for the case of a flat Bi_2Te_3 ingot with a thickness of 12 mm, a container diameter of d = 24 mm, a heater height of h_h = 72 mm, and a cooler height of h_c = 24 mm (the heater height is 3d, the cooler height is 1d), a heater temperature T_h = 760 °C, and a cooler temperature T_c = 30 °C.

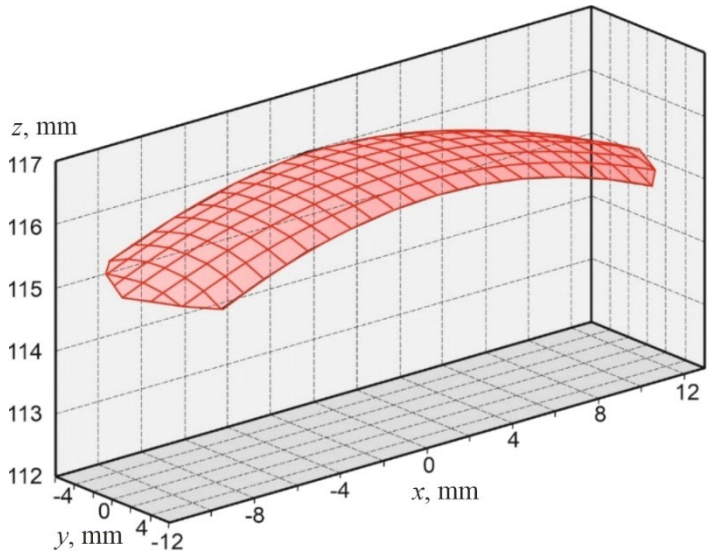

Fig. 2. Example of the shape of crystallization front (for a flat ingot with a thickness h = 12 mm, container diameter d = 24 mm, heater height h_h = 72 mm and cooler height h_c = 24 mm, heater temperature T_h = 760°C).

The shape of crystallization front in sections YZ ($x = 0$) and XZ ($y = 0$) at different sizes of the ingot, heater, and coolers, as well as at different temperatures of the heater, is shown in Figs. 3 – 13.

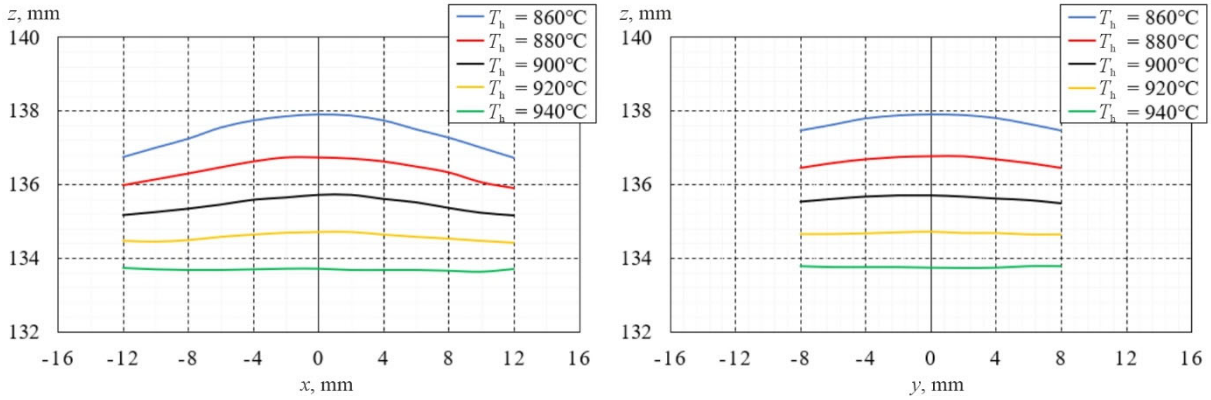

Fig. 3. The shape of crystallization front in sections XZ (y = 0) and YZ (x = 0) for different temperatures of the heater T_h (with ingot thickness h = 16 mm, container diameter d = 24 mm, heater height h_h = 1d = 24 mm, cooler height h_c = 1d = 24 mm).

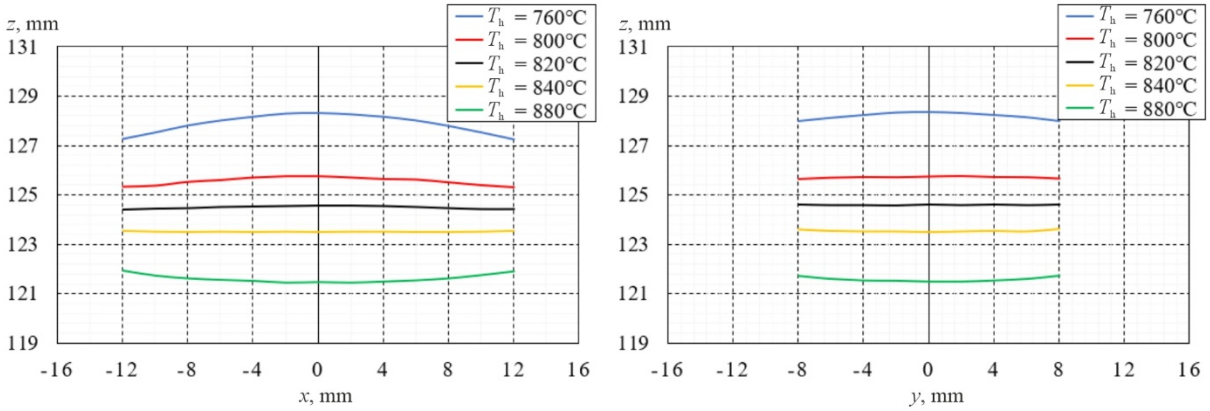

Fig. 4. The shape of crystallization front in sections XZ (y = 0) and YZ (x = 0) for different temperatures of the heater T_h (with ingot thickness h = 16 mm, container diameter d = 24 mm, heater height h_h = 2d = 48 mm, cooler height h_c = 1d = 24 mm).

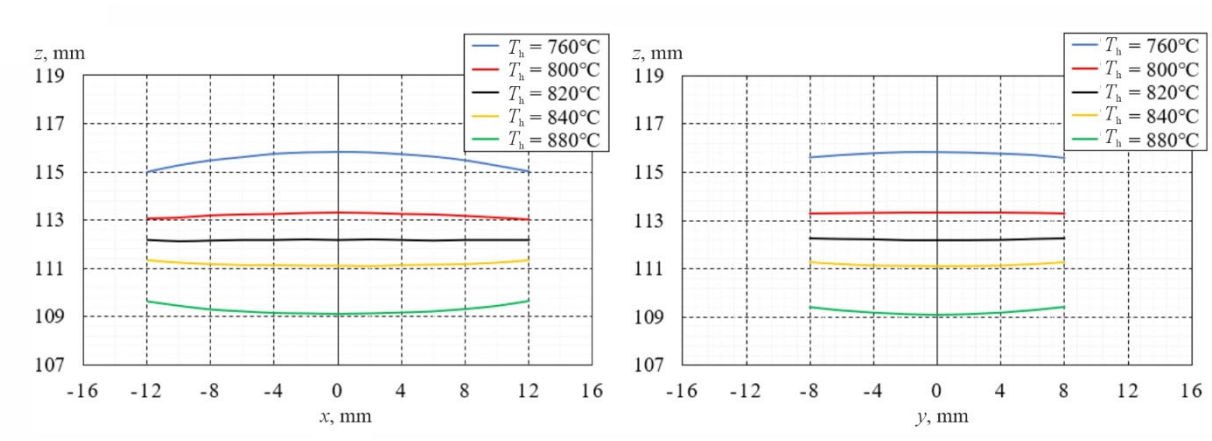

Fig. 5. The shape of crystallization front in sections XZ (y = 0) and YZ (x = 0) for different temperatures of the heater T_h (with ingot thickness h = 16 mm, container diameter d = 24 mm, heater height $h_h = 3d = 72$ mm, cooler height $h_c = 1d = 24$ mm).

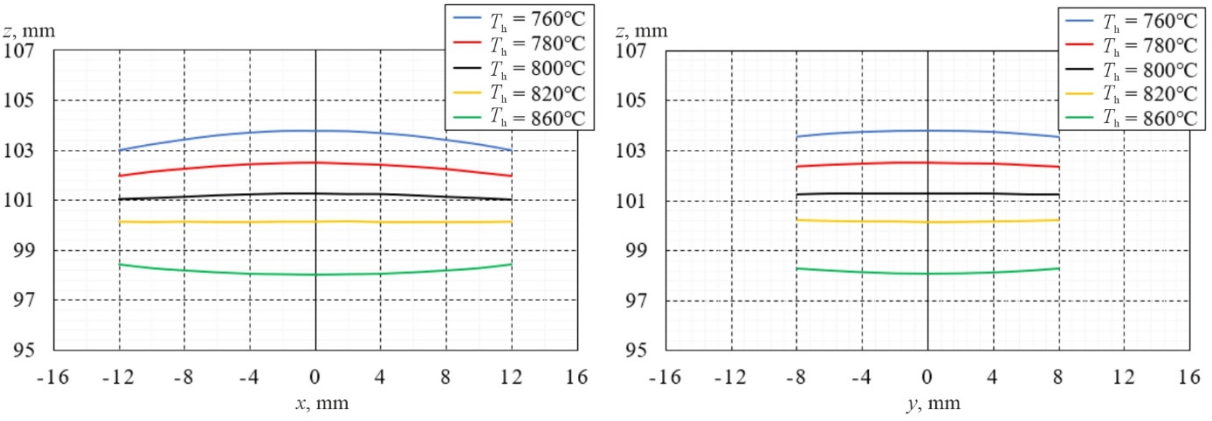

Fig. 6. The shape of crystallization front in sections XZ (y = 0) and YZ (x = 0) for different temperatures of the heater T_h (with ingot thickness h = 16 mm, container diameter d = 24 mm, heater height $h_h = 4d = 96$ mm, cooler height $h_c = 1d = 24$ mm).

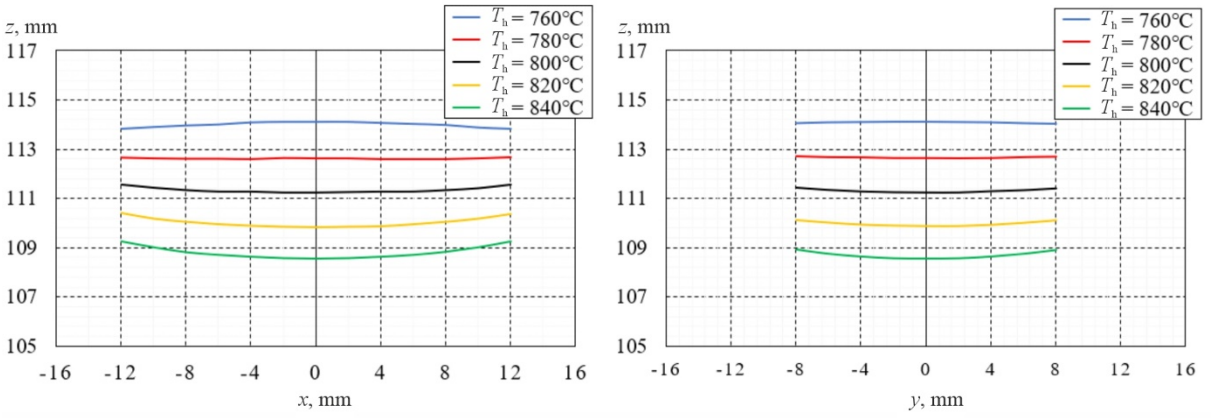

Fig. 7. The shape of crystallization front in sections XZ (y = 0) and YZ (x = 0) for different heater temperatures T_h (with ingot thickness h = 16 mm, container diameter d = 24 mm, heater height $h_h = 3d = 72$ mm, cooler height $h_c = 0.25d = 6$ mm).

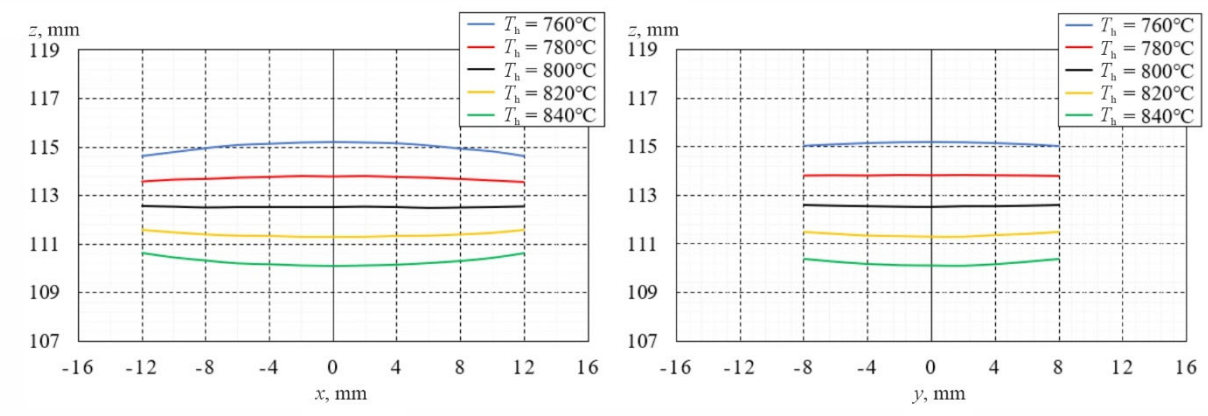

Fig. 8. The shape of crystallization front in sections XZ (y = 0) and YZ (x = 0) for different heater temperatures T_h (with ingot thickness h = 16 mm, container diameter d = 24 mm, heater height h_h = 3d = 72 mm, cooler height h_c = 0.5d = 12 mm).

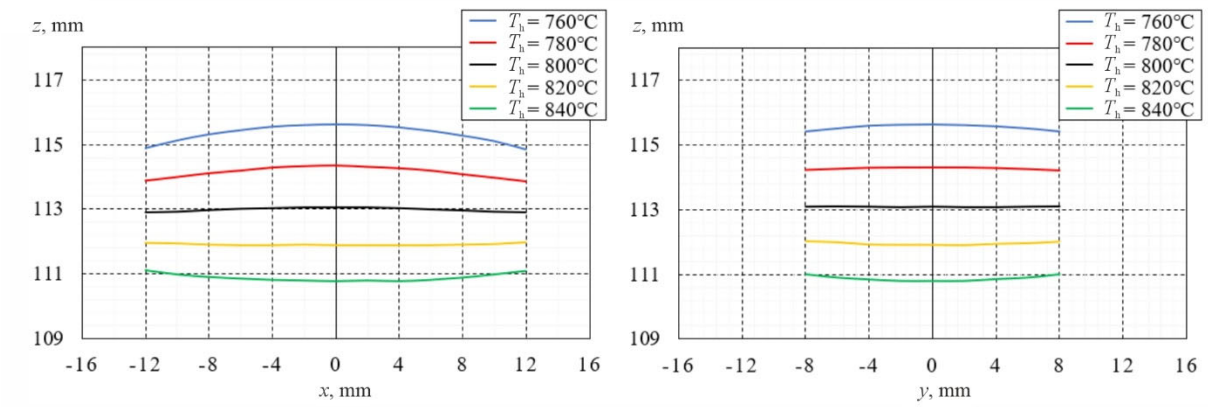

Fig. 9. The shape of crystallization front in sections XZ (y = 0) and YZ (x = 0) for different heater temperatures T_h (with ingot thickness h = 16 mm, container diameter d = 24 mm, heater height h_h = 3d = 72 mm, cooler height h_c = 0.75d = 18 mm).

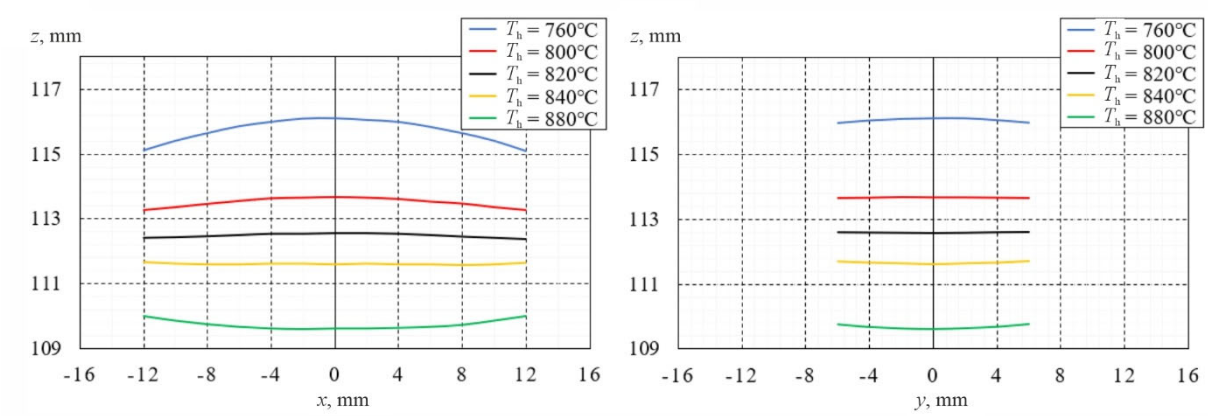

Fig. 10. The shape of crystallization front in sections XZ (y = 0) and YZ (x = 0) for different heater temperatures T_h (with ingot thickness h = 12 mm, container diameter d = 24 mm, heater height h_h = 3d = 72 mm, cooler height h_c = 1d = 24 mm).

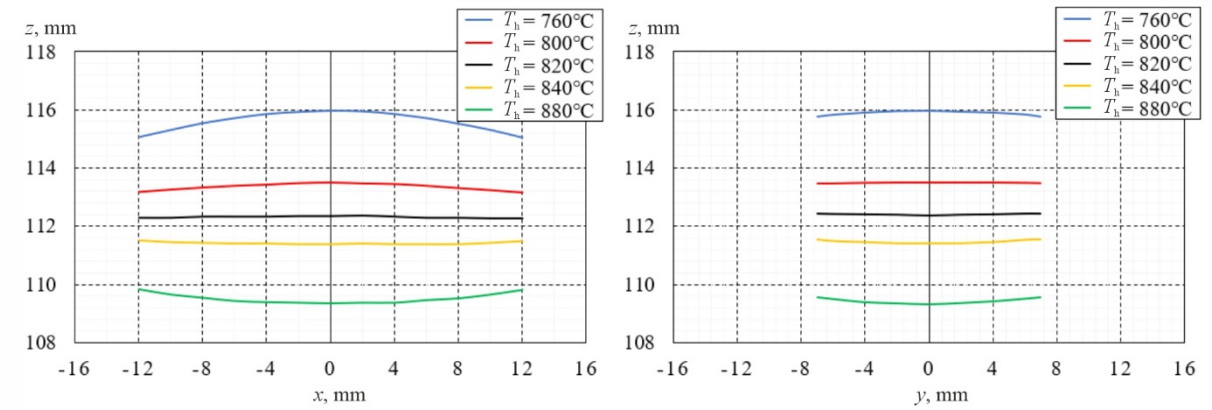

Fig. 11. The shape of crystallization front in sections XZ (y = 0) and YZ (x = 0) for different heater temperatures T_h (with ingot thickness h = 14 mm, container diameter d = 24 mm, heater height h_h = 3d = 72 mm, cooler height h_c = 1d = 24 mm).

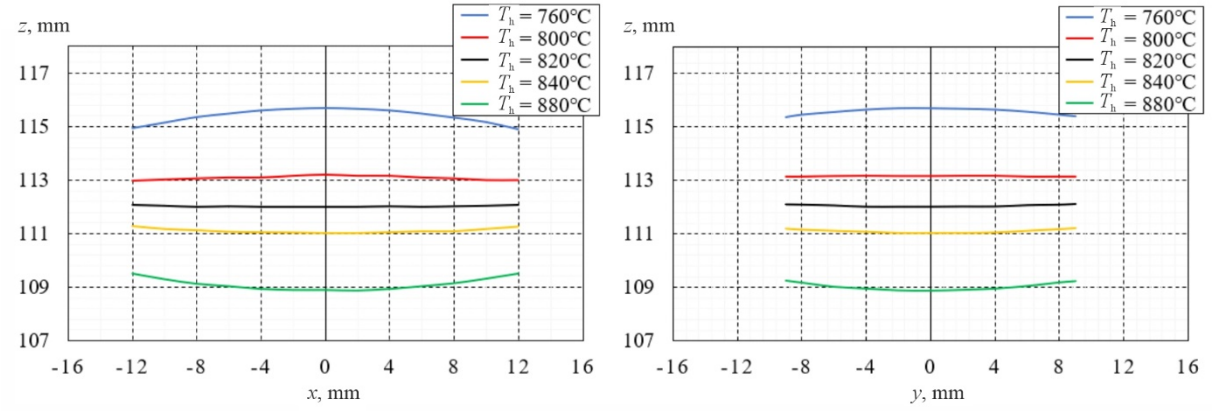

Fig. 12. The shape of crystallization front in sectionsx XZ (y = 0) and YZ (x = 0) for different heater temperatures T_h (with ingot thickness h = 18 mm, container diameter d = 24 mm, heater height h_h = 3d = 72 mm, cooler height h_c = 1d = 24 mm).

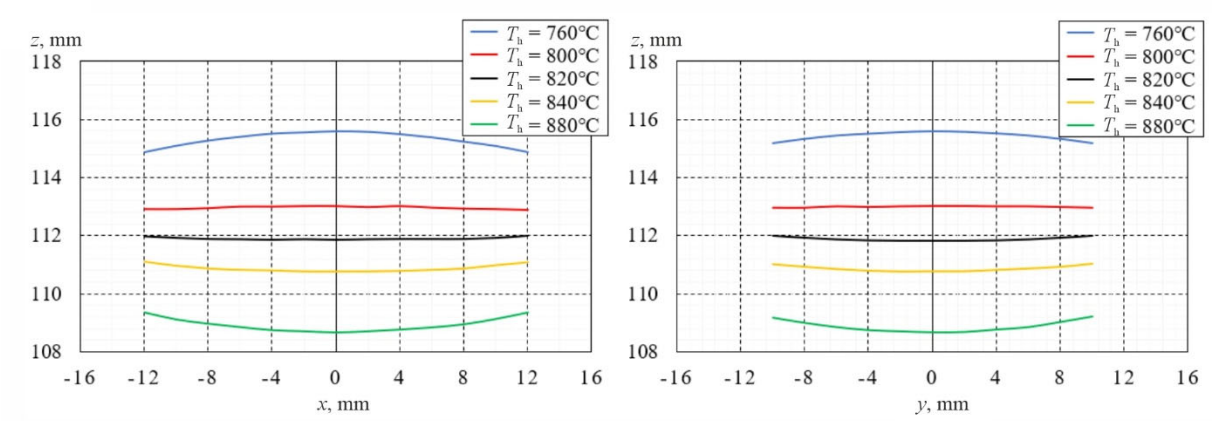

Fig. 13. The shape of crystallization front in sections XZ (y = 0) and YZ (x = 0) for different heater temperatures T_h (with ingot thickness h = 20 mm, container diameter d = 24 mm, heater height h_h = 3d = 72 mm, cooler height h_c = 1d = 24 mm).

As can be seen from Figs. 3 – 13, with an increase in the height of the heater, for a given temperature, the crystallization front is leveled. It can also be seen that at $h_h = 3d$ and $4d$, the crystallization front is flat at the same heater temperature of 820°C, which is optimal for growing a given material, and also conclude that $h_h = 3d$ is the optimal heater parameter. In this case, the optimal height of the coolers is $h_c = 1d$.

Also, based on the simulation results, the yield percentage of material with an improved structure was estimated when using the proposed technology for growing flat ingots depending on the thickness of the ingot h (Fig. 14). Coefficient K is the ratio of the percentage of material with an improved structure for a flat ingot to the percentage of material with an improved structure for a round ingot with the same diameter of the container, growing conditions and the criterion for evaluating the uniformity of the crystallization front.

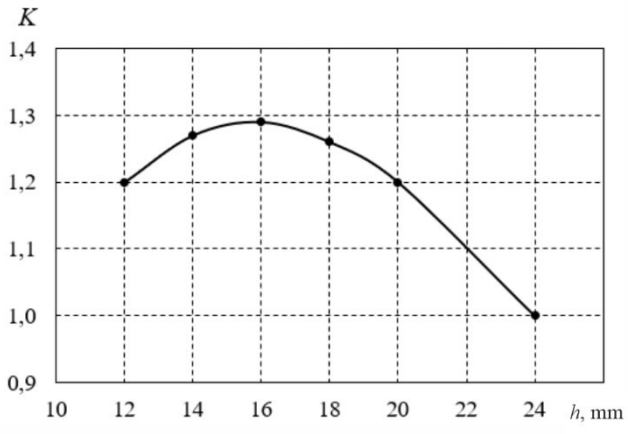

Fig. 14. Coefficient of increase in the yield of material with improved structure when growing flat ingots depending on ingot thickness h.

Therefore, when growing material in the form of flat ingots, the percentage of yield of material with an improved structure is 1.2 – 1.3 times higher compared to growing round ingots in a container of the same diameter. At the same time, the optimal thickness of the ingot for a container with a diameter of 24 mm is a thickness of 15 – 16 mm.

Conclusions

1. The results of computer simulation of the process of manufacturing flat ingots of thermoelectric materials based on Bi_2Te_3 by the method of vertical zone melting are presented. The dependence of the shape of the crystallization front on the geometric dimensions of the heater and coolers, their temperatures, movement speed, and other technological parameters is given.
2. The optimal container geometries, sizes of the heater and coolers, and their temperatures have been determined. It has been shown that with an increase in the heater height at a given temperature, the crystallization front is leveled. It has been established that at a heater temperature of 820 °C and coolers of 30 °C, the optimal heater height is equal to three container diameters, and the optimal cooler height is equal to one container diameter.
3. It has been shown that growing thermoelectric materials in the form of flat ingots allows increasing the percentage of yield of material with an improved structure by 1.2 – 1.3 times compared to round ingots of the same container diameter.

References

1. *Thermoelectric Modules Market – Global Industry Analysis and Forecast* (2023-2029) / MMR PVT. Ltd, 2023. https://www.maximizemarketresearch.com/market-report/thermoelectric-modules-mar-ket/2622/.
2. *Pat. CN216524233U*. Thermoelectric water kettle water level detection circuit. Published 13.05.2022.
3. *Pat. CN105167597B*. A kind of thermo-electric generation hot-water bottle. Published 02.01.2018.
4. *Pat. CN209391675U*. A kind of heating vessel. Published. 17.09.2019.
5. *Pat. CN208806757U*. Thermo-electric generation wild cooker. Published. 30.04.2019.
6. *Pat. GB2605345A*. Cooking vessel. Published 28.09.2022.
7. L.I. Anatychuk, V.V. Lysko. (2023). On the design of a trench thermoelectric source of heat and electricity. *J. Thermoelectricity*, 1, 93 – 100.
8. Montecucco A., Siviter J. & Knox A.R. (2017). Combined heat and power system for stoves with thermoelectric generators. *Applied Energy*, Elsevier, vol. 185(P2), 1336-1342. DOI: 10.1016/j.apenergy.2015.10.132.
9. Żołądek Maciej, Papis Karolina, Kuś Jakub, Zając Michal, Figaj Rafał and Rudykh Kyrylo. (2020). The use of thermoelectric generators with home stoves. *E3S Web Conf*., 173 (2020) 03005. DOI: https://doi.org/10.1051/e3sconf/202017303005.
10. *Wood stove thermoelectric generator rabbit ears* [Electronic resource] – Retrieved from: https://thermoelectric-generator.com/product/wood-stove-thermoelectric-generator-rabbit-ears/.
11. *45-watt teg generator for wood stoves with air-cooling* [Electronic resource] – Retrieved from: https://www.tegmart.com/thermoelectric-generators/wood-stove-air-cooled-45w-teg.
12. *Thermoelectric power generator for fireplace heater* [Electronic resource] – Retrieved from: http://www.thermonamic.com/pro_view.asp?id=828.
13. Cao T., Shi X.L., Li M., Hu B., Chen W., Liu W. Di, Lyu W., MacLeod J., Chen Z.G. (2023). Advances in bismuth-telluride-based thermoelectric devices: progress and challenges. *EScience,* 3(3), Article 100122. https://doi.org/0.1016/j.esci.2023.100122.
14. Goldsmid H.J. (2014). Bismuth telluride and its alloys as materials for thermoelectric generation. *Materials,* 7,2577-2592. https://doi.org/10.3390/ma7042577.
15. Tritt T. (2000). *Recent trends in thermoelectric materials research, Part Two* (Semiconductors and Semimetals, Volume 70). Academic Press. ISBN-13: 978-0127521794.
16. Lysko V.V., Tudoroi P.F. (2019). Computer simulation of extrusion process of Bi_2Te_3 based tape thermoelectric materials. *J. Thermoelectricity,* 2, 58 – 65.
17. Anatychuk L.I., Lysko V.V. (2020). *Thermoelectricity: Vol. 5. Metrology of thermoelectric materials.* Chernivtsi: Bukrek. ISBN 978-617-7770-40-3.
18. Anatychuk L.I., Havrylyuk N.V., Lysko V.V. (2012). Methods and equipment for quality control of thermoelectric materials. *Journal of Electronic Materials,* 41 (6), 1680 – 1685. https://doi.org/10.1007/s11664-012-1973-1.
19. Lysko V.V., Nitsovich O.V. (2023). Computer simulation of the process of manufacturing flat ingots of thermoelectric materials based on Bi_2Te_3 by vertical zone melting method. *J. Thermoelectricity*, 3, 18 – 25.
20. COMSOL Multiphysics, v.6.0.www.comsol.com. COMSOL AB, Stockholm, Sweden, 2021.

Submitted: 08.11.2023.

Лисько В.В., *канд. фіз.-мат. наук* [1,2]
Ніцович О.В., *канд. фіз.-мат. наук* [1]

[1] Інститут термоелектрики НАН та МОН України,
вул. Науки, 1, Чернівці, 58029, Україна;
[2] Чернівецький національний університет імені Юрія Федьковича,
вул. Коцюбинського 2, Чернівці, 58012, Україна
e-mail: anatych@gmail.com

КОМП'ЮТЕРНА ОПТИМІЗАЦІЯ МЕТОДУ ВЕРТИКАЛЬНОЇ ЗОННОЇ ПЛАВКИ ДЛЯ ВИГОТОВЛЕННЯ ПЛОСКИХ ЗЛИТКІВ ТЕРМОЕЛЕКТРИЧНИХ МАТЕРІАЛІВ НА ОСНОВІ Bi_2Te_3

Представлено результати комп'ютерного моделювання процесу виготовлення плоских злитків термоелектричних матеріалів на основі Bi_2Te_3 методом вертикальної зонної плавки. Наведено залежності форми фронту кристалізації від геометричних розмірів нагрівника та холодильників, їх температур, швидкості руху та інших технологічних параметрів. Проведено багатофакторну комп'ютерну оптимізацію технологічних режимів та конструкції обладнання для вирощування плоских злитків термоелектричних матеріалів на основі Bi_2Te_3. Бібл. 20, рис. 14.

Ключові слова: моделювання, вертикальна зонна плавка, термоелектричний матеріал, телурид вісмуту.

Література

1. *Thermoelectric Modules Market – Global Industry Analysis and Forecast* (2023-2029) / MMR PVT. Ltd, 2023. https://www.maximizemarketresearch.com/market-report/thermoelectric-modules-mar-ket/2622/.
2. *Pat. CN216524233U*. Thermoelectric water kettle water level detection circuit. Published 13.05.2022.
3. *Pat. CN105167597B*. A kind of thermo-electric generation hot-water bottle. Published 02.01.2018.
4. *Pat. CN209391675U*. A kind of heating vessel. Published. 17.09.2019.
5. *Pat. CN208806757U*. Thermo-electric generation wild cooker. Published. 30.04.2019.
6. *Pat. GB2605345A*. Cooking vessel. Published 28.09.2022.
7. L.I. Anatychuk, V.V. Lysko. (2023). On the design of a trench thermoelectric source of heat and electricity. *J. Thermoelectricity*, 1, 93 – 100.
8. Montecucco A., Siviter J. & Knox A.R. (2017). Combined heat and power system for stoves with thermoelectric generators. *Applied Energy*, Elsevier, vol. 185(P2), 1336-1342. DOI: 10.1016/j.apenergy.2015.10.132.
9. Żołądek Maciej, Papis Karolina, Kuś Jakub, Zając Michal, Figaj Rafał and Rudykh Kyrylo. (2020). The use of thermoelectric generators with home stoves. *E3S Web Conf.*, 173 (2020) 03005. DOI: https://doi.org/10.1051/e3sconf/202017303005.
10. *Wood stove thermoelectric generator rabbit ears* [Electronic resource] – Retrieved from: https://thermoelectric-generator.com/product/wood-stove-thermoelectric-generator-rabbit-ears/.

11. *45-watt teg generator for wood stoves with air-cooling* [Electronic resource] – Retrieved from: https://www.tegmart.com/thermoelectric-generators/wood-stove-air-cooled-45w-teg.
12. *Thermoelectric power generator for fireplace heater* [Electronic resource] – Retrieved from: http://www.thermonamic.com/pro_view.asp?id=828.
13. Cao T., Shi X.L., Li M., Hu B., Chen W., Liu W. Di, Lyu W., MacLeod J., Chen Z.G. (2023). Advances in bismuth-telluride-based thermoelectric devices: progress and challenges. *EScience,* 3(3), Article 100122. https://doi.org/0.1016/j.esci.2023.100122.
14. Goldsmid H.J. (2014). Bismuth telluride and its alloys as materials for thermoelectric generation. *Materials,* 7,2577-2592. https://doi.org/10.3390/ma7042577.
15. Tritt T. (2000). *Recent trends in thermoelectric materials research, Part Two* (Semiconductors and Semimetals, Volume 70). Academic Press. ISBN-13: 978-0127521794.
16. Lysko V.V., Tudoroi P.F. (2019). Computer simulation of extrusion process of Bi_2Te_3 based tape thermoelectric materials. *J. Thermoelectricity,* 2, 58 – 65.
17. Anatychuk L.I., Lysko V.V. (2020). *Thermoelectricity: Vol. 5. Metrology of thermoelectric materials.* Chernivtsi: Bukrek. ISBN 978-617-7770-40-3.
18. Anatychuk L.I., Havrylyuk N.V., Lysko V.V. (2012). Methods and equipment for quality control of thermoelectric materials. *Journal of Electronic Materials,* 41 (6), 1680 – 1685. https://doi.org/10.1007/s11664-012-1973-1.
19. Lysko V.V., Nitsovich O.V. (2023). Computer simulation of the process of manufacturing flat ingots of thermoelectric materials based on Bi_2Te_3 by vertical zone melting method. *J. Thermoelectricity*, 3, 18 – 25.
20. COMSOL Multiphysics, v.6.0.www.comsol.com. COMSOL AB, Stockholm, Sweden, 2021.

Надійшла до редакції: 08.11.2023.

L.I. Anatychuk, *Acad. NAS Ukraine* [1,2]
V.V. Lysko, *Cand. Sc (Phys-Math)* [1,2]
K.I. Strusovskyi [2]

[1]Institute of Thermoelectricity of the NAS
and MES of Ukraine,
1, Nauky str., Chernivtsi, 58029, Ukraine;
[2]Yuriy Fedkovych Chernivtsi National University,
2, Kotsiubynsky str., Chernivtsi, 58012, Ukraine
e-mail: anatych@gmail.com

COMPUTER RESEARCH ON THE ACCURACY OF PROBE METHOD FOR MEASURING THE ELECTRICAL CONTACT RESISTANCE OF "METAL – THERMOELECTRIC MATERIAL"

Physical and computer models have been created to study possible errors in measuring the electrical contact resistance of "metal-thermoelectric material" using the probe method. By means of computer simulation, the distributions of electric potential and temperature in the studied physical model were obtained for different sample geometries, current through the sample, and contact electrical resistance. It has been found that deviations from isothermal conditions in the sample, caused by the influence of the Joule and Peltier effects, can lead to very significant (over 100%) measurement errors. The possibilities of minimizing these errors by thermostating one side of the sample are considered. Bibl. 12, Figs. 14.
Key words: electrical contact resistance, measurement, computer simulation, accuracy, thermoelectric thermoelectric energy converters.

Introduction

The development of methods and equipment for studying the quality of contact structures in thermoelectric energy converters and their subsequent comprehensive optimization is an important and urgent task. It is due to the need of modern thermoelectrics to miniaturize thermoelectric energy converters, which will allow significantly reducing their cost, approaching that acceptable for wide practical use. The main obstacle to this is the relatively large values of contact resistances, since, as is known, the influence of contact resistance on the efficiency of a thermoelectric energy converter increases as it becomes smaller [1 – 5].

It is also important to ensure high-quality contacts for conducting high-precision measurements of the thermoelectric properties of materials both in materials science research aimed at finding ways to increase their thermoelectric figure of merit, and in the processes of developing and manufacturing thermoelectric energy converters [6-8].

To create a technology for manufacturing contact structures with acceptable contact resistance values, it is necessary to conduct a complex of experimental studies, which are possible only with the availability of high-precision methods and equipment for measuring contact resistances. In doing so, as literature analysis shows [9, 10], reliable equipment for studying contact resistances of "metal –

thermoelectric material" has not yet been created. The developed methods for measuring electrical contact resistance in thermoelectricity can be divided into those based on measuring the characteristics of "pack" contact structures, which are a series of series-connected thermoelements with contact resistances; probe and microelectronic methods, which require the manufacture of test structures

Works devoted to measuring contact resistance in thermoelectricity are not of a comprehensive nature aimed at developing high-precision measuring equipment for widespread use.

Therefore, the *purpose of this work* was to analyze the accuracy of the probe method for measuring the electrical contact resistance of "metal – thermoelectric material" through a detailed analysis of its real physical model and computer optimization to achieve minimal error values. This approach to the development of measuring equipment was successfully used at the Institute of Thermoelectricity (Ukraine) in creating equipment for determining the properties of thermoelectric parameters of materials by a complex absolute method, which is several times more accurate than its analogues [11, 12].

1. Description of the probe method for measuring electrical contact resistance of "metal – thermoelectric material"

The physical model of the probe method for measuring the electrical contact resistance of "metal – thermoelectric material" is shown in Fig. 1. The structure under study consists of a thermoelectric material sample 1 with a metal (e.g., nickel) coating 3 applied to its ends, a transient contact layer 2, a solder layer 4, and metal (e.g., copper) contact plates 5. A pointed probe is located on the side surface of the sample, which measures the potential distribution along the sample when a constant electric current of magnitude I is passed through it.

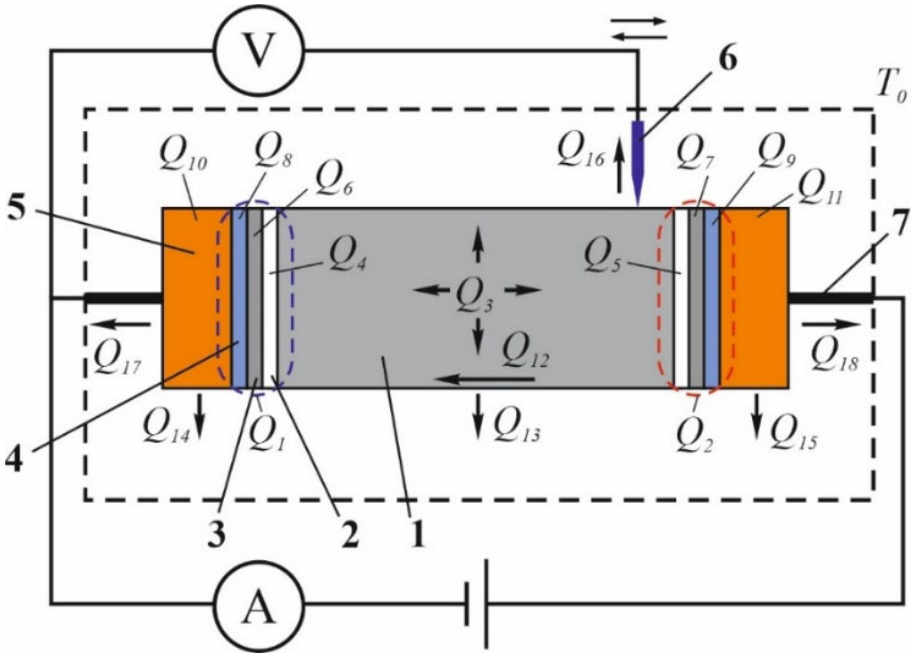

Fig. 1. Physical model of the probe method for measuring electrical contact resistance of "metal – thermoelectric material": 1 – thermoelectric material sample; 2 – transient contact layer; 3 – metal anti-diffusion coating; 4 – solder; 5 – metal contact plates; 6 – movable potential probe; 7 – current leads.

In Fig. 1: Q_1 is the Peltier heat absorbed at the "metal-thermoelectric material" contact; Q_2 is the Peltier heat released at the "metal-thermoelectric material" contact; Q_3 is the Joule heat released in the volume of thermoelectric material sample; Q_4, Q_5 is the Joule heat released on the transient contact layers; Q_6, Q_7 is the Joule heat released in the volume of metal anti-diffusion coatings; Q_8, Q_9 is the Joule heat released in the volume of solder layers; Q_{10}, Q_{11} is the Joule heat released in the volume of metal contact plates; Q_{12} is heat flow from the hot to cold "metal-thermoelectric material" contact; Q_{13}, Q_{14}, Q_{15} is heat transfer from the side surface of the sample and metal contact plates to the environment by radiation and convection; Q_{16}, Q_{17}, Q_{18} is heat transfer from the side surface of the sample and metal contact plates to the environment by thermal conductivity through the potential probe and current leads; T_0 is ambient temperature.

The value of electrical contact resistance of "metal – thermoelectric material" is determined by the formula

$$r_c = \frac{\Delta U}{I} \cdot S, \tag{1}$$

where r_c is specific electrical contact resistance of "metal-thermoelectric material", ΔU is voltage drop across the contact, S is contact area.

The main sources of errors in determining contact resistance using this method will be the following:

1. Errors of instruments for measuring current and electric potential.
2. Errors in measuring the geometric dimensions of the sample and the coordinates of the probe location.
3. Deviations from isothermal measurement conditions caused by the influence of Joule heat generated when passing electric current through the volume of the sample, current leads and contact resistance, as well as heat generated or absorbed at the points of contact of dissimilar materials.

2. Computer model

To determine the errors, the influence of various factors on them, and optimize the measurement method, it is necessary to find the distribution of the electric potential φ and the temperature T in the sample, which can be obtained based on the laws of conservation of electric charge and energy, written in the form:

$$\begin{cases} -\nabla\left(\left(\kappa_j + \alpha_j^{\,2}\sigma_j T + \alpha_j \varphi \sigma_j\right)\nabla T\right) - \nabla\left(\left(\alpha_j \sigma_j T + \varphi\sigma_j\right)\nabla\varphi\right) = 0, \\ -\nabla\left(\sigma_j \nabla\varphi\right) - \nabla\left(\sigma_j \alpha_j \nabla T\right) = 0. \end{cases} \quad (j = 1...10), \tag{2}$$

where: α_i, σ_i, κ_i are the Seebeck coefficient, electrical conductivity and thermal conductivity of the model elements.

The boundary conditions for such a model:

– the side surfaces of the sample, metal coating, contact plates and current leads are electrically isolated

$$\mathbf{n} \cdot \mathbf{j} = 0;$$

– a current of magnitude I flows through the current leads

$$\mathbf{n} \cdot \mathbf{j} = I / S_{cm.};$$

– the ends of current leads are maintained at ambient temperature T_0

$$T = T_0;$$

– the side surfaces of the sample, metal coating, contact plates and current leads are in a state of heat exchange with the environment

$$\mathbf{n} \cdot \mathbf{q} = h_i (T_0 - T),$$

where h_i are heat transfer coefficients.

To calculate such a problem, computer object-oriented simulation was used by applying the finite element method (Fig. 2), implemented in the Comsol Multiphysics application software package.

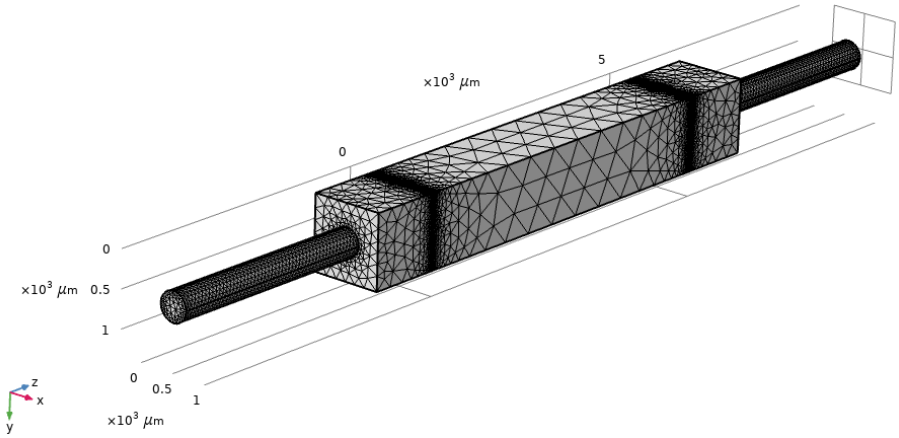

Fig. 2. Finite element method mesh for simulation of the probe method of measuring the electrical contact resistance in the Comsol Multiphysics application package.

Fig. 3 shows typical distributions of electric potential and temperature in the contact structure under study, obtained by computer simulation. Fig. 4 shows the distributions of electric potential and temperature along the line of movement of the measuring probe (for the case of a sample 5 mm long and 1 x 1 mm^2 in cross-section, with a current through the sample of 1 A; contact resistance is 10^{-6} Ohm·cm^2).

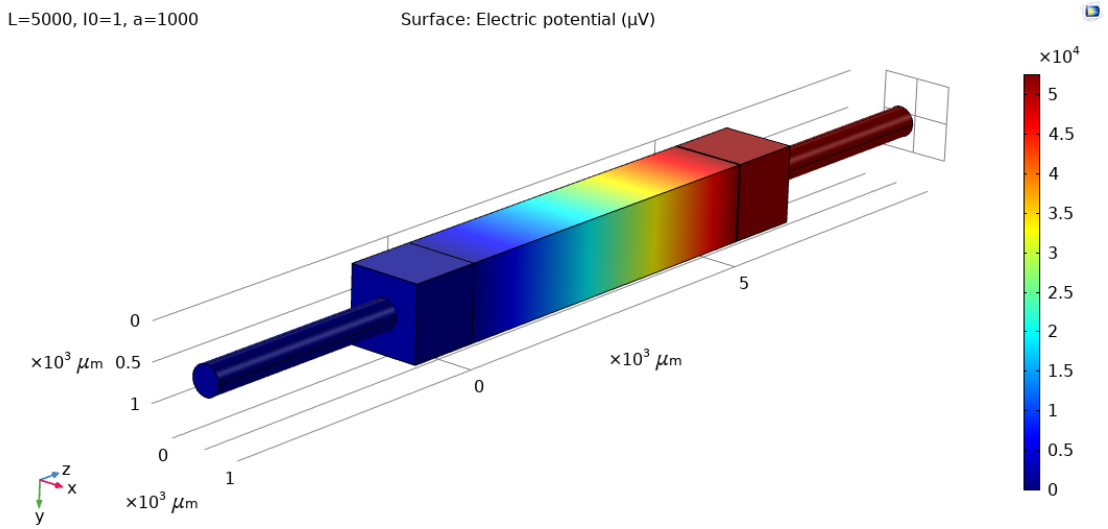

a)

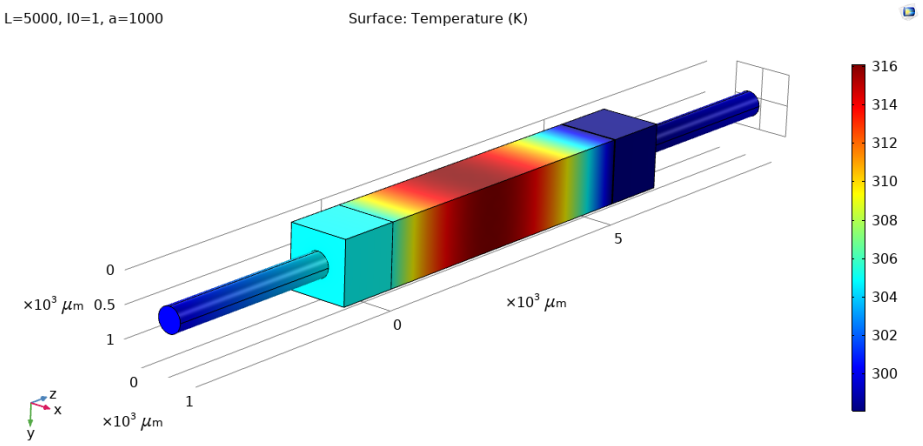

b)

Fig. 3. Typical distributions of electric potential (a) and temperature (b) in the studied contact structure, obtained by computer simulation using the Comsol Multyphysics package.

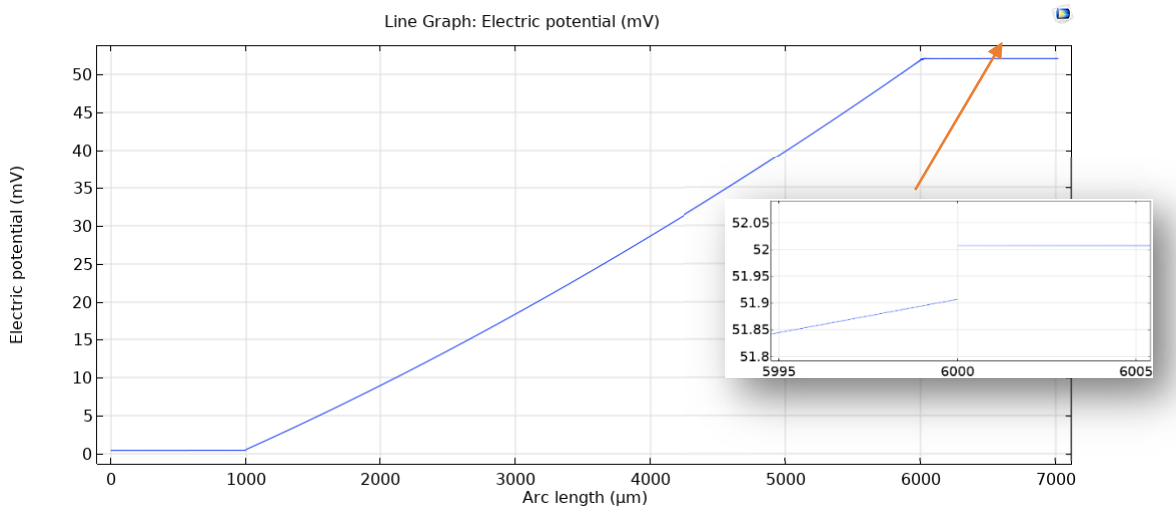

a)

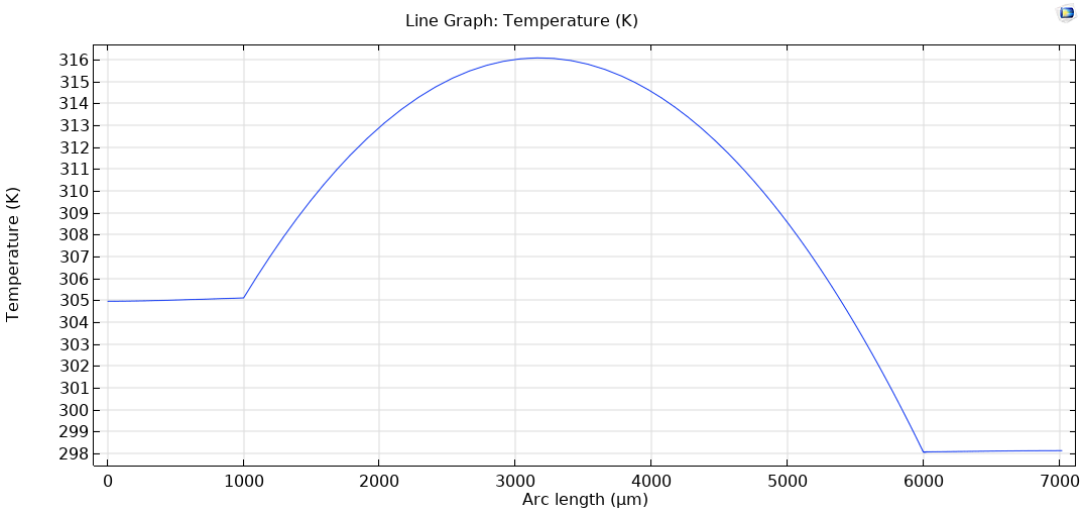

b)

Fig. 4. Distributions of electric potential (a) and temperature (b) on the surface of the studied contact structure along the line of movement of the measuring probe (for the case of a sample with a length of 5 mm and a cross-section of 1 mm², at a current of 1 A; contact resistance – 10^{-6} Ohm·cm²).

3. Results of the study of possible measurement errors and conditions for their minimization

By means of computer simulation, the distributions of electric potential and temperature in the studied model were obtained for different sample geometries, current through the sample, and contact electrical resistance.

Fig. 5 shows an example of the dependences of the voltage drop at the contact and on a section of the sample with a length of 50 μm on the current through the sample for different sample geometries, with a contact resistance of 10^{-6} Ohm·cm^2. From these dependences it is clear that to ensure sufficient accuracy of measurements of electric current and voltage by modern measuring devices (up to 0.05% with a resolution of 1 μV), it is necessary to use samples with a cross section of at least 1 mm^2 and a current of 0.5 – 1 A.

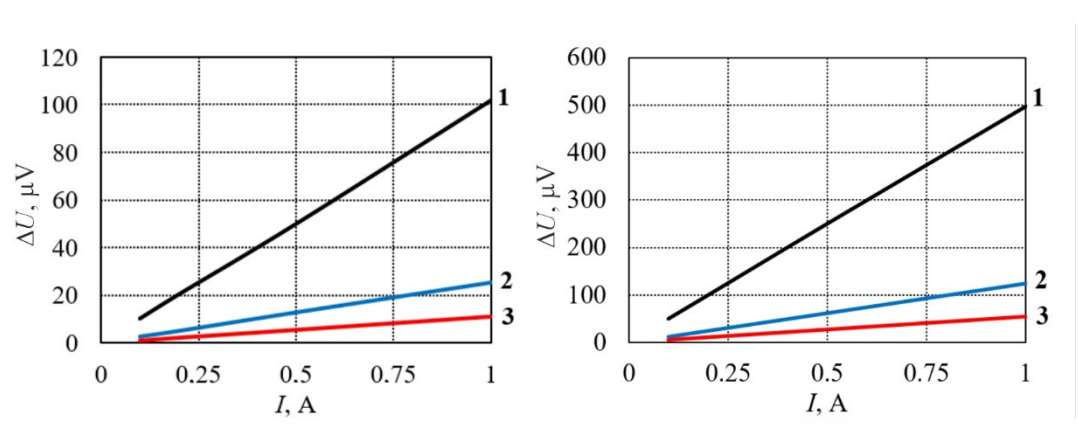

a) *b)*

Fig. 5. Dependence of the voltage drop at the contact (a) and on a section of the sample 50 μm long (b) on the current through the sample. Sample cross-section S: 1 – 1 x 1 mm ^{2}; 2 – 2 x 2 mm^2; 3 – 3 x 3 mm^2.

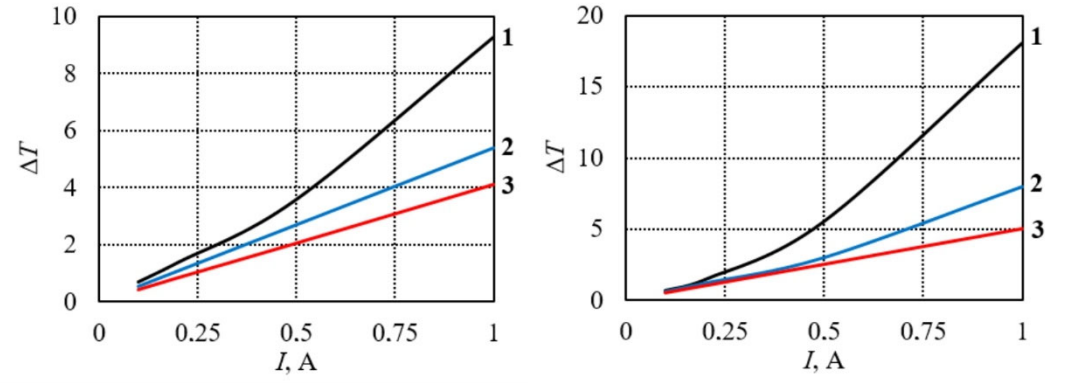

a) *b)*

Fig. 6. Dependence of the temperature difference on the sample on the current through the sample (for samples with a length of 3 mm (a) and 5 mm (b)): Section of the sample S: 1 – 1 x 1 mm2; 2 – 2 x 2 mm2; 3 – 3 x 3 mm2.

However, this poses a problem with ensuring the isothermality of the sample. Fig. 6 shows the dependences of the temperature difference on the sample, which will arise during measurements due to the Peltier and Joule effects (for the case of heat exchange of the sample with the environment by free convection and radiation). As can be seen from the figure, the temperature difference on the sample can reach 18 K, which will lead to very significant (over 100 %) measurement errors caused by the fact that thermoEMF will be added to the measured ohmic voltage drop, and the values of thermoEMF and ohmic

voltage drop on the sample will be commensurate.

To minimize the influence of the Peltier and Joule effects, glue one side of the sample to an electrical insulator with high thermal conductivity (for example, beryllium oxide ceramics) and place it on a thermostatic surface (Fig. 7).

The heat flows to the thermostat from this side of the sample, as well as from the corresponding sides of the metal contact plates, are designated Q_{19}, Q_{20}, Q_{21}, respectively. Other designations of heat flows $Q_1 – Q_{18}$ correspond to those given earlier for the physical model shown in Fig. 1.

As computer simulation has shown, when using thermostating of even one of the sides, the non-isothermality of the sample is significantly reduced. This is clearly seen by comparing the temperature distributions in the studied contact structure (Fig. 8) and along the line of movement of the measuring probe (Fig. 9) with similar distributions without thermostating (Fig. 3*b* and Fig. 4*b*).

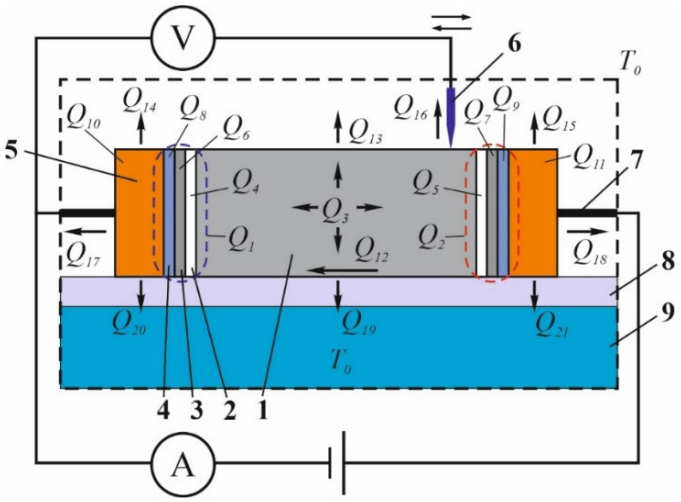

Fig. 7. Thermostating a sample when measuring electrical contact resistance using the probe method: 1 – sample of thermoelectric material; 2 – transient contact layer; 3 – metal anti-diffusion coating; 4 – solder; 5 – metal contact plates; 6 – movable potential probe; 7 – current leads; 8 – electrical insulator; 9 – thermostat.

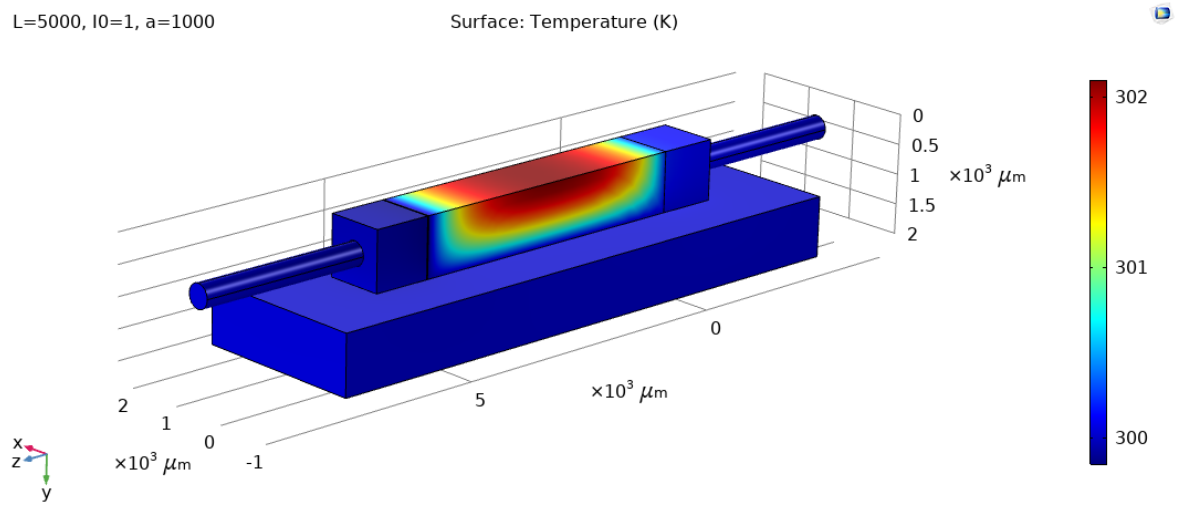

Fig. 8. Temperature distribution in the contact structure under study during thermostating of one of its surfaces.

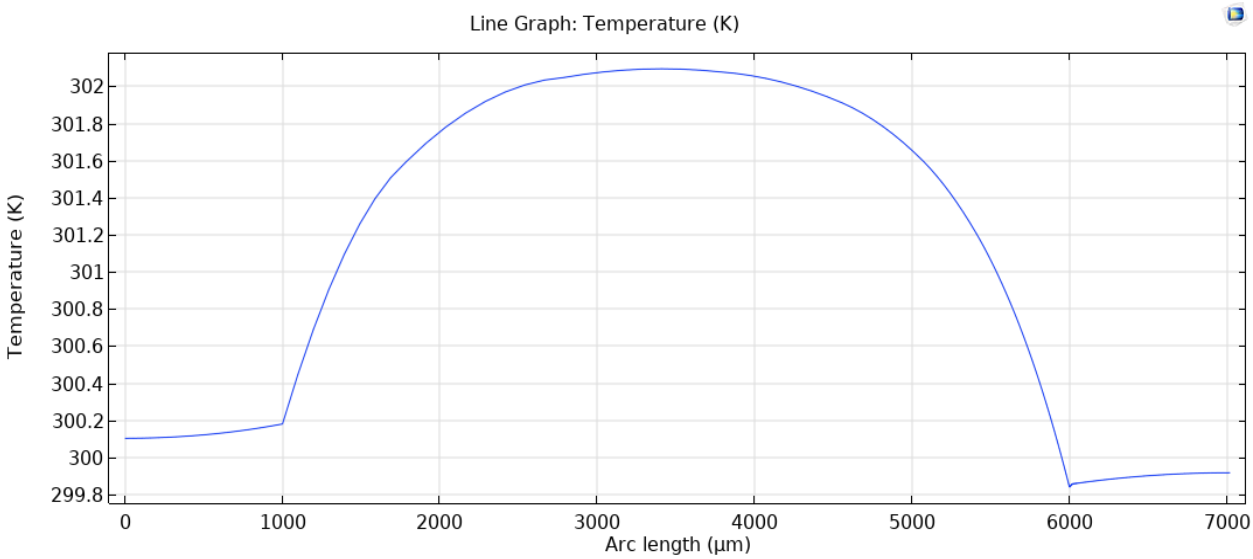

Fig. 9. Temperature distribution along the line of motion of the measuring probe over the surface of the investigated contact structure during thermostating of one of its surfaces (for the case of a sample with a length of 5 mm and a cross-section of 1 mm², at a current of 1A; contact resistance – 10^{-6} Ohm·cm²).

The dependence of the temperature difference on the sample on the current through the sample for different sample geometries is shown in Fig. 10.

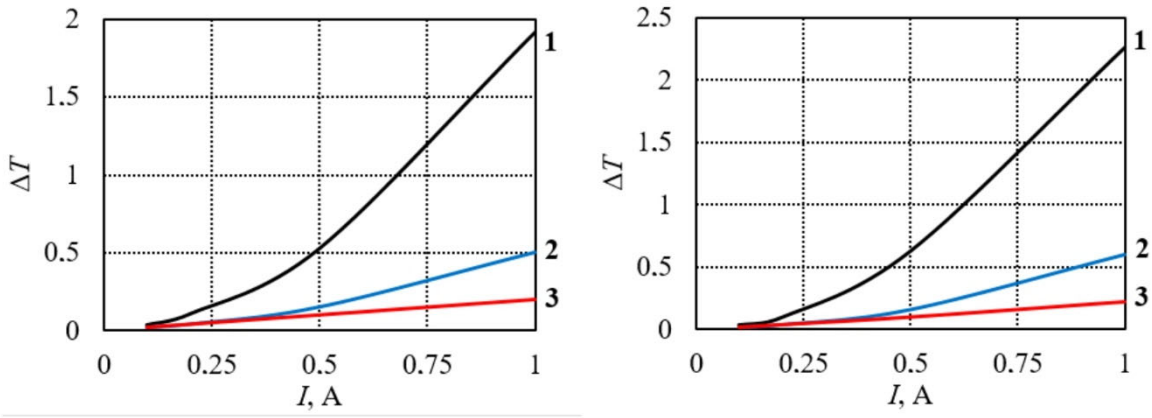

a) *b)*

Fig. 10. Dependence of the temperature difference on the sample on the current through the sample when thermostating one of its side surfaces (for samples with a length of 3 mm (a) and 5 mm (b)): Section of the sample S: 1 – 1 x 1 mm²; 2 – 2 x 2 mm²; 3 – 3 x 3 mm².

Thus, the error in determining the contact resistance, caused by the non-isothermal nature of the measurement conditions, will be significantly reduced – to a value of ~ 8 % (at a contact resistance of 10^{-6} Ohm·cm²).

Additional improvement can be achieved by using samples with a rectangular cross-section of the same area and placing them on a thermostatic surface with their wider side. The temperature distributions in the contact structure under study and along the line of movement of the measuring probe are shown in Figs. 11 and 12 (for a sample length of 5 mm, a cross-section of 0.5 mm by 2 mm, at a current of 1 A; contact resistance is 10^{-6} Ohm·cm²).

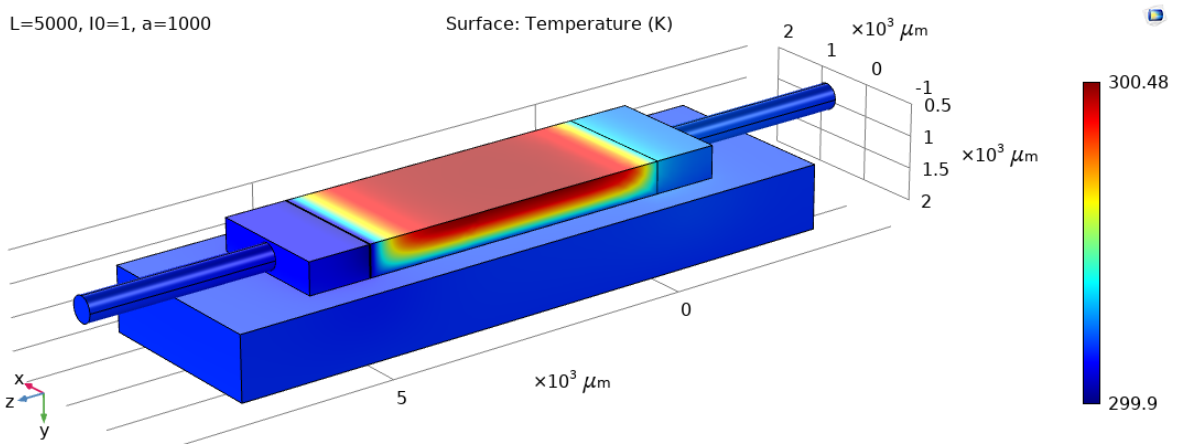

Fig. 11. Temperature distribution in the studied contact structure during thermostating of one of its surfaces (for the case of a sample with a length of 5 mm and a cross section of 0.5 mm by 2 mm, at a current of 1 A; contact resistance – 10^{-6} Ohm·cm²).

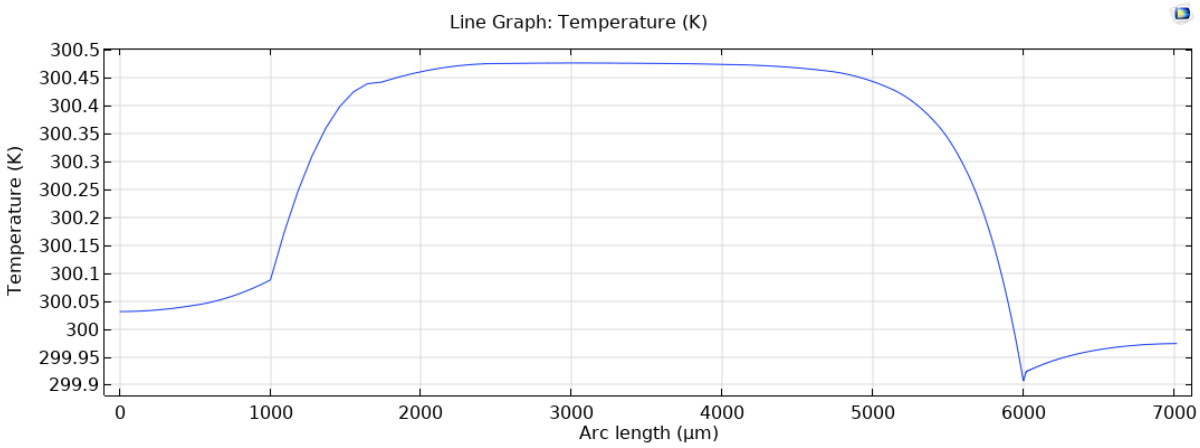

Fig. 12. Temperature distribution along the line of movement of the measuring probe on the surface of the contact structure under study during thermostating of one of its surfaces (for the case of a sample 5 mm long and 0.5 mm by 2 mm in cross-section at a current of 1 A; contact resistance is 10^{-6} Ohm·cm²).

In this case, the error in determining the contact resistance, caused by the non-isothermal nature of the measurement conditions, for a sample with a cross section of 0.5 mm by 2 mm and a length of 5 mm, will not exceed 2 %.

Conclusions

1. A computer model has been created to study possible errors in measuring the electrical contact resistance of "metal – thermoelectric material" using the probe method. By means of computer simulation, the distributions of electrical potential and temperature in the physical model under study have been obtained for different sample geometries, current values through the sample, and electrical contact resistance.
2. It has been established that deviations from isothermal conditions in the sample, caused by the influence of the Joule and Peltier effects, can lead to very significant (over 100 %) measurement errors, caused by the fact that the thermoEMF will be added to the measured ohmic voltage drop, and the values of the thermoEMF and the ohmic voltage drop on the sample will be commensurate.

3. It is shown that thermostating one side of the sample allows reducing measurement errors to 8 % for samples with a square cross-section and to 2 % for samples with a rectangular cross-section of a similar area, located with the wider side on the thermostat (with a contact resistance of 10^{-6} Ohm·cm^2).

References

1. Tritt T. (2000). Recent trends in thermoelectric materials research, Part Two (*Semiconductors and Semimetals, Volume 70*). Academic Press, ISBN-13: 978-0127521794.
2. Rowe D.M. (2006). *Thermoelectrics Handbook: Macro to Nano* (1st ed.). CRC Press. https://doi.org/10.1201/9781420038903.
3. Vikhor L.M., Anatychuk L.I. and Gorskyi P.V. (2019). Electrical resistance of metal contact to Bi_2Te_3 based thermoelectric legs. *Journal of Applied Physics*, 26, 64503-1 – 164503-8.
4. Anatychuk L.I., Vikhor L.M., Mitskaniuk N.V. (2019). Contact resistance due to potential barrier at thermoelectric material – metal boundary. *J. Thermoelectricity*, 4, 74 – 88.
5. Vikhor, L., Kotsur, M. (2023). Evaluation of efficiency for miniscale thermoelectric converter under the influence of electrical and thermal resistance of contacts. *Energies*, 16, 4082-1 – 22. https://doi.org/10.3390/en16104082.
6. Mykhailovsky V.Ya., Lysko V.V., Antoniuk V.V., Maksymuk M.V. (2017). Research on thermoelements based on *n-PbTe* and *p*-TAGS materials for thermoelectric generator cascade module. *J. Thermoelectricity*. 3, 37 – 44.
7. Anatychuk, L.I., Lysko V.V. (2014). Methods for assuring high quality electric and thermal contacts when measuring parameters of thermoelectric materials. *J. Thermoelectricity,* 4, 83 – 90.
8. Anatychuk L.I., Havrylyuk N.V., Lysko V.V. (2012). Methods and equipment for quality control of thermoelectric materials. *J. Electronic Materials,* 41 (6). 1680 – 1685. https://doi.org/10.1007/s11664-012-1973-1.
9. Vikhor L.M., Gorskyi P.V., Lysko V.V. (2022). Methods for measuring contact resistances of "metal-thermoelectric material" structures (part 1). *J. Thermoelectricity,* 2, 5 – 24.
10. Vikhor L.M., Gorskyi P.V., Lysko V.V. (2022). Methods for measuring contact resistances of "metal-thermoelectric material" structures (part 2). *J. Thermoelectricity,* 3-4, 5 – 17.
11. Anatychuk L.I., Lysko V.V. (2020). *Thermoelectricity: Vol. 5. Metrology of Thermoelectric Materials.* Chernivtsi: Bukrek. ISBN 978-617-7770-40-3.
12. Anatychuk L.I., Lysko V.V. (2014). On improvement of the accuracy and speed in the process of measuring characteristics of thermoelectric materials. *J. Electronic Materials*, 43 (10), 3863 – 3869. https://doi.org/10.1007/s11664-014-3300-5.

Submitted: 11.12.2023.

Анатичук Л.І., *акад. НАН України* [1,2]
Лисько В.В., *канд. фіз.-мат. наук* [1,2]
Струсовський К.І. [2]

[1] Інститут термоелектрики НАН та МОН України,
вул. Науки, 1, Чернівці, 58029, Україна;
[2] Чернівецький національний університет імені Юрія Федьковича,
вул. Коцюбинського 2, Чернівці, 58012, Україна, *e-mail: anatych@gmail.com*

КОМП'ЮТЕРНІ ДОСЛІДЖЕННЯ ТОЧНОСТІ ЗОНДОВОГО МЕТОДУ ВИМІРЮВАННЯ ЕЛЕКТРИЧНОГО КОНТАКТНОГО ОПОРУ «МЕТАЛ – ТЕРМОЕЛЕКТРИЧНИЙ МАТЕРІАЛ»

Створено фізичну та комп'ютерну моделі для дослідження можливих похибок вимірювань електричного контактного опору «метал – термоелектричний матеріал» зондовим методом. Шляхом комп'ютерного моделювання отримано розподіли електричного потенціалу та температури у досліджуваній фізичні моделі для різної геометрії зразків, величини струму через зразок та контактного електричного опору. Встановлено, що відхилення від ізотермічних умов у зразку, викликані впливом ефектів Джоуля та Пельтьє, можуть призводити до дуже значних (понад 100%) похибок при вимірюваннях. Розглянуто можливості мінімізації цих похибок за допомогою термостатування однієї зі сторін зразка. Бібл. 12, рис. 14.

Ключові слова: електричний контактний опір, вимірювання, комп'ютерне моделювання, точність, термоелектричні перетворювачі енергії.

Література

1. Tritt T. (2000). Recent trends in thermoelectric materials research, Part Two (*Semiconductors and Semimetals, Volume 70*). Academic Press, ISBN-13: 978-0127521794.
2. Rowe D.M. (2006). *Thermoelectrics Handbook: Macro to Nano* (1st ed.). CRC Press. https://doi.org/10.1201/9781420038903.
3. Vikhor L.M., Anatychuk L.I. and Gorskyi P.V. (2019). Electrical resistance of metal contact to Bi_2Te_3 based thermoelectric legs. *Journal of Applied Physics*, 26, 64503-1 – 164503-8.
4. Anatychuk L.I., Vikhor L.M., Mitskaniuk N.V. (2019). Contact resistance due to potential barrier at thermoelectric material – metal boundary. *J. Thermoelectricity*, 4, 74 – 88.
5. Vikhor, L., Kotsur, M. (2023). Evaluation of efficiency for miniscale thermoelectric converter under the influence of electrical and thermal resistance of contacts. *Energies*, 16, 4082-1 – 22. https://doi.org/10.3390/en16104082.
6. Mykhailovsky V.Ya., Lysko V.V., Antoniuk V.V., Maksymuk M.V. (2017). Research on thermoelements based on *n-PbTe* and *p*-TAGS materials for thermoelectric generator cascade module. *J. Thermoelectricity*. 3, 37 – 44.
7. Anatychuk, L.I., Lysko V.V. (2014). Methods for assuring high quality electric and thermal contacts when measuring parameters of thermoelectric materials. *J. Thermoelectricity,* 4, 83 – 90.
8. Anatychuk L.I., Havrylyuk N.V., Lysko V.V. (2012). Methods and equipment for quality control of thermoelectric materials. *J. Electronic Materials,* 41 (6). 1680 – 1685. https://doi.org/10.1007/s11664-012-1973-1.
9. Vikhor L.M., Gorskyi P.V., Lysko V.V. (2022). Methods for measuring contact resistances of "metal-thermoelectric material" structures (part 1). *J. Thermoelectricity,* 2, 5 – 24.
10. Vikhor L.M., Gorskyi P.V., Lysko V.V. (2022). Methods for measuring contact resistances of "metal-thermoelectric material" structures (part 2). *J. Thermoelectricity,* 3-4, 5 – 17.
11. Anatychuk L.I., Lysko V.V. (2020). *Thermoelectricity: Vol. 5. Metrology of Thermoelectric Materials.* Chernivtsi: Bukrek. ISBN 978-617-7770-40-3.
12. Anatychuk L.I., Lysko V.V. (2014). On improvement of the accuracy and speed in the process of measuring characteristics of thermoelectric materials. *J. Electronic Materials*, 43 (10), 3863 – 3869. https://doi.org/10.1007/s11664-014-3300-5.

Надійшла до редакції: 11.12.2023.

R.R. Kobylianskyi, *Cand.Sc.(Phys-Math)* [1,2]
V.V. Lysko, *Cand. Sc (Phys-Math)* [1,2]
A.V. Prybyla, *Cand. Sc (Phys-Math)* [1,2]
I.A. Konstantynovych, *Cand. Sc. (Phys-Math)* [1,2]
A.K. Kobylianska, *Cand. Sc (Phys-Math)* [1]
N.R. Bukharayeva, [1]
V.V. Boychuk [2]

[1] Institute of Thermoelectricity of the NAS and MES of Ukraine,
1 Nauky str., Chernivtsi, 58029, Ukraine;
[2] Yuriy Fedkovych Chernivtsi National University, 2 Kotsiubynskyi str.,
Chernivtsi, 58000, Ukraine
e-mail: anatych@gmail.com

TECHNOLOGICAL MODES OF MANUFACTURING MEDICAL PURPOSE THERMOELECTRIC SENSORS

This work presents technological modes of manufacturing thermoelectric heat flux converters. It has been established that the optimal thermoelectric material for a thermopile is low-temperature materials based on Bi_2Te_3. The effectiveness of using such technological modes for manufacturing thermoelectric microthermopiles capable of recording laser radiation with an improved conversion coefficient of 1 – 1.5 orders of magnitude compared to existing measuring transducers has been experimentally confirmed. The specified technological modes significantly simplify and mechanize the method of manufacturing medical purpose thermoelectric heat flux sensors and microgenerators for powering low-power medical equipment.

Key words: technological mode, thermoelectric converter, medical purpose thermoelectric heat flux sensor.

Introduction

General characterization of the problem. Thermoelectric heat flux sensors are widely used in medicine due to their ability to accurately measure changes in the heat release of the human body [1 – 20]. This allows them to be used for diagnostics and monitoring of the condition of patients, especially in cases where it is important to detect local changes in body temperature [21 – 40]. The main aspects of thermoelectric sensors [1 – 40]:

1. Operating principle:
- is based on the thermoelectric Seebeck effect, where a temperature difference between two points causes an electric voltage to arise;
- the sensor responds to the heat flux that occurs due to the temperature difference between the two sides of the sensor.

2. Medical applications:
- blood flow distribution: heat flux measurement can be used to assess blood microcirculation, which is useful in diagnosing diabetic foot or for studying skin pathologies;

- monitoring of wound conditions: in wounds or postoperative sutures, changes in heat flux may indicate inflammation or healing;
- tumor diagnosis: tumors are usually accompanied by a local increase in heat flux due to intense blood circulation in the affected area;
- neurophysiology: sensors help in measuring thermal changes caused by neural activity.

3. Sensor types:
- disposable or reusable devices;
- high-sensitivity sensors for localized measurement, for example in dermatology.

4. Advantages:
- high accuracy;
- small size, which allows them to be integrated into wearable devices;
- rapid response to changes in heat flux.

5. Production technologies:
- use of biocompatible materials;
- micromechanical design (MEMS) to ensure compactness and accuracy.

The prospects for the development of such sensors in medicine include their integration into multifunctional diagnostic and rehabilitation systems, which contributes to more accurate and comfortable monitoring of patients' health.

The purpose of this work is to develop special technological modes for the production of improved thermoelectric microthermopiles for medical purpose heat flux sensors.

1. Selection of thermoelectric material for manufacturing microthermopile

Thermoelectric semiconductor materials (TEM) must satisfy a number of requirements: maintain a high figure of merit in a wide temperature range, have significant mechanical strength, be easy to process when manufacturing samples of the required sizes, not be subject to the oxidizing action of the atmosphere, not sublimate or decompose at elevated temperatures, etc. The most important of these requirements is to achieve high values of the thermoelectric figure of merit, on which in most cases the possibility of using a thermoelectric material depends [1 – 3].

Thermoelectric materials are classified according to their operating temperature range: low-, medium-, and high-temperature. Low-temperature materials are semiconductors with the operating temperature of 0 – 350 °C, medium-temperature materials are semiconductors with the operating temperature of 350 °C – 650 °C, and high-temperature materials are semiconductors with the operating temperature of 700 °C – 1000 °C.

In this case, low-temperature materials are used to manufacture thermoelectric sensors.

As mentioned, the TEM is characterized by the figure of merit:

$$Z = \frac{\alpha^2 \sigma}{\chi} \tag{1}$$

where α is the Seebeck coefficient, σ is electrical conductivity, χ is the thermal conductivity.

$$\alpha = \frac{E}{\Delta T}, \tag{2}$$

$$\sigma = \frac{Il}{Us}, \tag{3}$$

$$\chi = \frac{I^2 Rl}{\Delta Ts}. \quad (4)$$

The most effective low-temperature materials are solid solutions based on Bi_2Te_3.

In the process of selecting the material for manufacturing the thermopile legs, low-temperature materials based on Bi_2Te_3 obtained by different methods were tested: single crystals (the Bridgman, Czochralski, zone melting), extrusion and pressing. Fig. 1 shows samples of n- and p-type thermoelectric material obtained by extrusion.

Fig. 1. Extruded bars of thermoelectric material of n- and p-type conductivity.

In the process of manufacturing a thermopile, such bars are cut into thin plates (Fig. 2), which are then glued together in pairs.

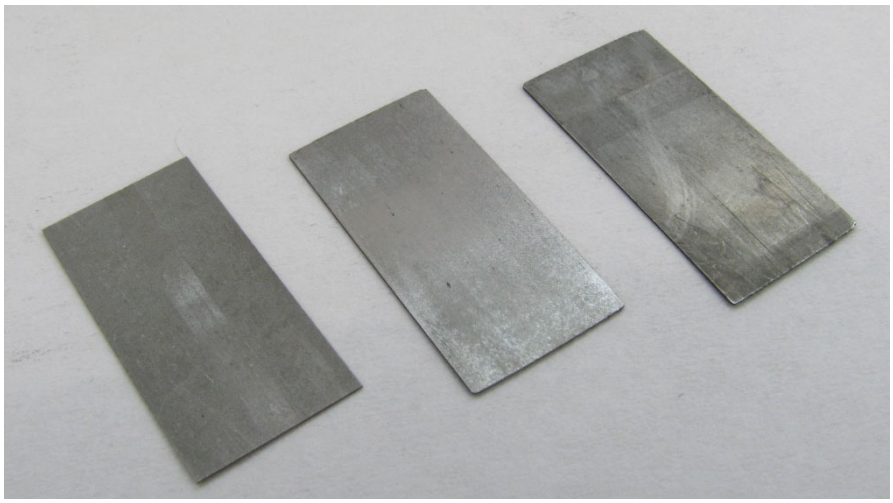

Fig. 2. Plates of thermoelectric material of n- and p-type conductivity.

Unlike single crystals grown by the Bridgman, Czochralski, and zone melting methods, the extruded material has high mechanical and technological properties; uniformity along the length of the rods, high mechanical strength, which is especially important in the manufacture of small-sized legs [1 – 3].

In the process of obtaining thermoelectric material, internal stress occurs as a result of various thermal and mechanical loads. The presence of final stresses, reaching ultimate strength values, can lead to the occurrence of micro- and macrocracks, which significantly weaken the strength of the material and can worsen its thermoelectric properties. The best strength is demonstrated by samples obtained by

extrusion. The high mechanical strength of the extruded material is explained by its relatively high homogeneity.

The thermopile legs were made of semiconductor material obtained by the extrusion method.

Of great importance for the materials used in thermoelements is the degree of their homogeneity. Inhomogeneities create closed thermoelectric currents in the middle of the leg, which reduce the efficiency of thermoelements.

TEMs obtained from powders by hot or cold pressing are currently the most widely used due to their technological simplicity and the possibility of manufacturing thermoelements of the required sizes [1 – 3].

In the simplest case, when the material of all grains is homogeneous and isotropic, the contact between grains is ideal and the influence of various microscopic defects (cracks, holes, various types of inclusions and cavities) is so small that it can be neglected, the expressions for describing the electrical and thermal conductivity of pistons are isomorphic, therefore, regardless of the configuration of the grains, their sizes, mutual orientation and contact area, the ratio σ/χ should remain constant. The Seebeck coefficient should also not depend on the listed factors, so the values of powder and single-crystal materials should coincide. In most cases, the figure of merit of powder materials is somewhat lower than that of single crystals, due to additional scattering of phonons and current carriers at grain boundaries, dislocations, vacancies, microcracks; due to the presence of oxide films, etc.

When using powders from anisotropic materials, the figure of merit of pressed powders may be significantly lower than that of single crystals. The anisotropy of thermoelectric power during grain misorientation leads to the appearance of eddy currents, which also deteriorates the properties of the material.

To achieve maximum figure of merit, it is necessary to perform grain orientation. In layered materials (in low-temperature TEMs operating in the temperature range of 0 ÷ 300 °C), represented by Bi_2Te_3-based alloys, such orientation is achieved during hot pressing [1 – 3] – the grains are arranged with cleavage planes perpendicular to the pressing direction. Orientation is also achieved when manufacturing samples by extrusion. When using such techniques, the powder material becomes anisotropic and approaches single crystals in the figure of merit.

2. Design of a thermoelectric microthermopile

The disadvantage of the above-mentioned technology for manufacturing thermoelectric microthermopiles is a significant percentage of defective plates of thermoelectric material due to microcracks that may occur during their grinding.

The operating principle of a semiconductor thermopile is based on the direct thermal into electrical energy conversion in accordance with the Seebeck effect, which states that in a closed circuit consisting of two dissimilar conductors, the junctions of which are at different temperatures, a thermoelectric power arises.

The thermopile design is a monolithic block with dimensions not exceeding (22 × 22 × 20) mm^3. The block consists of 1600 *p*- and *n*-type semiconductor legs of square cross-section and insulated from each other. The *p*- and *n*-type legs are connected in pairs in a series electrical circuit (Fig. 3) and are arranged parallel to the heat flux, i.e. the heat flux passes along the thermopile legs (along the height). The extreme *p*- and *n*-type legs in the electrical circuit are connected to nickel buses, which are glued to two opposite side surfaces of the semiconductor thermopile [1 – 3].

The dimensions of the manufactured thermocouple leg are: (20 × 0.5 × 0.5) mm^3. The thermopile legs are made of extruded thermoelectric semiconductor material based on Bi_2Te_3 alloys. The average values of the electrical parameters of this material are: α_{av} = 190 μV K^{-1}, σ_{av} = 900 $Ohm^{-1}cm^{-1}$.

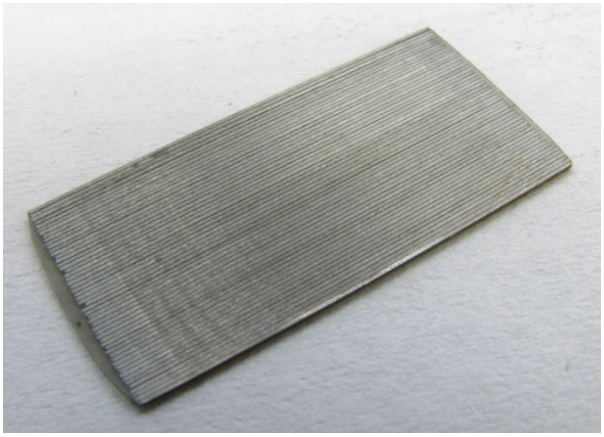

Fig. 3. Glued thermopile legs made of extruded thermoelectric material.

3. Technological modes of manufacturing thermoelectric microthermopile

Micromodules are, as a rule, single-stage thermopiles made of low-temperature thermoelectric materials based on ternary alloys of bismuth telluride [1 – 3], which acquire *p*- or *n*-type conductivity depending on their doping. The process flow chart of micromodules includes the following stages: synthesis of low-temperature thermoelectric alloys of *p*- and *n*-type conductivity; crushing of alloy ingots into powder with the required grain size with its subsequent extrusion through dies measuring 7×7 mm^2 or 5×10 mm^2. The obtained thermoelectric legs with the appropriate cross-section are characterized by high parameter values in the temperature range of 200 ÷ 600 K and good mechanical properties, which allows them to be used in production conditions. From these legs, bars of the required length and an average value of 180 ÷ 200 μV/K and 900 ÷ 1200 Ohm^{-1}cm^{-1} are cut with a diamond disk. Then the bars are cut using a mechanical wire cutting into 0.7 mm thick plates and after appropriate chemical treatment, the plates are glued together, maintaining the sequence of alternating *p*- and *n*-conductivity. The electrical insulation between the plates is a polyamide film with a thickness of 10 microns, the adhesive chosen is epoxy compound K-400 with a plasticizer. The blocks obtained after drying were cut into rows of legs of the required thickness (in our case – 0.7 mm). After chemical etching, the ends of the rows of glued legs were covered with an anti-diffusion layer, followed by the creation of interconnect coating. After these operations, we obtain the required number of micromodule units, each of which contains a selected number of half-elements (legs) connected electrochemically.

The structure of micromodule fragment is shown in Fig. 4.

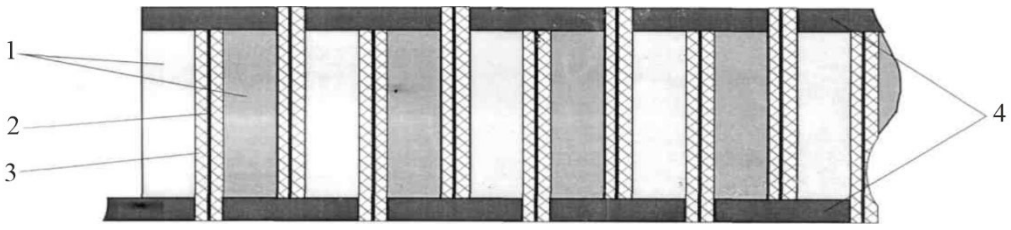

Fig. 4. Fragment of thermopile micromodule: 1 – half-elements of p- and n- type conductivity, 2 – polyamide film, 3 – epoxide compound, 4 – interconnects.

According to the above-mentioned process flow chart, 4 units of micromodules were assembled, which were glued into a block through a polyamide film and connected to each other from the heat-generating side. Fig. 5 shows the assembled and connected micromodule.

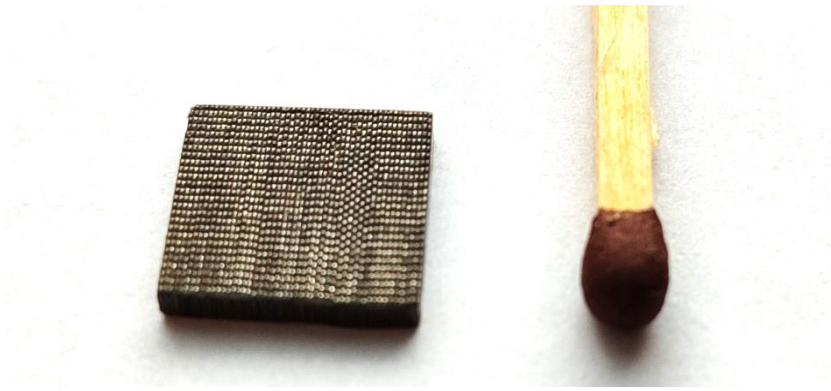

Fig. 5. Assembled and connected thermopile micromodule.

Electrical leads were soldered to the micromodule block, which is actually a thermopile, and its heat-exchange sides were covered with a heat-conducting protective layer containing boron nitrite.

In general, the technological chain for manufacturing a thermopile can be reduced to the following diagram (Fig. 6):

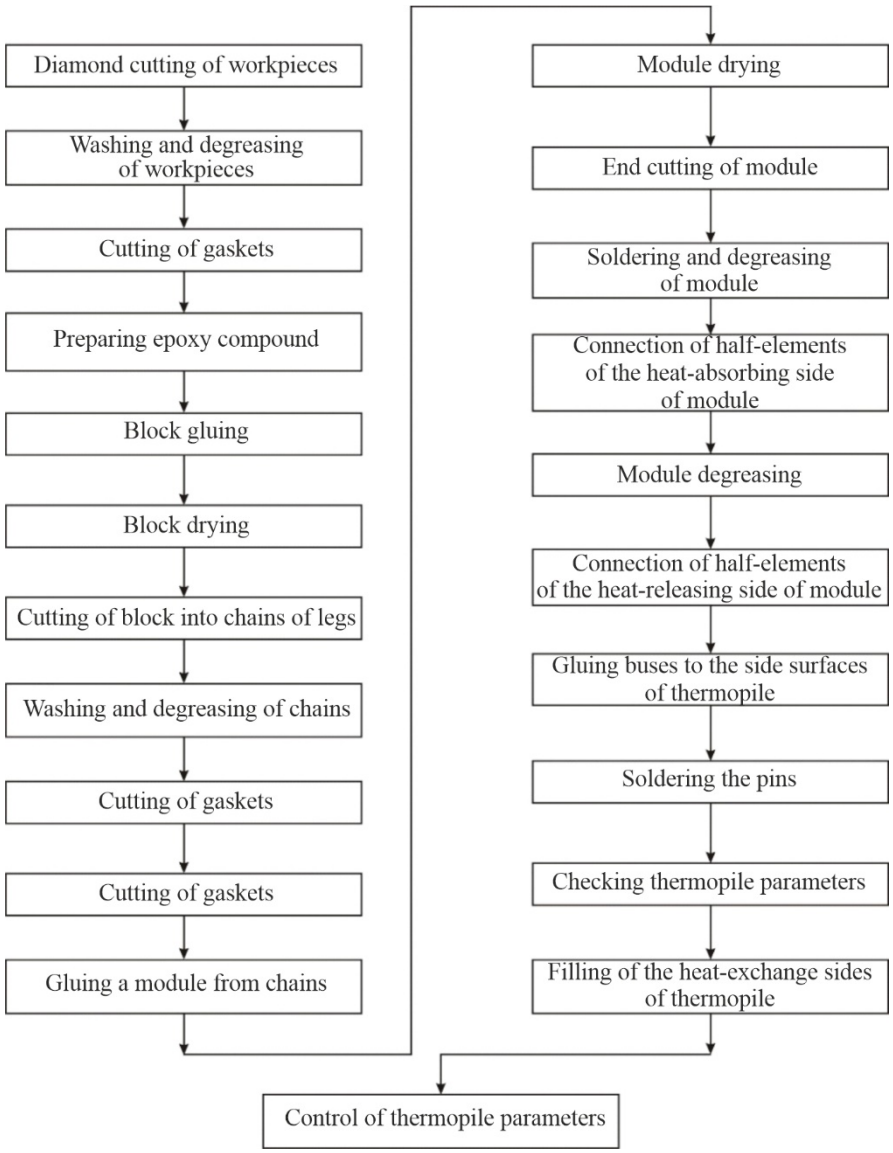

Fig. 6. Process flow chart for the production of thermopile.

3.1. Anti-diffusion layers and interconnects of thermoelectric micromodules

To create thermopiles, highly efficient low-temperature thermoelectric materials are used, which are ternary alloys based on bismuth telluride Bi_2Te_3 [1 – 3] and which acquire *p*- or *n*-type conductivity depending on their doping.

The relatively high operating temperature of the hot junctions of the micromodule half-elements requires the use of anti-diffusion layers on the surfaces of the contact half-elements. Various technologies and methods for sputtering anti-diffusion metal layers are known: chemical, electrochemical, melt immersion, mechanical deposition, vacuum sputtering, vapor phase deposition, cathodic sputtering, plasma spraying. Each of the above methods has negative and positive features. Cathode sputtering provides the best results. However, the extremely slow deposition rate and high energy consumption of the process do not allow this method to be used. Plasma spraying allows for a significant increase in the rate of coating deposition, but requires the use of rather complex and energy-intensive technological equipment. At the same time, galvanic methods are not characterized by low cost of the technological process, relative simplicity of equipment and sufficiently high quality of metal layers. The choice of materials for galvanic anti-diffusion layers is quite limited.The point is that it is necessary to ensure, in addition to significant adhesion, also a small contact resistance r_0, which significantly affects the thermoelectric figure of merit Z_{TE} of the thermoelement [1 – 3]:

$$Z_{\text{TE}} = Z_{\text{TEM}} \frac{1}{1 + \frac{2r_0}{r}}, \tag{5}$$

where Z_{TEM} is the figure of merit of thermoelectric material, *r* is half-element resistance.

Nickel *Ni* is considered one of the most suitable for creating anti-diffusion contact layers. It provides contact resistance at the level of $1 \div 5 \cdot 10^{-6}$ Ohm·cm^2.

The reliability of *Ni* antidiffusion layers is determined by the existence of internal stresses in the metal coatings. Classical Watts sulfuric acid electrolytes are characterized by rather large values of internal stresses, therefore they cannot be used to create antidiffusion layers and interconnects of highly reliable thermoelectric microbatteries.

Ni coatings with zero internal stress values can be obtained using modern electrolytes: fluoroborate, sulfanate, sulfamate, fluoroborate, and sulfamate sulfate.

The most promising is the sulfamic acid electrolyte, which allows, by changing the electrodeposition modes, to regulate the values of stresses from tensile to compressive. The work investigated the influence of the concentration of *Ni* sulfamic acid on the values of stresses in the deposited layers obtained in electrolytes of the following composition

1. Nickel sulfamic acid, g/l	100 – 800
2. Nickel chloride, g/l	20
3. Boric acid, g/l	30
pH	4.0
t_e, °C	40 – 60
I_K, A/dm^2	3.10

The obtained results indicate that with an increase in the concentration of *Ni* sulfamic acid from 100 to 800 g/l, the tensile stress in the deposited layers decreases and reaches zero values at 650 g/l (t_e = 40 °C). If the concentration of *Ni* sulfamic acid is further increased, the tensile stresses are transformed into compressive stresses.

For the application of anti-diffusion layers and interconnects in micromodules, nickel sulfamic acid electrolyte was used. The thickness of the *Ni* layer was 100 – 120 μm. To ensure minimal internal stress values, deposition was carried out at reduced cathodic current density values. Also, in order to reduce stresses, immediately after the nickel plating, the thermopile was annealed at a temperature of 150 °C for 4 hours. As a result, a high-quality protective interconnect coating with adhesion of at least 120 kg/cm^2 and high cyclic stability was obtained.

3.2. Improving the reliability of thermoelectric microthermopile

One of the effective methods of increasing the reliability of multi-element systems is the use of redundant elements, which, in the event of a system element failure, take over the functions of the failed element in whole or in part. In this work, the so-called passive redundancy method was used. It consists of the fact that the legs of a multi-element thermopile are shunted by passive resistors, which, in the event of a leg failure, prevent the opening of the thermopile electrical circuit, and therefore the failure only entails a decrease in the thermopile power, but not a complete failure of the thermopile (Fig. 7).

This method is economical and effective with the optimal choice of the ratio of resistances of the redundant legs and redundant shunts, which depends on the failure criterion of the thermopile. Such a criterion for passive redundancy is the permissible percentage of decrease in the output power of the thermopile for the guaranteed operating time.

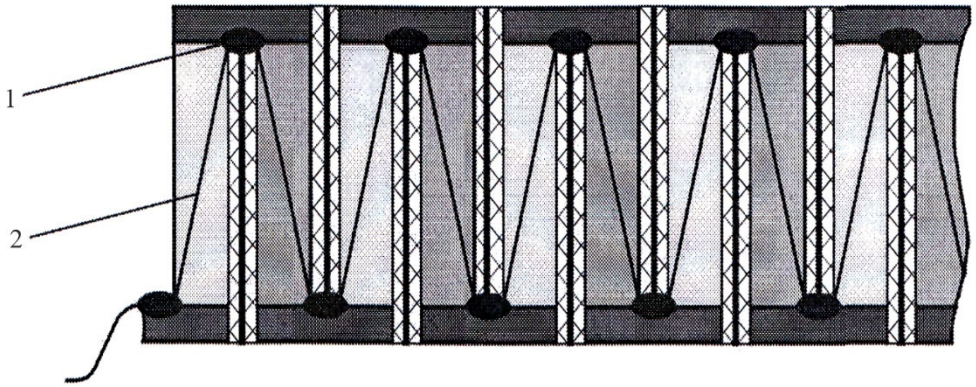

Fig. 7. Fragment of thermopile micromodule with passive resistors:
1 – soldering of passive resistor, 2 – passive resistor.

To calculate the reliability of the thermopile and optimize the ratio of the thermopile resistances and redundant elements, methods and computer programs developed at the Institute of Thermoelectricity of the National Academy of Sciences and the Ministry of Education and Science of Ukraine were used. The calculation results are given in Table 1.

Table 1

Dependence of thermopile parameters on the number of broken legs.

	T_c – 50 °C			T_h – 250 °C		
Number of broken legs	*U*, B	%	*W*	%	η,%	%
0	6.75	0	0.180	0	2.95	0
1	6.61	2.0	0.172	4.1	2.85	3.5
2	6.53	3.2	0.168	6.9	2.77	6.0
3	6.45	4.4	0.164	9.0	2.65	10.0
4	6.36	5.8	0.159	11.7	2.57	13.0
5	6.27	7.1	0.155	13.8	2.45	17.0

Experimental studies on the dependence of the parameters of a micro thermopile on the number of broken legs showed good agreement and coincidence with the calculation results given in Table 1.

Conclusions

1. Special technological modes for manufacturing thermoelectric micro thermopiles with an increased density of elements (up to several thousand) based on highly efficient semiconductor materials have been developed, which significantly simplifies and mechanizes the method of manufacturing thermoelectric medical purpose heat flux sensors and microgenerators for powering low-power medical equipment.
2. The dependences of the parameters of thermoelectric microthermopiles on the number of broken legs and methods for increasing the failure rate of such microthermopiles by optimally selecting the ratio of the resistances of the redundant legs and redundant shunts are established, thereby achieving an acceptable percentage of reduction in the output power of the thermoelectric thermopile for the guaranteed operating time.
3. It has been established that thermoelectric heat flux sensors are promising for monitoring and early diagnosis of inflammatory processes and cancer. The introduction of such sensors into medical practice will become an effective means of diagnosing various human diseases.

References

1. Anatychuk L.I. (2003). *Thermoelectricity. Vol. 2. Thermoelectric power converters*. Kyiv, Chernivtsi: Institute of Thermoelectricity.
2. Anatychuk L.I. (1998). *Thermoelectricity. Vol.1. Physics of thermoelectricity*. Kyiv, Chernivtsi: Institute of Thermoelectricity.
3. Anatychuk L.I. (2007). Current status and some prospects of thermoelectricity. *J. Thermoelectricity*, 2, 7 – 20.
4. Demchuk B.M., Kushneryk L.Ya., Rublenyk I.M. (2002). Thermoelectric sensors for orthopaedics. *J. Thermoelectricity*, 4, 80 – 85.

5. Patent of Ukraine 53104 A. (2003). Sensor for preliminary diagnosis of inflammatory processes of the mammary glands. A.A. Ashcheulov, A.V. Klepikovsky, L.Ya. Kushneryk, et al.
6. Ashcheulov A.A., Kushneryk L.Ya. (2004). Thermoelectric device for medico-biological express diagnostics. *Technology and Design in Electronic Equipment,* 4, 38 – 39.
7. *Patent of Ukraine 71619* (2012). Thermoelectric medical heat meter. L.I. Anatychuk, R.R. Kobylianskyi. Institute of Thermoelectricity (In Ukrainian).
8. *Patent of Ukraine 72032* (2012). Thermoelectric sensor for temperature and heat flux measurement. L.I. Anatychuk, R.R. Kobylianskyi. Institute of Thermoelectricity (In Ukrainian).
9. *Patent of Ukraine 73037* (2012). Thermoelectric medical device. P.D. Mykytiuk, R.R. Kobylianskyi, T.V. Slepeniuk. Institute of Thermoelectricity (In Ukrainian).
10. *Patent of Ukraine 78619* (2013). Method for determination of heat flux density. L.I. Anatychuk, R.R. Kobyliansky. Institute of Thermoelectricity (In Ukrainian).
11. *Patent of Ukraine 79929* (2013). Thermoelectric converter of heat flux for gradient heat meters. L.I. Anatychuk. Institute of Thermoelectricity (In Ukrainian).
12. Gischuk V.S. (2012). Electronic recorder of human heat flux sensor signals. *J. Thermoelectricity*, 4, 105 – 108.
13. Gischuk V.S. (2013). Electronic recorder with signal processing of thermoelectric heat flux sensor. *J. Thermoelectricity,* 1, 82 – 86.
14. Gischuk V.S. (2013). Modernized device for measuring human heat fluxes. *J. Thermoelectricity,* 2, 91 – 95.
15. Anatychuk L.I., Kobylianskyi R.R. (2012). Study of the influence of thermoelectric heat meter on determination of human heat release. *J. Thermoelectricity,* 4, 60 – 66.
16. Anatychuk L.I., Kobylianskyi R.R. (2012). 3D-model for determination of the influence of thermoelectric heat meter on the accuracy of measuring human heat release. *Scientific Herald of Chernivtsi University: Collected papers. Physics. Electronics. Vol. 2, Issue 1*. Chernivtsi: Chernivtsi National University, 15 – 20.
17. Anatychuk L.I., Kobylianskyi R.R. (2013). Computer simulation of thermoelectric heat meter readings in real-world operating conditions. *J. Thermoelectricity,* 1, 53 – 60.
18. Anatychuk L.I., Giba R.G., Kobylianskyi R.R. On some features of the use of medical heat meters in the study of local human heat release. *J. Thermoelectricity,* 2, 67 – 73.
19. Anatychuk L.I., Kobylianskyi R.R., Konstantynovich I.A. (2013). On the influence of a thermoelectric power source on the accuracy of temperature and heat flux measurement. *J. Thermoelectricity,* 6, 53 – 61.
20. Ivashchuk O.I., Morar I.K., Kobylianskyi R.R., Nepelyak L.V., Deley V.D. (2013). The role of abdominal heat flow in monitoring acute destructive pancreatitis. *Abstracts of scientific and practical conference "Current issues in surgery"*, Chernivtsi, Ukraine, 254 – 259.
21. Kobylianskyi R.R. (2016). The influence of thermal insulation on the readings of thermoelectric medical sensor. *Scientific Herald of Chernivtsi University: Collected papers. Physics. Electronics. Vol. 5, Issue 1.* Chernivtsi: Chernivtsi National University, 45 – 49.
22. Kobylianskyi R.R. (2016). Computer simulation of readings of a medical thermoelectric sensor. *J. Thermoelectricity,* 4, 69 – 77.
23. . Gischuk V.S., Kobylianskyi R.R., Cherkez R.G. (2014). Multichannel device for measuring the temperature and density of heat fluxes. *Scientific Herald of Chernivtsi University: Collected papers. Physics. Electronics. Vol. 3, Issue. 1*. Chernivtsi: Chernivtsi National University, 96 – 100.

24. The use of thermoelectric heat meters in medical diagnostics. *Scientific Herald of Chernivtsi University: Collected papers. Physics. Electronics. Vol. 4, Issue 1.* Chernivtsi: Chernivtsi National University, 90 – 96.
25. Anatychuk L.I., Ivashchuk O.I., Kobylianskyi R.R., Postevka I.D., Bodiaka V.Yu., Gushul I.Ya. (2016). Thermoelectric device for measuring the temperature and density of heat flux "ALTEC-10008". *J. Thermoelectricity*, 1, 76 – 84.
26. Anatychuk L.I., Yuryk O.E., Kobylianskyi R.R., Roy I.V., Fishchenko Ya.V., Slobodianiuk N.P., Yuryk N.E., Duda B.S. (2017). Thermoelectric device for diagnosing inflammatory processes and neurological manifestations of osteochondrosis of the human spine. *J. Thermoelectricity,* 3, 54 – 67.
27. Yuryk O.E., Anatychuk L.I., Roy I.V., Kobylianskyi R.R., Fishchenko Ya.V., Slobodianuk N.P., Yuryk N.E., Duda B.S. (2017). Peculiarities of heat exchange in patients with neurological manifestations of osteochondrosis in the lumbosacral spine. *Trauma*, 18 (6).
28. Anatychuk L.I., Luste O.J, Kobylianskyi R.R. (2017). Information and energy theory of thermoelectric temperature and heat flux sensors for medical purposes. *J. Thermoelectricity,* 4, 5 – 20.
29. Anatychuk L.I., Kobylianskyi R.R., Cherkez R.G., Konstantynovych I.A., Hoshovskyi V.I., Tiumentsev V.A. (2017). Thermoelectric device with electronic control unit for diagnostics of inflammatory processes in the human organism. Tekhnologiya i konstruirovanie v elektronnoi apparature – Technology and Design in Electronic Equipment, 6, 44 – 48.
30. Anatychuk L.I., Ivashchuk O.I., Kobylianskyi R.R., Postevka I.D., Bodiaka V.Yu., Gushul I.Ya., Chuprovska Yu.Ya. (2018). On the influence of ambient temperature on the readings of thermoelectric medical sensors. *Sensor Electronics and Microsystem Technologies*, 15 (1), 17 – 29.
31. Anatychuk L.I., Pasyechnikova N.V., Naumenko V.O., Zadorozhnyi O.S., Havryliuk M.V., Kobylianskyi R.R. (2018). Thermoelectric device for determination of heat flux from the surface of eyes. *J. Thermoelectricity,* 5, 52 – 67.
32. Anatychuk L.I., Kobylianskyi R.R., Konstantynovich I.A. (2014). Calibration of thermoelectric heat flux sensors. *Proc. of XV International scientific and practical conference "Modern information and electronic technologies"* (Odesa, Ukraine, May 26-30, 2014.) Vol. 2, 30 – 31.
33. Anatychuk L.I., Kobylianskyi R.R., Konstantynovich I.A., Lysko V.V., Pugantseva O.V., Rozver Yu.Yu., Tiumentsev V.A. (2016). Calibration bench for thermoelectric heat flux converters. *J. Thermoelectricity,* 5, 71 – 79.
34. Anatychuk L.I., Kobylianskyi R.R., Konstantynovich I.A., Kuz R.V., Manyk O.M., Nitsovich O.V., Cherkez R.G. (2016). Manufacturing technology of thermoelectric microthermopiles. *J. Thermoelectricity,* 6, 49 – 54.
35. Anatychuk L.I., Razinkov V.V., Bukharayeva N.R., Kobylianskyi R.R. (2017). Thermoelectric bracelet. *J. Thermoelectricity,* 2, 58 – 72.
36. Anatychuk L.I., Todurov B.M., Kobylianskyi R.R., Dzhal S.A. (2019). On the use of thermoelectric microgenerators to power pacemakers. *J. Thermoelectricity,* 5, 63 – 88.
37. Anatychuk L.I., Yuryk O.E., Strafun S.S., Stashkevich A.T., Kobylianskyi R.R., Cheviuk A.D., Yuryk N.E., Duda B.S. (2021). Thermometric indicators in patients with chronic low back pain. *J. Thermoelectricity,* 1, 51 – 64.
38. Chunzhi Wang, Hongzhe Jiao, Lukyan Anatychuk, Nataliya Pasyechnikova, Volodymyr Naumenko, Oleg Zadorozhnyy, Lyudmyla Vikhor, Roman Kobylianskyi, Roman Fedoriv, Orest Kochan (2022). Development of a temperature and heat flux measurement system based on

microcontroller and its application in ophthalmology. *Measurement Science Review*, 22 (2), 73 – 79.

39. Kobylianskyi R.R., Prybyla A.V., Konstantynovich I.A., Boychuk V.V. (2022). Results of experimental investigations of thermoelectric medical heat flux sensors, *J. Thermoelectricity*, 3-4, 70 – 83.
40. Yuryk O., Anatychuk L., Kobylianskyi R., Yuryk N. (2023*). Measurement of heat flux density as a new method of diagnosing neurological diseases.* Kharkiv: PC Technology Center, 31 – 68.

Submitted: 01.12.2023.

Кобилянський Р.Р., *канд. фіз.-мат. наук* [1,2]
Лисько В.В., *канд. фіз.-мат. наук* [1,2]
Прибила А.В., *канд. фіз.-мат. наук* [1,2]
Константинович І.А., *канд. фіз.-мат. наук* [1,2]
Кобилянська А.К., *канд. фіз.-мат. наук* [1]
Бухараєва Н.Р., [1]
Бойчук В.В. [1,2]

[1] Інститут термоелектрики НАН та МОН України,
вул. Науки, 1, Чернівці, 58029, Україна;
[2] Чернівецький національний університет імені Юрія Федьковича,
вул. Коцюбинського 2, Чернівці, 58012, Україна
e-mail: anatych@gmail.com

ТЕХНОЛОГІЧНІ РЕЖИМИ ВИГОТОВЛЕННЯ ТЕРМОЕЛЕКТРИЧНИХ СЕНСОРІВ МЕДИЧНОГО ПРИЗНАЧЕННЯ

У роботі наведено технологічні режими виготовлення термоелектричних перетворювачів теплового потоку. Встановлено, що оптимальним термоелектричним матеріалом для термобатареї є низькотемпературні матеріали на основі Bi_2Te_3. Експериментально підтверджено ефективність використання таких технологічних режимів для виготовлення термоелектричних мікробатарей, здатних реєструвати лазерне випромінювання з покращеним коефіцієнтом перетворення в 1 – 1.5 порядки у порівнянні з існуючими вимірювальними перетворювачами. Вказані технологічні режими значно спрощують та механізують методику виготовлення термоелектричних сенсорів теплового потоку медичного призначення та мікрогенераторів для живлення малопотужної медичної апаратури.

Ключові слова: технологічний режим, термоелектричний перетворювач, термоелектричний сенсор теплового потоку медичного призначення.

Література

1. Анатичук Л.І. Термоелектрика. Т.2. Термоелектричні перетворювачі енергії. Київ, Чернівці: Інститут термоелектрики, 2003. – 376 с.
2. Anatychuk L.I. (1998). *Thermoelectricity. Vol.1. Physics of thermoelectricity*. Kyiv, Chernivtsi: Institute of Thermoelectricity.

3. Анатичук Л.І. Сучасний стан і деякі перспективи термоелектрики // Термоелектрика. – 2007. – № 2. – С. 7 – 20.
4. Демчук Б.М., Кушнерик Л.Я., Рубленик І.М. Термоелектричні датчики для ортопедії.// Термоелектрика. – 2002. – №4. – С. 80 – 85.
5. Патент України 53104 А. Датчик для попередньої діагностики запальних процесів молочних залоз // А.А. Ашеулов, А.В. Клепіковський, Л.Я. Кушнерик та ін. – 2003.
6. Ащеулов А.А., Кушнерик Л.Я. Термоелектричний прилад для медико-біологічної експрес-діагностики // Технологія та конструювання в електронній апаратурі. – №4. – 2004. – С. 38 – 39.
7. Пат. 71619 Україна, МПК H01L 35/00. Термоелектричний медичний тепломір / Анатичук Л.І., Кобилянський Р.Р.; Інститут термоелектрики. – № u 2011 14007; заявл. 28.11.11; опубл. 25.07.12, Бюл. № 14.
8. Пат. 72032 Україна, МПК H01L 35/00. Термоелектричний сенсор для вимірювання температури і теплового потоку / Анатичук Л.І., Кобилянський Р.Р.; Інститут термоелектрики. – № u 2011 14005; заявл. 28.11.11; опубл. 10.08.12, Бюл. № 15.
9. Пат. 73037 Україна, МПК H01L 35/02. Термоелектричний медичний пристрій / Микитюк П.Д., Кобилянський Р.Р., Слепенюк Т.В.; Інститут термоелектрики. – № u 2012 01922; заявл. 20.02.12; опубл. 10.09.12, Бюл. № 17.
10. Пат. 78619 Україна, МПК H01L 35/00. Метод визначення густини теплового потоку / Анатичук Л.І., Кобилянський Р.Р.; Інститут термоелектрики. – № u 2012 11018; заявл. 21.09.12; опубл. 25.03.13, Бюл. № 6.
11. Пат. 79929 Україна, МПК H01L 35/00. Термоелектричний перетворювач теплового потоку для градієнтних тепломірів / Анатичук Л.І.; Інститут термоелектрики. – № u 2012 11857; заявл. 15.10.12; опубл. 13.05.13, Бюл. № 9.
12. Гищук В.С. Електронний регістратор сигналів сенсорів теплового потоку людини // Термоелектрика. − № 4. – 2012. – С. 105 – 108.
13. Гищук В.С. Електронний регістратор з обробкою сигналів термоелектричного сенсора теплового потоку // Термоелектрика. − № 1. – 2013. – С. 82 – 86.
14. Гищук В.С Модернізований прилад для вимірювання теплових потоків людини // Термоелектрика. – №2. – 2013. – С. 91 – 95.
15. Анатичук Л.І., Кобилянський Р.Р. Дослідження впливу термоелектричного тепломіра на визначення тепловиділення людини // Термоелектрика. − № 4. – 2012. – С. 60 – 66.
16. Анатичук Л.І., Кобилянський Р.Р. 3D-модель для визначення впливу термоелектричного тепломіра на точність вимірювання тепловиділення людини // Науковий вісник Чернівецького університету: збірник наук. праць. Фізика. Електроніка. – Т. 2, Вип. 1. – Чернівці: Чернівецький національний університет, 2012. – С. 15 – 20.
17. Анатичук Л.І., Кобилянський Р.Р. Комп’ютерне моделювання показів термоелектричного тепломіра в умовах реальної експлуатації // Термоелектрика. − № 1. – 2013. – С. 53 – 60.
18. Анатичук Л.І., Гіба Р.Г., Кобилянський Р.Р. Про деякі особливості використання медичних тепломірів при дослідженні локальних тепловиділень людини // Термоелектрика. − № 2. – 2013. – С. 67 – 73.
19. Анатичук Л.І., Кобилянський Р.Р., Константинович І.А. Про вплив термоелектричного джерела живлення на точність вимірювання температури і теплового потоку // Термоелектрика. − № 6. – 2013. – С. 53 – 61.

20. Іващук О.І., Морар І.К., Кобилянський Р.Р., Непеляк Л.В., Делей В.Д. Роль теплового потоку черевної порожнини в моніторингу гострого деструктивного панкреатиту // Збірник тез науково-практичної конференції "Актуальні питання хірургії", м. Чернівці, Україна. – 2013. – С. 254 – 259.
21. Кобилянський Р.Р. Про вплив теплової ізоляції на покази термоелектричного сенсора медичного призначення // Науковий вісник Чернівецького університету: збірник наук. праць. Фізика. Електроніка. – Т. 5, Вип. 1. – Чернівці: Чернівецький національний університет, 2016. – С. 45 – 49.
22. Кобилянський Р.Р. Комп'ютерне моделювання показів термоелектричного сенсора медичного призначення // Термоелектрика. − № 4. – 2016. – С. 69 – 77.
23. Гищук В.С., Кобилянський Р.Р., Черкез Р.Г. Багатоканальний прилад для вимірювання температури і густини теплових потоків // Науковий вісник Чернівецького університету: збірник наук. праць. Фізика. Електроніка. – Т. 3, Вип. 1. – Чернівці: Чернівецький національний університет, 2014. – С. 96 – 100.
24. Кобилянський Р.Р., Бойчук В.В. Використання термоелектричних тепломірів у медичній діагностиці // Науковий вісник Чернівецького університету: збірник наук. праць. Фізика. Електроніка. – Т. 4, Вип. 1. – Чернівці: Чернівецький національний університет, 2015. – С. 90 – 96.
25. Анатичук Л.І., Іващук О.І., Кобилянський Р.Р., Постевка І.Д., Бодяка В.Ю., Гушул І.Я. Термоелектричний прилад для вимірювання температури і густини теплового потоку "АЛТЕК-10008" // Термоелектрика. − № 1. – 2016. – С. 76 – 84.
26. Анатичук Л.І., Юрик О.Є., Кобилянський Р.Р., Рой І.В., Фіщенко Я.В., Слободянюк Н.П., Юрик Н.Є., Дуда Б.С. Термоелектричний прилад для діагностики запальних процесів та неврологічних проявів остеохондрозу хребта людини // Термоелектрика. − № 3. – 2017. – С. 54 – 67.
27. Юрик О.Є., Анатичук Л.І., Рой І.В., Кобилянський Р.Р., Фіщенко Я.В., Слободянюк Н.П., Юрик Н.Є., Дуда Б.С. Особливості теплового обміну у пацієнтів з неврологічними проявами остеохондрозу в попереково-крижовому відділі хребта // Травма. − Т.18. – № 6. – 2017.
28. Анатичук Л.І., Лусте О.Я., Кобилянський Р.Р. Інформаційно-енергетична теорія термоелектричних сенсорів температури і теплового потоку медичного призначення // Термоелектрика. − № 4. – 2017. – С. 5 – 20.
29. Anatychuk L.I., Kobylianskyi R.R., Cherkez R.G., Konstantynovych I.A., Hoshovskyi V.I., Tiumentsev V.A. (2017). Thermoelectric device with electronic control unit for diagnostics of inflammatory processes in the human organism. Tekhnologiya i konstruirovanie v elektronnoi apparature – Technology and Design in Electronic Equipment, 6, 44 – 48.
30. Анатичук Л.І., Іващук О.І., Кобилянський Р.Р., Постевка І.Д., Бодяка В.Ю., Гушул І.Я., Чупровська Ю.Я. Про вплив температури навколишнього середовища на покази термоелектричних сенсорів медичного призначення // Сенсорна електроніка і мікросистемні технології. − Т. 15. – № 1. – 2018. – С. 17 – 29.
31. Анатичук Л.І., Пасєчнікова Н.В., Науменко В.О., Задорожний О.С., Гаврилюк М.В., Кобилянський Р.Р. Термоелектричний прилад для визначення теплового потоку з поверхні очей // Термоелектрика. − № 5. – 2018. – С. 52 – 67.
32. Анатичук Л.І., Кобилянський Р.Р., Константинович І.А. Градуювання термоелектричних сенсорів теплового потоку // Труди XV Міжнародної науково-практичної конференції

«Сучасні інформаційні та електронні технології» 26-30 травня 2014 року. – Т. 2. – Одеса, Україна. – 2014. – С. 30 – 31.

33. Анатичук Л.І., Кобилянський Р.Р., Константинович І.А., Лисько В.В., Пуганцева О.В., Розвер Ю.Ю., Тюменцев В.А. Стенд для градуювання термоелектричних перетворювачів теплового потоку // Термоелектрика. − № 5. – 2016. – С. 71 – 79.
34. Анатичук Л.І., Кобилянський Р.Р., Константинович І.А., Кузь Р.В., Маник О.М., Ніцович О.В., Черкез Р.Г. Технологія виготовлення термоелектричних мікробатарей // Термоелектрика. − № 6. – 2016. – С. 49 – 54.
35. Анатичук Л.І., Разіньков В.В., Бухараєва Н.Р., Кобилянський Р.Р. Термоелектричний браслет // Термоелектрика. − № 2. – 2017. – С. 58 – 72.
36. Анатичук Л.І., Тодуров Б.М., Кобилянський Р.Р., Джал С.А. Про використання термоелектричних мікрогенераторів для живлення електрокардіостимуляторів // Термоелектрика. − № 5. – 2019. С. 63 – 88.
37. Анатичук Л.І., Юрик О.Є., Страфун С.С., Сташкевич А.Т., Кобилянський Р.Р., Чев'юк А.Д., Юрик Н.Є., Дуда Б.С. Теплометричні показники у пацієнтів з хронічним болем у попереку // Термоелектрика. − № 1. – 2021. С. 51 – 64.
38. Chunzhi Wang, Hongzhe Jiao, Lukyan Anatychuk, Nataliya Pasyechnikova, Volodymyr Naumenko, Oleg Zadorozhnyy, Lyudmyla Vikhor, Roman Kobylianskyi, Roman Fedoriv, Orest Kochan (2022). Development of a temperature and heat flux measurement system based on microcontroller and its application in ophthalmology. *Measurement Science Review*, 22 (2), 73 – 79.
39. Кобилянський Р.Р., Прибила А.В., Константинович І.А., Бойчук В.В. Результати експериментальних досліджень термоелектричних медичних сенсорів теплового потоку // Термоелектрика №3-4. – 2022. С. 70 – 83.
40. Yuryk O., Anatychuk L., Kobylianskyi R., Yuryk N. (2023*). Measurement of heat flux density as a new method of diagnosing neurological diseases.* Kharkiv: PC Technology Center, 31 – 68.

Надійшла до редакції: 01.12.2023.

O.S. Kshevetsky, *Cand. Sc (Phys-Math)* [1]
R.G. Cherkez, *DSc (Phys-Math)* [1,2]
Yu.I. Mazar [1]

[1] Institute of Thermoelectricity of the NAS and MES of Ukraine,
1 Nauky str., Chernivtsi, 58029, Ukraine;
[2] Yuriy Fedkovych Chernivtsi National University, 2 Kotsiubynskyi str.,
Chernivtsi, 58000, Ukraine
e-mail: anatych@gmail.com

ESTIMATION OF THE EFFICIENCY OF PARTIAL CASE OF HEAT AND MASS TRANSFER PROCESSES BETWEEN HEAT PUMPS AND MOVING SUBSTANCE. PART 4

A theoretical model is presented for estimating the efficiency of a partial case of processes in which there is thermal contact of a moving substance (or at least part of this moving substance) with the heat-absorbing and heat-releasing heat-exchange parts of at least two heat pumps for the case of heating the moving substance in its input flow by all individual heat pumps. Mathematical expressions for the corresponding estimation calculations and examples of the results of such calculations are presented.
Key words: heat pump, moving substance, heat and mass transfer, efficiency, energy efficiency, thermoelectric heat pump, thermoelements.

Introduction

This work (part 4) is a continuation of the previous works [1, 2, 3] (parts 1 – 3). In this part 4 we will use the notations, abbreviations (in particular, word combinations) and acronyms that were introduced in [1, 2, 3], in the same meaning as in [1, 2, 3]. In [3], mathematical expressions were obtained to assess the efficiency of the investigated heat and mass transfer method and examples of corresponding calculations were given for the case of cooling the MS in its input flow by all individual THPs, provided that $T_{1.n}^{PP} = T_{2.n}^{PP}$ according to Fig. 2 [1] (the case of heating the MS in its input flow by all individual THPs is not considered in [3]).

The purpose of this work is to create theoretical prerequisites for an approximate quantitative estimation of the efficiency (primarily energy efficiency) of the *investigated heat and mass transfer method* [1 – 6] using THPs, which can operate in different modes, for the case of heating of the MS in its input flow by all individual THPs according to Fig. 3 [1].

To achieve this goal, the *objectives of this work* are to create an estimation model, obtain mathematical expressions for estimation calculations and obtain examples of corresponding calculations for the case of heating the MS in its input flow by all individual THPs according to Fig. 3 [1], in particular, for the case when $T_{1.n}^{PP} \neq T_{2.n}^{PP}$.

Description of estimation model and equations for estimation calculations

Let us consider the following example of the *investigated processes*. Consider processes involving a MS and at least one THP (all HPs used in these processes are THPs based on thermoelements [7]), in which, according to Fig. 3 [1], the MS in its input flow is heated by all the THPs taken separately. Let the useful effect of these processes be to maintain the temperature difference of the MS in its input flow between positions 1.0 and 1.n according to Fig. 3 [1] (for some inlet temperature of MS in position 1.0). This useful action is carried out due to the total electrical power consumed by all THPs W^{TTH} (and more directly due to the total heat output of all THPs Q_{hot}^{TTH}). In this work (part 4), we will not take into account the energy consumption for creating the MS flow.

Let us consider the *i*-th THP separately.

We use the well-known ratio to determine the heating coefficient μ_i^{TE} of the thermoelements of the *i*-th THP [18]:

$$\mu_i^{TE} = \frac{Q_{hot,i}^{TE}}{W_i^{TE}}, \tag{4.1}$$

where

$$Q_{hot,i}^{TE} = \alpha_i I_i T_{hot,i}^{TE} + \frac{1}{2} I_i^2 r_i - k_i \left(T_{hot,i}^{TE} - T_{cool,i}^{TE} \right); \tag{4.2}$$

$$W_i^{TE} = I_i^2 r_i + \alpha_i \left(T_{hot,i}^{TE} - T_{cool,i}^{TE} \right) I_i; \tag{4.3}$$

$Q_{hot,i}^{TE}$ is general (total) heat productivity of thermoelements of the *i*-th THP; W_i^{TE} is general (total) electric power consumed by thermoelements of the *i*-th THP; α_i is general (total) differential Seebeck coefficient of the material of thermoelements of the *i*-th THP; I_i is the strength of the current flowing through thermoelements of the *i*-th THP; r_i is general (total) electric resistance of thermoelements of the *i*-th THP; k_i is general (total) thermal conductivity of thermoelements of the *i*-th THP; $T_{hot,i}^{TE}$ is temperature of the heat releasing junctions of thermoelements of the *i*-th THP; $T_{cool,i}^{TE}$ is temperature of the heat absorbing junctions of thermoelements of the *i*-th THP.

Heating coefficient of the *i*-th THP operating in the *investigated process* according to Fig. 3 [1] and with regard to assumption 6 [1] ($d = const$) μ_i^{TTH}:

$$\mu_i^{TTH} = \frac{Q_{hot,i}^{TTH}}{W_i^{TTH}} = \frac{T_{hot,i}^{PP} - T_{hot,(i-1)}^{PP}}{\left(T_{hot,i}^{PP} - T_{hot,(i-1)}^{PP} \right) - \left(T_{cool,i}^{PP} - T_{cool,(i-1)}^{PP} \right)}, \tag{4.4}$$

where $Q_{hot,i}^{\text{TTH}}$ is heat productivity of the *i*-th THP; W_i^{TTH} is power consumed by the *i*-th THP; $T_{hot,i}^{PP}$ is temperature of the MS immediately after its TC with the heat releasing HE of the *i*-th THP; $T_{hot,(i-1)}^{PP}$ is temperature of the MS immediately before its TC with the heat releasing HE of the *i*-th THP; $T_{cool,i}^{PP}$ is temperature of the MS immediately before its TC with the heat absorbing HE of the *i*-th THP; $T_{cool,(i-1)}^{PP}$ is temperature of the MS immediately after its TC with the heat absorbing HE of the *i*-th THP.

Let $Q_{hot,i}^{\text{TTH}} = Q_{hot,i}^{TE}$ and $W_i^{TTH} = W_i^{TE}$. Then, on the basis of equations (4.1) and (4.4) it can be written:

$$\mu_i^{TE} = \mu_i^{TTH}, \tag{4.5}$$

$$\frac{T_{hot,i}^{PP}-T_{hot,(i-1)}^{PP}}{\left(T_{hot,i}^{PP}-T_{hot,(i-1)}^{PP}\right)-\left(T_{cool,i}^{PP}-T_{cool,(i-1)}^{PP}\right)}=\frac{\alpha_i I_i T_{hot,i}^{TE}+\frac{1}{2}I_i^2 r_i-k_i\left(T_{hot,i}^{TE}-T_{cool,i}^{TE}\right)}{I_i^2 r_i+\alpha_i\left(T_{hot,i}^{TE}-T_{cool,i}^{TE}\right)I_i}. \quad (4.6)$$

We will assume that the heat transfer from the heat releasing junctions of the thermoelements of the *i*-th THP to the MS is carried out through a medium characterized by the corresponding heat transfer resistance (thermal resistance) $R_{hot,i}$, and the heat transfer from the MS to the heat-absorbing junctions of the thermoelements of the *i*-th THP is carried out through a medium characterized by the corresponding heat transfer resistance (thermal resistance) $R_{cool,i}$. We will also assume that there are no other additional factors that could affect the heat exchange between the MS and the *i*-th THP. Then we can write the following equations, which, in particular, reflect the relationship between the junction temperatures of the thermoelements of the *i*-th THP and the MS (in the corresponding positions of its movement):

$$T_{hot,i}^{TE}-T_{hot,i}^{PP}=Q_{hot,i}^{TE}R_{hot,i}, \quad (4.7)$$

$$T_{hot,i}^{TE}-T_{hot,i}^{PP}=\left(\alpha_i I_i T_{hot,i}^{TE}+\frac{1}{2}I_i^2 r_i-k_i\left(T_{hot,i}^{TE}-T_{cool,i}^{TE}\right)\right)R_{hot,i} \quad (4.8)$$

(Eq. (4.8) was obtained using Eq. (4.2));

$$T_{cool,(i-1)}^{PP}-T_{cool,i}^{TE}=Q_{cool,i}^{TE}R_{cool,i}, \quad (4.9)$$

$$T_{cool,(i-1)}^{PP}-T_{cool,i}^{TE}=\left(\alpha_i I_i T_{cool,i}^{TE}-\frac{1}{2}I_i^2 r_i-k_i\left(T_{hot,i}^{TE}-T_{cool,i}^{TE}\right)\right)R_{cool,i}, \quad (4.10)$$

where $Q_{cool,i}^{TE}$ is general (total) cooling capacity of thermoelements of the *i*-th THP ($Q_{cool,i}^{TE}=\alpha_i I_i T_{cool,i}^{TE}-\frac{1}{2}I_i^2 r_i-k_i\left(T_{hot,i}^{TE}-T_{cool,i}^{TE}\right)$ [8]).

Taking into account assumption 6 [1] and the information given above, we write an equation that, in particular, reflects the relationship between the general (total) heating capacity of the thermoelements of the *i*-th THP, the change in the temperature of the MS as a result of its TC with the heat-generating HE of the *i*-th THP, and the heat capacity flow rates of the MS, V_C^{PP} [3]:

$$V_C^{PP}\left(T_{hot,i}^{PP}-T_{hot,(i-1)}^{PP}\right)=\alpha_i I_i T_{hot,i}^{TE}+\frac{1}{2}I_i^2 r_i-k_i\left(T_{hot,i}^{TE}-T_{cool,i}^{TE}\right). \quad (4.11)$$

Taking into account assumption 6 [1] and the information given above, we write an equation that, in particular, reflects the relationship between the general (total) cooling capacity of the thermoelements of the *i*-th THP, the change in the temperature of the MS as a result of its TC with the heat-absorbing HE of the *i*-th THP, and the heat capacity flow rates of the MS:

$$V_C^{PP}\left(T_{cool,i}^{PP}-T_{cool,(i-1)}^{PP}\right)=\alpha_i I_i T_{cool,i}^{TE}-\frac{1}{2}I_i^2 r_i-k_i\left(T_{hot,i}^{TE}-T_{cool,i}^{TE}\right). \quad (4.12)$$

Taking into account assumption 6 [1] and the information provided above, we write an equation that, in particular, reflects the relationship between the general (total) power consumption of thermoelements of the *i*-th THP, the total change in the temperature of the MS as a result of its TC with the heat-absorbing and heat-releasing HE of the *i*-th THP, and the heat capacity flow rates of the MS:

$$V_C^{PP}\left(\left(T_{hot,i}^{PP}-T_{hot,(i-1)}^{PP}\right)-\left(T_{cool,i}^{PP}-T_{cool,(i-1)}^{PP}\right)\right)=I_i^2 r_i+\alpha_i\left(T_{hot,i}^{TE}-T_{cool,i}^{TE}\right)I_i. \quad (4.13)$$

In this paper (part 4) we will consider that the values $R_{hot,i}$, $R_{cool,i}$, α_i, r_i, k_i are temperature independent.

Eqs. (4.6), (4.7), (4.9), (4.11), (4.12), (4.13) can be used for estimation calculations of the operating modes of individual THPs and *the investigated processes* in general.

For the example described above, we will use the energy efficiency indicator of the investigated process ω_{hot}:

$$\omega_{hot} = \frac{Q_{hot}^{\mathrm{TTH}}}{W^{TTH}} = \frac{\Delta T_{hot}^{PP}}{\Delta T_{hot}^{PP} - \Delta T_{cool}^{PP}} \tag{4.15}$$

(the right-hand side of this expression was obtained using Eqs. (1), (54) and (55) [1]), where ΔT_{hot}^{PP} – according to the diagram in Fig. 3 [1], is the temperature difference of the MS, which is formed as a result of heating the MS in its input flow by all individual THPs; ΔT_{cool}^{PP} – according to the diagram in Fig. 3 [1], the temperature difference of the MS, which is formed as a result of cooling the MS in its output flow by all individual THPs.

Note that when only one THP is used in the *investigated process*, then ω_{hot} is equal to the heating coefficient of this single THP μ_1^{TTH} [9 – 11].

To implement one of the objectives of this work, some estimation calculations were carried out using the estimation model and equations for estimation calculations described above.

Results of estimated calculations and their features

The initial data and some results of the corresponding calculations, which are relevant to the example of the investigated process considered in this work, are presented (in abbreviated form) in Table 4.1. The column headings of Table 4.1 contain, sequentially, from top to bottom, a text description of the corresponding quantities, their symbolic designation (if any) and dimension (if any), which are separated by dotted lines. In Table 4.1, the initial data and calculation results are marked with different colors (the initial data are in this color, and the calculation results are in this other color).

Also, information about calculations is presented in Figs. 4.1 – 4.7.

For all cases of the considered example, the total temperature difference of the MS in its input flow according to Eq. (54) [1] and the diagram in Fig. 3 [1] is the same and equal to 5 *K*:

$$\Delta T_1^{PP} = \Delta T_{hot}^{PP} = 5\ K\ . \tag{4.16}$$

Also, for all cases of the considered example, the inlet temperature of the MS is the same according to Fig. 3 [1]:

$$T_{1.0}^{PP} = 298.15\ K\ . \tag{4.17}$$

In those cases of the considered example when several THPs are used, these several THPs are the same (the values of α_i, r_i, k_i, $R_{hot,i}$ and $R_{cool,i}$ for all these THPs are the same), and also for all these THPs the strength of current flowing through them, I_i is the same.

Let us assume that for the implementation of *the investigated process* according to the diagram in Fig. 3 [1] there is a THP with known given parameters, for example, those given in Table 4.1 for the 1st or 2nd or 5th cases of the considered example of the *investigated heat and mass transfer method.* Fixed temperature $T_{1.n}^{PP}$ and temperature difference $\Delta T_1^{PP} = \Delta T_{hot}^{PP} = 5\ K$ are also specified (4.16). Heat capacity flow rates of MS can change (are not fixed). Examples of calculated results for such cases are presented in Table 4.1 (1st, 2nd and 5th cases) and in Figs 4.1 - 4.6 (for initial data corresponding to the 1st and 2nd cases in Table 4.1).

Table 4.1

Initial data and some results of corresponding estimation calculations of the efficiency of the investigated heat and mass transfer method with the use of THP for the case of heating the MS in its input flow by all individual THPs (according to Fig. 3 [1]*; according to assumptions 1, 2, 4-7* [1]*;* $T_{1.0}^{PP} = 298.15\ K$ *)*

Case number of the example under consideration	Total number of THPs n	Thermoelectric figure of merit of thermoelements of each individual i-th THP	Total differential Seebeck coefficient of the material (legs) of the thermoelements of each individual i-th THP	Total electrical resistance of thermoelements of each individual i-th THP	Total thermal conductivity of the thermoelement legs of each individual i-th THP	Current flowing through each thermoelement of each individual i-th THP	Total resistance of heat transfer from the heat releasing junctions of the thermoelements of each individual i-th THP to the MS	Total resistance of heat transfer from the MS to the heat absorbing junctions of the thermoelements of each individual i-th THP	Heat capacity flow rates of the MS	MS temperature in position 1.n	MS temperature in position 2.n	Temperature difference across thermoelements of the nth THP	Heating coefficient of thermoelements of the nth THP	Energy efficiency indicator of *the investigated process*
l	n	z_i	α_i	r_i	k_i	I_i	$R_{hot.i}$	$R_{cool.i}$	V_C^{PP}	$T_{1.n}^{PP}$	$T_{2.n}^{PP}$	ΔT_n^{TE}	μ_n^{TE}	ω_{hot}
		1/K	V	Ohm	W/K	A	K/W	K/W	W/K	K	K	K		
1(1)	1	0.0026	0.048	2.6	0.34	0.2422	0.1	0.1	0.3917	303.15	303.15	4.8377	9.379 (1)	9.379 (1)
2(1)	1	0.0026	0.048	1.3	0.68	0.4749	0.1	0.1	0.7185	303.15	303.15	5.1074	8.77 (1)	8.77 (1)
3(2)	1	0.0026	0.048	3.082	0.287	0.2245	0.1	0.1	0.3917	303.15	303.15	4.8411	9.436 (2)	9.436 (2)
4(2)	1	0.0026	0.048	1.783	0.496	0.4106	0.1	0.1	0.7185	303.15	303.15	5.1197	8.951 (2)	8.951 (2)
5(1)	1	0.0026	0.048	2.6	0.34	0.2913	0.1	0.1	0.4755	303.15	302.15	5.8103	7.874 (1)	7.874 (1)
6(2)	1	0.0026	0.048	3.692	0.239	0.2227	0.1	0.1	0.3917	303.15	302.15	5.7432	8.013 (2)	8.013 (2)
7(2)	2	0.0026	0.048	3.077	0.287	0.1153	0.1	0.1	0.3917	303.15	303.15	2.5301	17.7	17.923 (2)
8	1	0.0027	0.048	1.008	0.847	0.403	0.1	0.1	0.3917	303.15	303.15	4.7153	7.682	7.682
9	2	0.0027	0.048	1.008	0.847	0.2079	0.1	0.1	0.3917	303.15	303.15	2.4649	14.1	14.443
10	8	0.0026	0.048	3.232	0.274	0.0288	0.1	0.1	0.3917	303.15	303.15	0.6555	67.236	68.748

(1) the value of V_C^{PP} is selected and specified such that the maximum value of ω_{hot} is achieved; (2) the value of r_i (and k_i) is selected and specified such that the maximum value of ω_{hot} is achieved.

Now let us assume that it is necessary to implement *the investigated process* according to the diagram in Fig. 3 [1], for which a fixed temperature $T_{1.n}^{PP}$, a fixed temperature difference $\Delta T_1^{PP} = \Delta T_{hot}^{PP} = 5\ K$ (4.16), fixed heat capacity flow rates of the MS, a fixed thermoelectric figure of merit of thermoelements of each individual ith *THP* z_i and a fixed total differential Seebeck coefficient of material (legs) of thermoelements of each individual ith *THP* are given, for instance, those given in Table 4.1 for the 3d or 4th or 6th or 7th cases of the considered example *of the investigated heat and mass transfer method*. At the same time, the values of r_i and, accordingly, k_i are not fixed and cannot be selected (calculated) to achieve the maximum value of ω_{hot}. Examples of calculated results for such cases are presented in Table 4.1 (3rd, 4th, 6th and 7th cases) and in Fig. 4.7 (for the initial data corresponding to the 3rd and 7th cases in Table 4.1; Fig. 4.7 shows, in particular, some calculated results that are not in Table 4.1).

For the 8th, 9th and 10th cases of the considered example of *the investigated heat and mass transfer method* according to Table 4.1, optimization was not carried out.

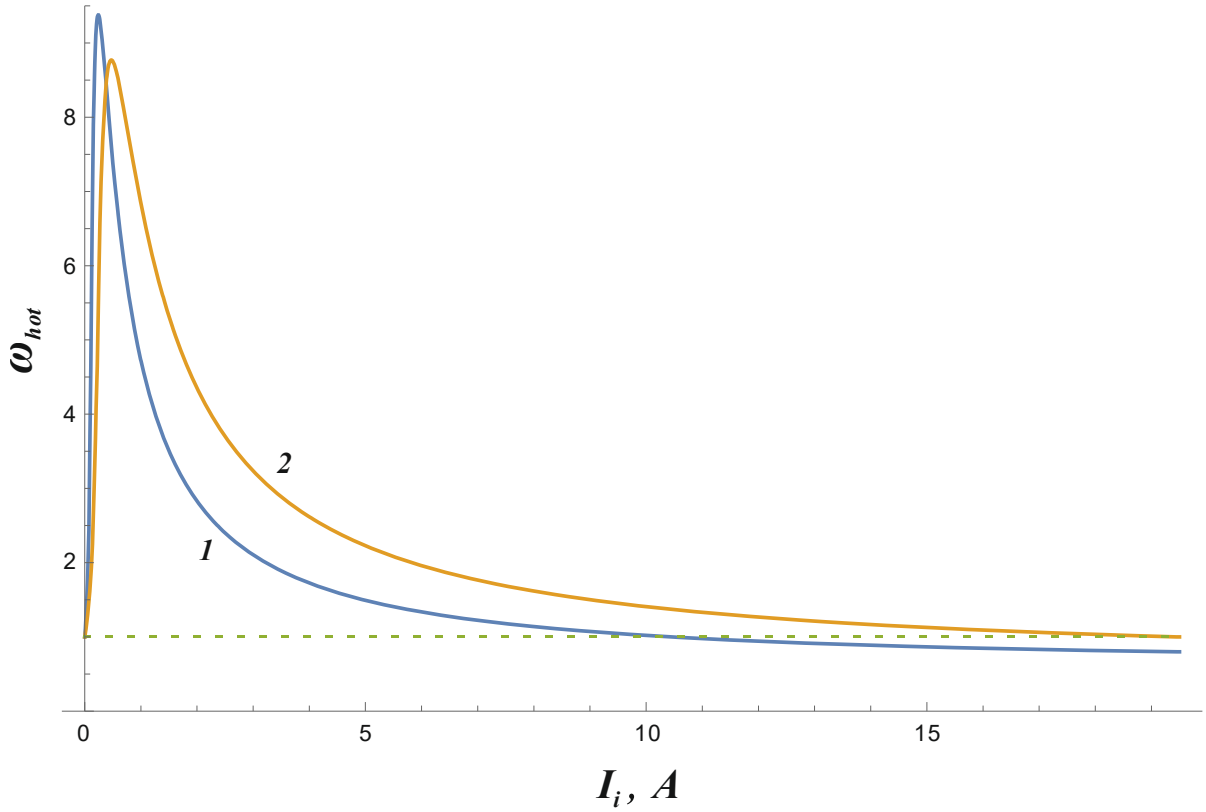

Fig. 4.1. Plots of dependence of ω_{hot} on I_i of the considered example of the investigated process for the initial data that correspond to the 1st and 2nd cases in Table 4.1 ($\Delta T_{hot}^{PP} = const = 5\ K$, $V_C^{PP} \neq const$): 1 – for the initial data of the 1st case from Table 4.1, 2 – for the initial data of the 2nd case from Table 4.1.

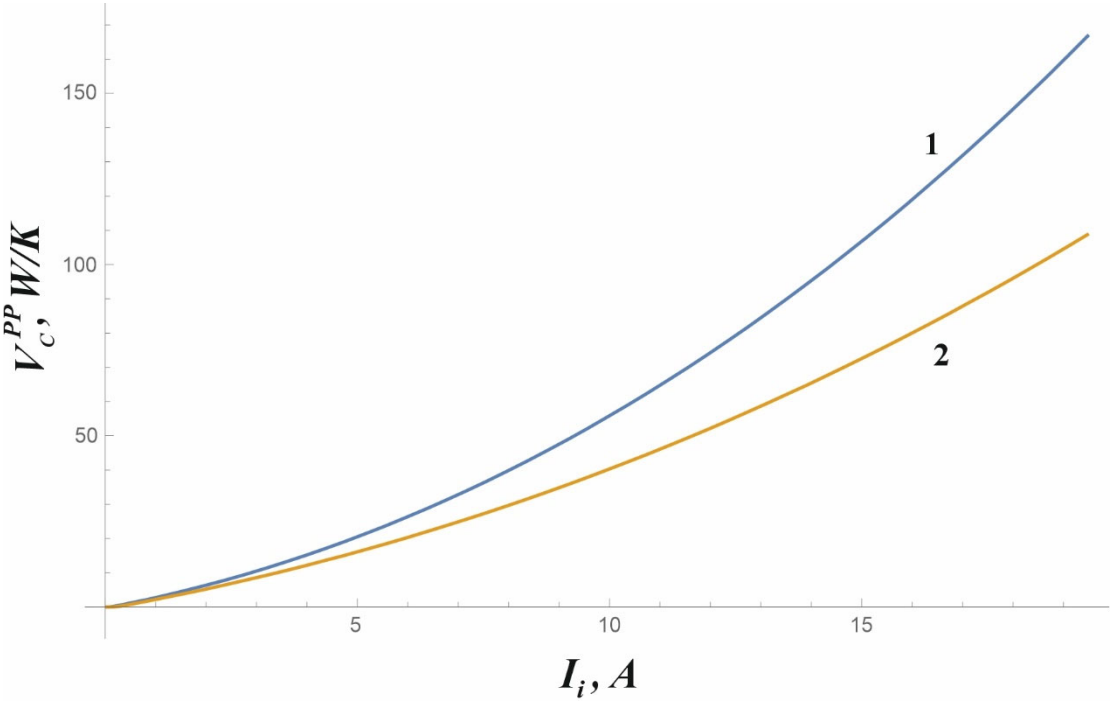

Fig. 4.2. Plots of dependence of V_C^{PP} on I_i of the considered example of the investigated process for the initial data that correspond to the 1st and 2nd cases in Table 4.1 ($\Delta T_{hot}^{PP} = const = 5$ K): 1 –for the initial data of the 1st case from Table 4.1, 2 – for the initial data of the 2nd case from Table 4.1.

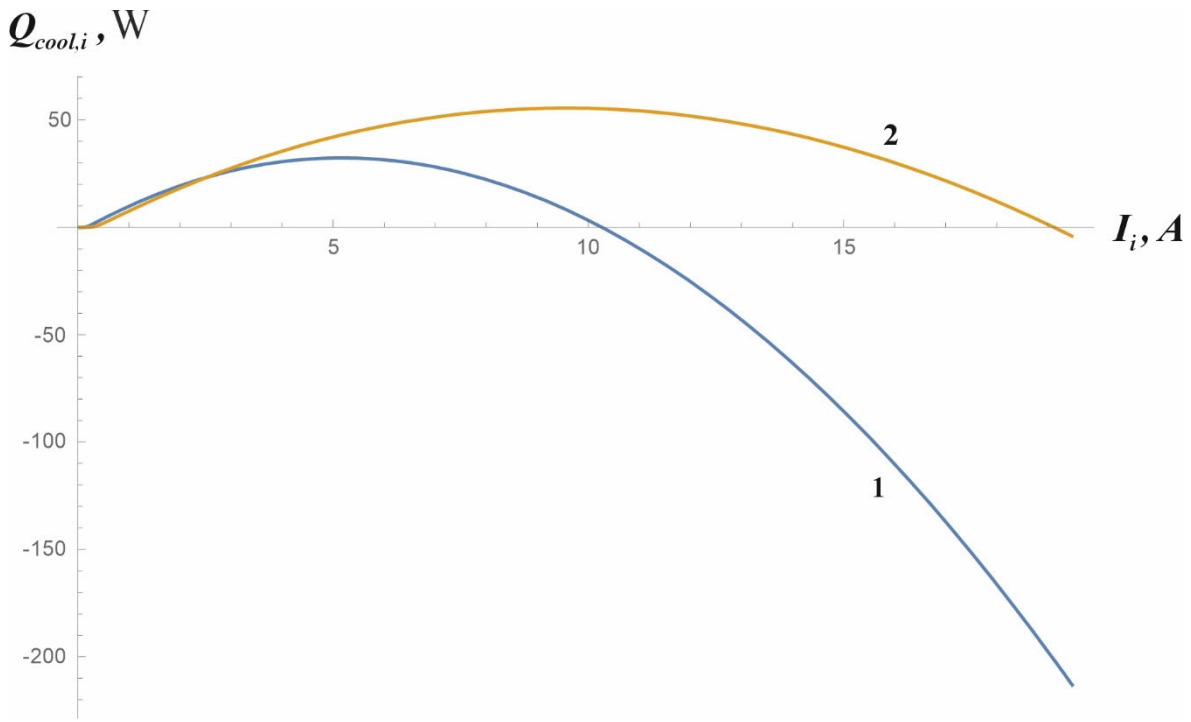

Fig. 4.3. Plots of dependence of heat flow from the MS to the heat absorbing junctions of thermoelements of the i^{th} THP $Q_{cool,i}$ on I_i of the considered example of the investigated process for the initial data that correspond to the 1st and 2nd cases in Table 4.1 ($\Delta T_{hot}^{PP} = const = 5$ K, $V_C^{PP} \neq const$): 1 – for the initial data of the 1st case from Table 4.1, 2 – for the initial data of the 2nd case from Table 4.1.

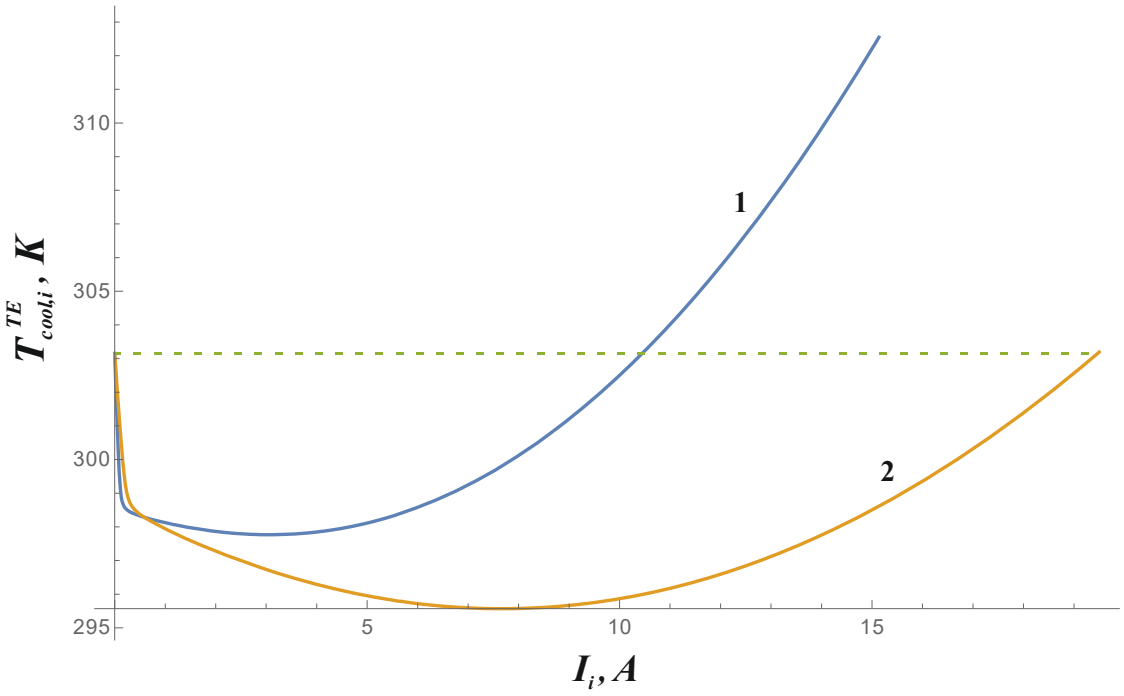

Fig. 4.4. Plots of dependence of $T^{TE}_{cool,i}$ on I_i of the considered example of the investigated process for the initial data that correspond to the 1st and 2nd cases in Table 4.1 ($\Delta T^{PP}_{hot} = const = 5\ K$, $V^{PP}_C \neq const$): 1 – for the initial data of the 1st case from Table 4.1, 2 – for the initial data of the 2nd case from Table 4.1.

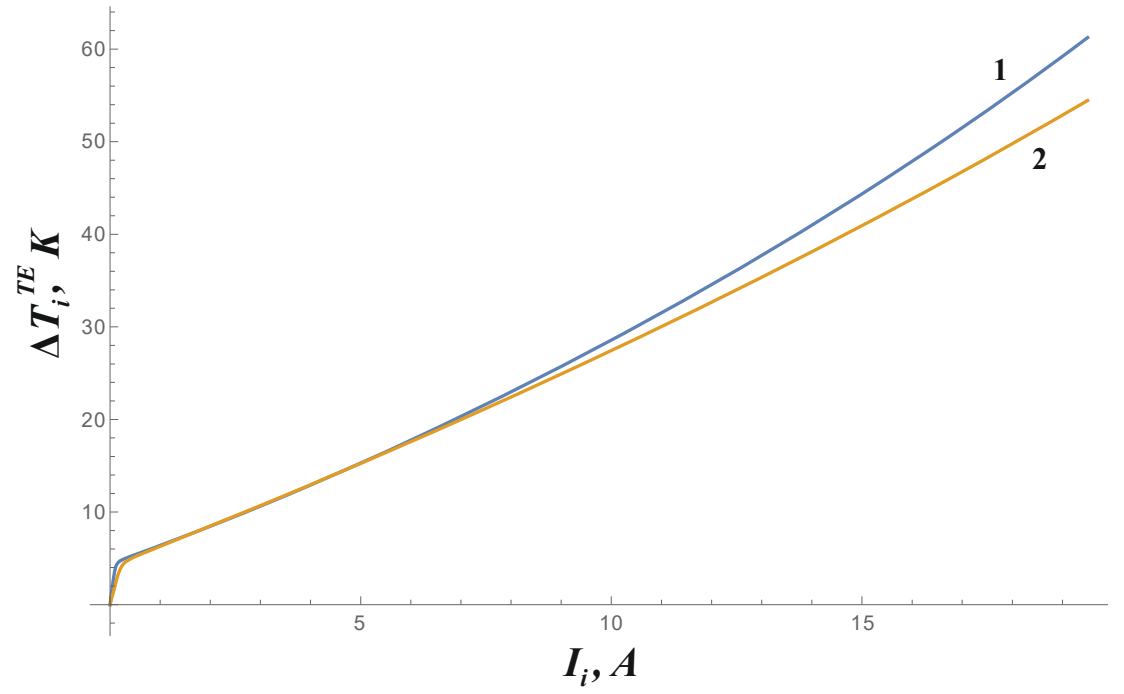

Fig 4.5. Plots of dependence of ΔT^{TE}_i on I_i of the considered example of the investigated process for the initial data that correspond to the 1st and 2nd cases in Table 4.1 ($\Delta T^{PP}_{hot} = const = 5\ K$, $V^{PP}_C \neq const$): 1 – for the initial data of the 1st case from Table 4.1, 2 – for the initial data of the 2nd case from Table 4.1.

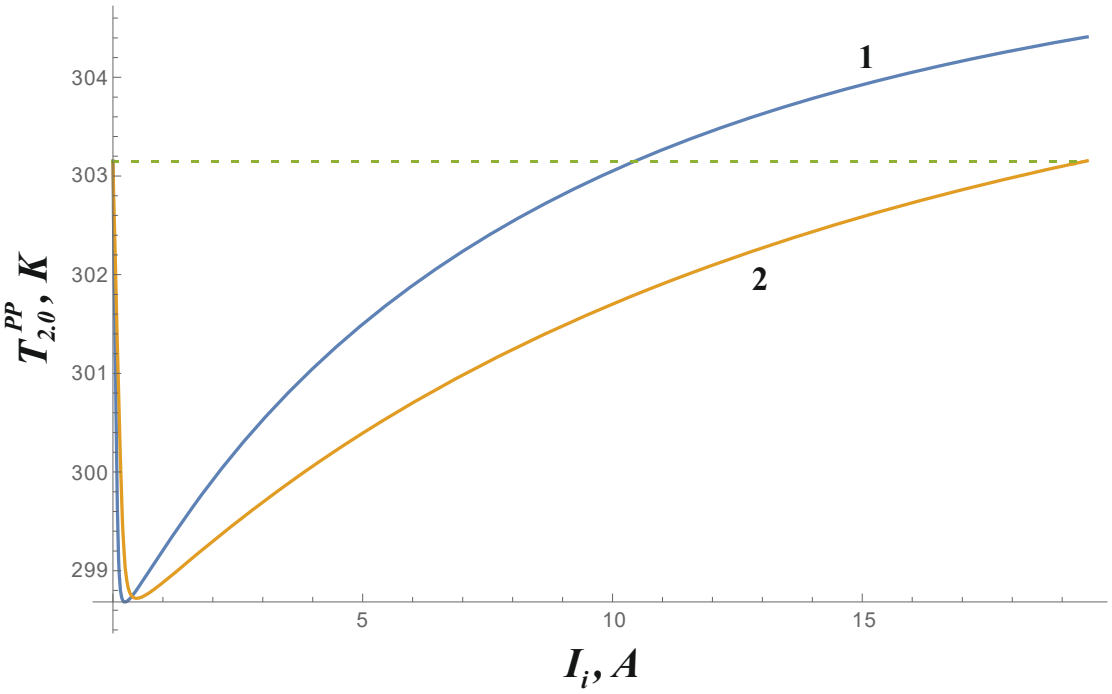

Fig. 4.6. Plots of dependence of the MS outlet temperature according to diagram in Fig. 3 [1] $T_{2.0}^{PP}$ *on* I_i *of the considered example of the investigated process for the initial data that correspond to the 1st and 2nd cases in Table 4.1 (*$\Delta T_{hot}^{PP} = const = 5\ K$, $V_C^{PP} \neq const$*): 1 –for the initial data of the 1st case from Table 4.1, 2 – for the initial data of the 2nd case from Table 4.1.*

a)

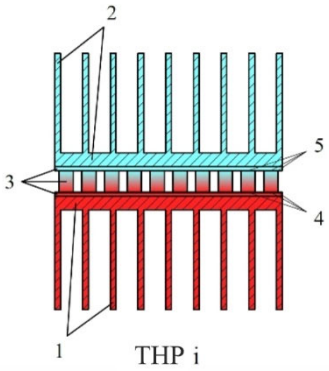

b)

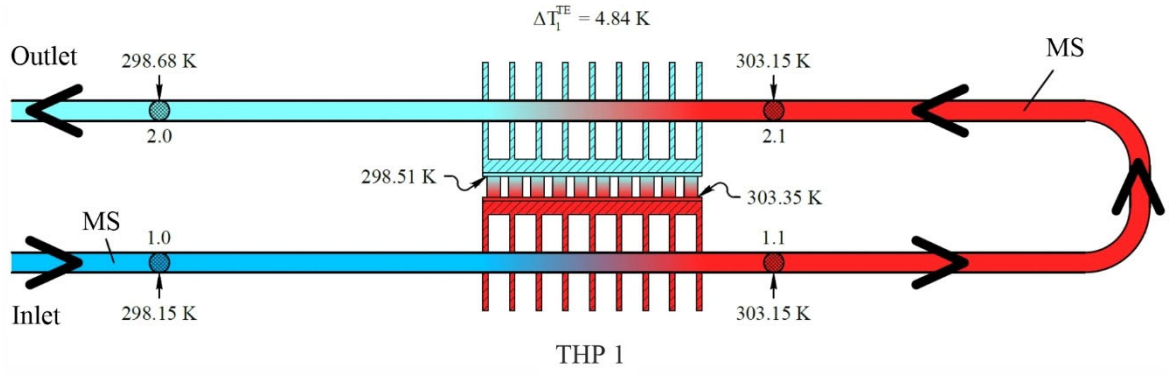

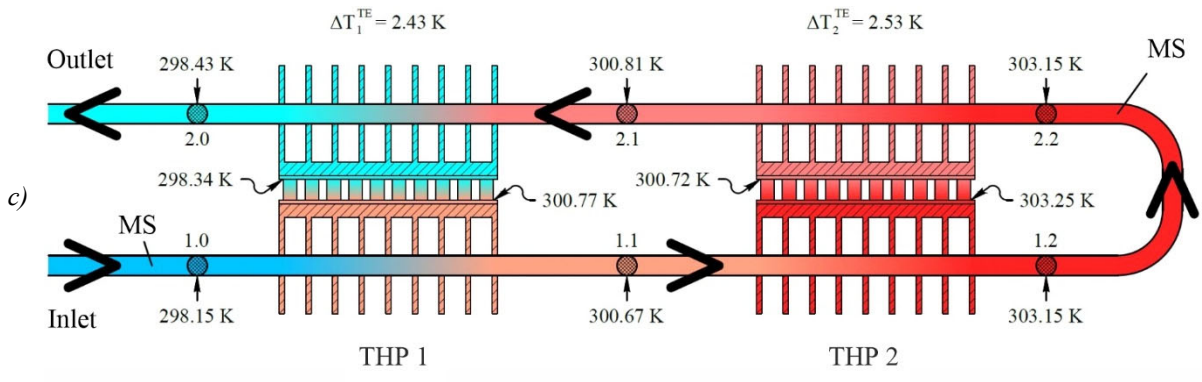

Fig. 4.7. Figure illustrating the calculated results for the 3rd and 7th cases of the considered example of the investigated heat and mass transfer method (according to Table 4.1): a) simplified diagram of individual ith THP: 1 – heat releasing heat exchanger, 2 –heat absorbing heat exchanger, 3 – thermoelectric module, 4 – location of the heat releasing junctions of THP thermoelements, 5 – location of the heat absorbing junctions of THP thermoelements; ***b)*** *simplified diagram of the 3rd case of the considered example of the investigated process with certain corresponding calculated results: 1.0, 1.1, 2.1, 2.0 – successive positions of the MS during its movement (1.0 – immediately before TC of MS to the heat releasing (1st) HE of THP 1, 1.1 – immediately after TC of MS to the heat releasing (1st) HE of THP 1, 2.1 – immediately before TC of the MS to the heat absorbing (2nd) HE of THP 1, 2.0 – immediately after TC of the MS to the heat absorbing (2nd) HE of THP 1; c) simplified diagram of the 7th case of the considered example of the investigated process with certain corresponding calculated results: 1.0, 1.1, 1.2, 2.2, 2.1, 2.0 – successive positions of the MS during its movement (1.0 – immediately before TC of the MS to the heat releasing (1st) HE of THP 1, 1.1 – immediately after TC of the MS to the heat releasing (1st) HE of THP 1, 1.2 – immediately after TC of the MS to the heat releasing (1st) HE of THP 2, 2.2 – immediately before TC of the MS to the heat absorbing (2nd) HE of THP 2, 2.1 – immediately after TC of the MS with the heat absorbing (2nd) HE of THP 2, 2.0 – immediately after TC of the MS to the heat absorbing (2nd) HE of THP 1.*

Conclusions

1. A theoretical model is presented for estimating the efficiency of using the investigated heat and mass transfer method for the case of heating the MS in its input flow by all individual THPs. Mathematical expressions for the corresponding estimation calculations and examples of the results of such calculations are presented.
2. The energy efficiency of the studied process may depend on its features, on the number of THPs used in the process, and on the parameters of the THP thermoelements.
3. Further theoretical and/or experimental studies may be required to make decisions regarding practical applications of the *investigated heat and mass transfer method*.

References

1. Kshevetsky O.S. (2017). Estimation of the efficiency of partial case of heat and mass transfer processes between heat pumps and moving substance, part 1. *J. Thermoelectricity, 6,* 39 – 55.
2. Kshevetsky O.S. (2018). Estimation of the efficiency of partial case of heat and mass transfer processes between heat pumps and moving substance, part 2. *J. Thermoelectricity, 2,* 56 – 68.

3. Kshevetsky O.S., Orletskyi O.V. (2019). Estimation of the efficiency of partial case of heat and mass transfer processes between heat pumps and moving substance, part 3. *J. Thermoelectricity, 4*, 40 – 53.
4. Kshevetsky O.S. (2019). About some of the possibilities of using heat pumps in processes that involve the movement of substance. *Thermophysics and Thermal Power Engineering*, *41* (3), 70 – 76. https://doi.org/https://doi.org/10.31472/ttpe.3.2019.10
5. Kshevetsky O.S. (2017). On the possibility of increasing the energy efficiency of heat and mass transfer processes that involve heating and cooling of moving matter.*Chemical Technology and Engineering: collection of abstracts of International Scientific and Practical Conference* (June 26 – 30, 2017, Lviv). Lviv: Lvivska Politechnica Publ., 96 – 97.
6. *Patent of Ukraine №118972*. O.S. Kshevetsky (2019). Method of heat and mass exchange between movable substance and heat pumps, Bul. №7.
7. Anatychuk L.I. (2005). *Thermoelectricity. Vol. 2. Thermoelectric Power Converters*. Kyiv, Chernivtsi, Institute of Thermoelectricity, 2005. 348 p.
8. Anatychuk L.I., Prybyla A.V. (2016). Comparative analysis of thermoelectric and compression heat pumps for individual air conditioners. *J. Thermoelectricity,* 2, 33 – 42.
9. Cherkez R. (2012). Theoretical studies on the efficiency of air conditioner based on permeable thermoelectric converter. *Applied Thermal Engineering*, 38, 7 – 13. DOI: http://dx.doi.org/10.1016/j.applthermaleng.2012.01.012
10. Anatychuk L.I. and Cherkez R.G. (2012). Energy potential of permeable segmented thermoelements in cooling mode. *Journal of Electronic Materials*, 41 (6), 1115 – 1119. DOI: 10.1007/s11664-012-1946-4
11. Prybyla A.V. and Cherkez R.G. (2012). Effect of heat-exchange systems on the efficiency of thermoelectric devices. *AIP Conf. Proc*. 1449, 443, 443 – 446; doi: http://dx.doi.org/10.1063/1.4731591

Submitted: 15.11.2023.

Кшевецький О.С., *канд. фіз.-мат. наук* [1]
Черкез Р.Г, *доктор фіз.-мат. наук* [1,2]
Мазар Ю.І. [1]

[1] Чернівецький національний університет імені Юрія Федьковича,
вул. Коцюбинського 2, Чернівці, 58012, Україна;
[2] Інститут термоелектрики НАН та МОН України,
вул. Науки, 1, Чернівці, 58029, Україна;
e-mail: anatych@gmail.com

ОЦІНКА ЕФЕКТИВНОСТІ ЧАСТИННОГО ВИПАДКУ ПРОЦЕСІВ ТЕПЛОМАСООБМІНУ МІЖ ТЕПЛОВИМИ НАСОСАМИ І РУХОМОЮ РЕЧОВИНОЮ. ЧАСТИНА 4

Представлена теоретична модель для оцінки ефективності роботи частинного випадку процесів, в яких має місце тепловий контакт рухомої речовини (або принаймні частини цієї рухомої речовини) з теплопоглинальною і тепловиділяючою теплообмінними частинами принаймні двох теплових насосів для випадку нагрівання рухомої речовини у її вхідному потоці всіма окремо взятими термоелектричними тепловими насосами. Наведені математичні вирази для відповідних оціночних розрахунків та приклади результатів таких розрахунків.

Ключові слова: тепловий насос, рухома речовина, тепломасообмін, ефективність, енергоефективність, термоелектричний тепловий насос, термоелементи.

Література

1. Kshevetsky O.S. (2017). Estimation of the efficiency of partial case of heat and mass transfer processes between heat pumps and moving substance, part 1. *J. Thermoelectricity, 6,* 39 – 55.
2. Kshevetsky O.S. (2018). Estimation of the efficiency of partial case of heat and mass transfer processes between heat pumps and moving substance, part 2. *J. Thermoelectricity, 2,* 56 – 68.
3. Kshevetsky O.S., Orletskyi O.V. (2019). Estimation of the efficiency of partial case of heat and mass transfer processes between heat pumps and moving substance, part 3. *J. Thermoelectricity, 4*, 40 – 53.
4. Kshevetsky O.S. (2019). About some of the possibilities of using heat pumps in processes that involve the movement of substance. *Thermophysics and Thermal Power Engineering*, *41* (3), 70 – 76. https://doi.org/https://doi.org/10.31472/ttpe.3.2019.10
5. Kshevetsky O.S. (2017). On the possibility of increasing the energy efficiency of heat and mass transfer processes that involve heating and cooling of moving matter.*Chemical Technology and Engineering: collection of abstracts of International Scientific and Practical Conference* (June 26 – 30, 2017, Lviv). Lviv: Lvivska Politechnica Publ., 96 – 97.
6. Кшевецький О.С. Патент UA №118972, МПК (2006) F26B 9/06 (2006.01), B01J 8/00, F26B 9/00 на винахід «Спосіб тепломасообміну між рухомою речовиною і тепловими насосами», 10.04.2019, Бюл. №7.
7. Anatychuk L.I. (2005). *Thermoelectricity. Vol. 2. Thermoelectric Power Converters*. Kyiv, Chernivtsi, Institute of Thermoelectricity, 2005. 348 p.
8. Anatychuk L.I., Prybyla A.V. (2016). Comparative analysis of thermoelectric and compression heat pumps for individual air conditioners. *J. Thermoelectricity,* 2, 33 – 42.
9. Cherkez R. (2012). Theoretical studies on the efficiency of air conditioner based on permeable thermoelectric converter. *Applied Thermal Engineering*, 38, 7 – 13. DOI: http://dx.doi.org/10.1016/j.applthermaleng.2012.01.012
10. Anatychuk L.I. and Cherkez R.G. (2012). Energy potential of permeable segmented thermoelements in cooling mode. *Journal of Electronic Materials*, 41 (6), 1115 – 1119. DOI: 10.1007/s11664-012-1946-4
11. Prybyla A.V. and Cherkez R.G. (2012). Effect of heat-exchange systems on the efficiency of thermoelectric devices. *AIP Conf. Proc*. 1449, 443, 443 – 446; doi: http://dx.doi.org/10.1063/1.4731591

Надійшла до редакції: 15.11.2023.

ARTICLE SUBMISSION GUIDELINES

For publication in a specialized journal, scientific works are accepted that have never been printed before. The article should be written on an actual topic, contain the results of an in-depth scientific study, the novelty and justification of scientific conclusions for the purpose of the article (the task in view).

The materials published in the journal are subject to internal and external review which is carried out by members of the editorial board and international editorial board of the journal or experts of the relevant field. Reviewing is done on the basis of confidentiality. In the event of a negative review or substantial remarks, the article may be rejected or returned to the author(s) for revision. In the case when the author(s) disagrees with the opinion of the reviewer, an additional independent review may be done by the editorial board. After the author makes changes in accordance with the comments of the reviewer, the article is signed to print.

The editorial board has the right to refuse to publish manuscripts containing previously published data, as well as materials that do not fit the profile of the journal or materials of research pursued in violation of ethical norms (for instance, conflicts between authors or between authors and organization, plagiarism, etc.). The editorial board of the journal reserves the right to edit and reduce the manuscripts without violating the author's content. Rejected manuscripts are not returned to the authors.

Submission of manuscript to the journal

The manuscript is submitted to the editorial office of the journal in paper form in duplicate and in electronic form on an electronic medium (disc, memory stick). The electronic version of the article shall fully correspond to the paper version. The manuscript must be signed by all co-authors or a responsible representative.

In some cases it is allowed to send an article by e-mail instead of an electronic medium (disc, memory stick).

English-speaking authors submit their manuscripts in English. Russian-speaking and Ukrainian-speaking authors submit their manuscripts in English and in Russian or Ukrainian, respectively. Page format is A4. The number of pages shall not exceed 15 (together with References and extended abstracts). By agreement with the editorial board, the number of pages can be increased.

To the manuscript is added:

1. Official recommendation letter, signed by the head of the institution where the work was carried out.

2. License agreement on the transfer of copyright (the form of the agreement can be obtained from the editorial office of the journal or downloaded from the journal website – Dohovir.pdf). The license agreement comes into force after the acceptance of the article for publication. Signing of the license agreement by the author(s) means that they are acquainted and agree with the terms of the agreement.

3. Information about each of the authors – full name, position, place of work, academic title, academic degree, contact information (phone number, e-mail address), ORCID code (if available). Information about the authors is submitted as follows:

authors from Ukraine - in three languages, namely Ukrainian, Russian and English;

authors from the CIS countries - in two languages, namely Russian and English;

authors from foreign countries – in English.

4. Medium with the text of the article, figures, tables, information about the authors in electronic form.

5. Colored photo of the author(s). Black-and-white photos are not accepted by the editorial staff. With the number of authors more than two, their photos are not shown.

Requirements for article design

The article should be structured according to the following sections:

- *Introduction*. Contains the problem statement, relevance of the chosen topic, analysis of recent research and publications, purpose and objectives.
- *Presentation of the main research material* and the results obtained.
- *Conclusions* summing up the work and the prospects for further research in this direction.
- *References*.

The first page of the article contains information:

1) in the upper left corner – UDC identifier (for authors from Ukraine and the CIS countries);

2) surname(s) and initials, academic degree and scientific title of the author(s);

3) the name of the institution where the author(s) work, the postal address, telephone number, e-mail address of the author(s);

4) article title;

5) abstract to the article – not more than 1 800 characters. The abstract should reflect the consistent logic of describing the results and describe the main objectives of the study, summarize the most significant results;

6) key words – not more than 8 words.

The text of the article is printed in Times New Roman, font size 11 pt, line spacing 1.2 on A4 size paper, justified alignment. There should be no hyphenation in the article.

Page setup: "mirror margins" – top margin – 2.5 cm, bottom margin – 2.0 cm, inside – 2.0 cm, outside – 3.0 cm, from the edge to page header and page footer – 1.27 cm.

Graphic materials, pictures shall be submitted in color or, as an exception, black and white, in .opj or .cdr formats, .jpg or .tif formats being also permissible. According to author's choice, the tables and partially the text can be also in color.

Figures are printed on separate pages. The text in the figures must be in the font size 10 pt. On the charts, the units of measure are separated by commas. Figures are numbered in the order of their arrangement in the text, parts of the figures are numbered with letters – a, b, .. On the back of the figure, the title of the article, the author (authors) and the figure number are written in pencil. Scanned images and graphs are not allowed to be inserted.

Tables are provided on separate pages and must be executed using the MSWord table editor. Using pseudo-graph characters to design tables is inadmissible.

Formulae shall be typed in Equation or MatType formula editors. Articles with formulae written by hand are not accepted for printing. It is necessary to give definitions of quantities that are first used in the text, and then use the appropriate term.

Captions to figures and tables are printed in the manuscript after the references.

Reference list shall appear at the end of the article. References are numbered consecutively in the order in which they are quoted in the text of the article. References to unpublished and unfinished works are inadmissible.

Attention! In connection with the inclusion of the journal in the international bibliographic abstract database, the reference list should consist of two blocks: CITED LITERATURE and REFERENCES (this requirement also applies to English articles):

CITED LITERATURE – sources in the original language, executed in accordance with the

Ukrainian standard of bibliographic description DSTU 8302:2015. With the aid of VAK.in.ua (http://vak.in.ua) you can automatically, quickly and easily execute your "Cited literature" list in conformity with the requirements of State Certification Commission of Ukraine and prepare references to scientific sources in Ukraine in understandable and unified manner. This portal facilitates the processing of scientific sources when writing your publications, dissertations and other scientific papers.

REFERENCES – the same cited literature list transliterated in Roman alphabet (recommendations according to international bibliographic standard APA-2010, guidelines for drawing up a transliterated reference list "References" are on the site http//www.dse.org.ua, section for authors).

To speed up the publication of the article, please adhere to the following rules:

- in the upper left corner of the first page of the article – the UDC identifier;
- family name and initials of the author(s);
- academic degree, scientific title;

begin a new line, Times New Roman font, size 12 pt, line spacing 1.2, center alignment;

- name of organization, address (street, city, zip code, country), e-mail of the author(s);

begin a new line 1 cm below the name and initials of the author(s), Times New Roman font, size 11 pt, line spacing 1.2, center alignment;

- the title of the article is arranged 1 cm below the name of organization, in capital letters, semi-bold, font Times New Roman, size 12 pt, line spacing 1.2, center alignment. The title of the article shall be concrete and possibly concise;
- the abstract is arranged 1 cm below the title of the article, font Times New Roman, size 10 pt, in italics, line spacing 1.2, justified alignment in Ukrainian or Russian (for Ukrainian-speaking and Russian-speaking authors, respectively);
- key words are arranged below the abstract, font Times New Roman, size 10 pt, line spacing 1.2, justified alignment. The language of the key words corresponds to that of the abstract. Heading "Key words" - font Times New Roman, size 10 pt, semi-bold;
- the main text of the article is arranged 1 cm below the abstract, indent 1 cm, font Times New Roman, size 11 pt, line space spacing 1.2, justified alignment;
- formulae are typed in formula editor, fonts Symbol, Times New Roman. Font size is "normal" – 12 pt, "large index" – 7 pt, "small index" – 5 pt, "large symbol" – 18 pt, "small symbol" – 12 pt. The formula is arranged in the text, center aligned and shall not occupy more than 5/6 of the line width, formulae are numbered in parentheses on the right;
- dimensions of all quantities used in the article are represented in the International System of Units (SI) with the explication of the symbols employed;
- figures are arranged in the text. The figures and pictures shall be clear and contrast; the plot axes – parallel to sheet edges, thus eliminating possible displacement of angles in scaling; figures are submitted in color, black-and-white figures are not accepted by the editorial staff of the journal;
- tables are arranged in the text. The width of the table shall be 1 cm less than the line width. Above the table its ordinary number is indicated, right alignment. Continuous table numbering throughout the text. The title of the table is arranged below its number, center alignment;

• references should appear at the end of the article. References within the text should be enclosed in square brackets behind the text. References should be numbered in order of first appearance in the text. Examples of various reference types are given below.

Examples of LITERATURE CITED

Journal articles

Anatychuk L.I., Mykhailovsky V.Ya., Maksymuk M.V., Andrusiak I.S. Experimental research on thermoelectric automobile starting pre-heater operated with diesel fuel. *J.Thermoelectricity*. 2016. №4. P.84–94.

Books

Anatychuk L.I. *Thermoelements and thermoelectric devices. Handbook.* Kyiv, Naukova dumka, 1979. 768 p.

Patents

Patent of Ukraine № 85293. Anatychuk L.I., Luste O.J., Nitsovych O.V. Thermoelement.

Conference proceedings

Lysko V.V. *State of the art and expected progress in metrology of thermoelectric materials.* Proceedings of the XVII International Forum on Thermoelectricity (May 14-18, 2017, Belfast). Chernivtsi, 2017. 64 p.

Authors' abstracts

Kobylianskyi R.R. *Thermoelectric devices for treatment of skin diseases*: extended abstract of candidate's thesis. Chernivtsi, 2011. 20 p.

Examples of REFERENCES

Journal articles

Gorskiy P.V. (2015). Ob usloviakh vysokoi dobrotnosti i metodikakh poiska perspektivnykh sverhreshetochnykh termoelektricheskikh materialov [On the conditions of high figure of merit and methods of search for promising superlattice thermoelectric materials]. *Termoelektrichestvo - J.Thermoelectricity,* 3, 5 – 14 [in Russian].

Books

Anatychuk L.I. (2003). *Thermoelectricity. Vol.2. Thermoelectric power converters*. Kyiv, Chernivtsi: Institute of Thermoelectricity.

Patents

Patent of Ukraine № 85293. Anatychuk L. I., Luste O.Ya., Nitsovych O.V. Thermoelements [In Ukrainian].

Conference proceedings

Rifert V.G. Intensification of heat exchange at condensation and evaporation of liquid in 5 flowing-down films. In: *Proc. of the 9th International Conference Heat Transfer.* May 20-25, 1990, Israel.

Authors'abstracts

Mashukov A.O. *Efficiency hospital state of rehabilitation of patients with color carcer.* PhD (Med.) Odesa, 2011 [In Ukrainian].

ISSN 1607 - 8829. Journal of Thermoelectricity. 2023. № 4. 1-80